Regulation of cell death signaling by the thioredoxin system in healthy and malignant cells

Dissertation

zur Erlangung des Doktorgrades

der Naturwissenschaften

vorgelegt am Fachbereich 14 Biochemie, Chemie und Pharmazie

der Johann Wolfgang Goethe-Universität

in Frankfurt am Main

von

Vanessa Ehrenfeld geb. Zimmermann

aus Aschaffenburg

Frankfurt am Main, 2020

(D30)

Vom Fachbereich Biochemie, Chemie und Pharmazie (FB14) der Johann Wolfgang Goethe-Universität Frankfurt am Main als Dissertation angenommen.

Dekan: Prof. Dr. Clemens Glaubitz

1. Gutachter: Prof. Dr. Volker Dötsch

2. Gutachter: Prof. Dr. Simone Fulda

Datum der Disputation: 23.11.2020

Table of contents

List of abbreviations

AIF	Apoptosis inducing factor
ALDH4	Aldehyde dehydrogenase
ALL	Acute lymphoblastic leukemia
ALN	Another-regulin
APAF1	Apoptotic peptidase activating factor 1
APIP	APAF1-interacting protein
APS	Ammounium persulfate
ARE	Antioxidant Response Element
ASK-1	Apoptosis signal-regulating kinase 1
A-T	Ataxia-telangiectasia
ATF4	Activating transcription factor 4
ATM	Ataxia-telangiectasia mutated
α-Toc	α-Tocopherol
ATP	Adenosine triphosphate
BAD	BCL-2 antagonist of cell death
BAK	BCL-2 antagonist/killer
BAX	BCL-2-associated X protein
BCAT1	Branched-chain aminotransferase
BCL-2	B-cell lymphoma 2
BCL2A1	BCL-2-related protein A1
BCL-W	BCL-2-like protein 2
BCL-X$_L$	BCL-2-like protein 1
BH	BCL-2 homology
BHA	Butylated hydroxyanisole
BIAM	EZ-Link™ Iodoacetyl-PEG2-Biotin
BID	BH3-interacting domain death agonist
BIM	BCL-2-interacting mediator of cell death
BMF	BCL-2-modifying factor
BODIPY	BODIPY 581/591-C11
BOK	BCL-2-related ovarian killer
BSA	Bovine serum albumin
BSO	Buthionine sulfoximine
Ca^{2+}	Calcium

CAD	Caspase-activated DNase
CAR	Chimeric antigen receptor
CBP	CREB-binding protein
CHAPS	Cholamidopropyldimethyl ammonio propane sulfonate
cIAP1/2	Cellular inhibitor of apoptosis protein 1/2
CLL	Chronic myelogenous leukemia
Ctrl	Control
CUL3	Cullin 3
CYLD	Cylindromatosis
CYP450	Cytochrome P450
CYPD	Cyclophilin D
Dab	Dabrafenib
DD	Death domain
DED	Death effector domain
DISC	Death inducing signaling complex
DMEM	Dulbecco's Modified Eagle Medium
DMSO	Dimethyl sulfoxide
DRP1	Dynamin-related protein 1
DSMZ	Deutsche Sammlung von Mikroorganismen und Zellkulturen
DTT	Dithiothreitol
DUOX1/2	Dual oxidase 1/2
EDTA	Ethylene diamine tetraacetic acid
EGF	Epidermal growth factor
EGFR	EGF receptor
ELN	Endoregulin
EndoG	Endonuclease G
ER	Endoplasmic reticulum
ERK	Extracellular signal-regulated kinase
ETC	Electron transport chain
FADD	Fas-associated protein with death domain
$FAD/FADH_2$	Flavin adenine dinucleotide
FCS	Fetal calf serum
FD	FADD-deficient
[Fe-S]	Iron-sulphur cluster
FOXO	Forkhead box protein O
FSC	Forward scatter

G6PDH	Glucose-6-phosphate dehydrogenase
GdmCl	Guanidinium chloride
GLS2	Glutaminase 2
GPX	Glutathione peroxidase
Grx	Glutaredoxin
GSH	Glutathione
GSK	GSK'872
GSSG	Glutathione disulfide
H_2DCF	$CM\text{-}H_2DCFDA$
HIF	Hypoxia-inducible factor
H_2O_2	Hydrogen peroxide
HO•	Hydroxyl radical
HRP	Horseradish peroxidase
IAP	Inhibitor of apoptosis protein
ICAD	Inhibitor of caspase-activated DNase
IMM	Inner mitochondrial membrane
JNK	c-Jun N-terminal kinase
KD	knock-down
KEAP1	Kelch-like ECH-associated protein 1
LC/MS	Liquid chromatography/mass spectrometry
MAPK	Mitogen-activated protein kinase
MCL-1	Myeloid cell leukemia-1
MEF	Mouse embryonic fibroblast
MFF	Mitochondrial fission factor
MID49/51	Mitochondrial dynamics protein of 49/51 kDa
MLKL	Mixed lineage kinase domain-like
MnSOD	Manganese superoxide dismutase
MnTBAP	Mn(III)tetrakis(4-benzoic acid)porphyrin chloride
MOMP	Mitochondrial outer membrane permeabilization
MPT	Mitochondrial permeability transition
MPTP	MPT pore
MS	Mass spectrometry
NAA40	N-alpha-acetyltransferase 40
NAC	N-acetylcysteine
$NAD^+/NADH$	Nicotinamide adenine dinucleotide
$NADP^+/NADPH$	Nicotinamide adenine dinucleotide phosphate

Nec-1s	Necrostatin-1s
NEM	N-ethylmaleimide
NOX	NADPH oxidase
NRF2	NF-E2-related factor 2
ns	Not significant
$O_2^{\bullet-}$	Superoxide anion
OMM	Outer mitochondrial membrane
PAGE	Polyacrylamid gel electrophoresis
PARP	poly(ADP-ribose) polymerase
PBS	Phosphate buffered saline
PCR	Polymerase chain reaction
PDGF	Platelet-derived growth factor
PDI	Protein disulfide isomerase
PDLIM1	PDZ and LIM domain protein 1
PFN2	Profilin-2
PHPT1	Phosphohistidine phosphatase 1
PI	Propidium iodide
PI3K	Phosphoinositide 3-kinase
PIC	Protease Inhibitor Cocktail
PIG3/6	p53-inducible gene 3/6
PMSF	Phenylmethylsulfonyl fluoride
PPP	Pentose phosphate pathway
PRDX	Peroxiredoxin
PRMT1	Proteine arginine N-methyltransferase 1
PS	Phosphatidylserine
PTEN	Phosphatase and tensin homolog
PTP	Protein tyrosine phosphatase
PTP4A2	Protein tyrosine phoshphatase type IVA 2
PUMA	p53 upregulated modulator of apoptosis
RAB11A/RAB11B	Ras-related protein Rab-11A/Rab-11B
RIPK1/3	Receptor-interacting protein kinase 1/3
RNAi	RNA interference
ROS	Reactive oxygen species
RPMI	Roswell Park Memorial Institute Medium
RT	Room temperature
SD	Standard deviation

SDS	Sodium dodecyl sulfate
SERCA	Sarcoplasmic-endoplasmic reticulum Ca^{2+} ATPase
siRNA	small-interfering RNA
SMAC	Second mitochondrial activator of caspase
SOD	Superoxide dismutase
SSC	Side scatter
Tbhq	tert-Butylhydoquinone
tBID	truncated BID
TCA	Trichloroacetic acid
TCEP	Tris(2-carboxyethyl)phosphine
TEMED	Tetramethylethylendiamine
TIGAR	TP53-inducible glycolysis and apoptosis regulator
TGR	Thioredoxin glutathione reductase
TNF	Tumor necrosis factor
TNFR	TNF receptor
TOMM20	Protein translocase of outer mitochondrial membrane 20
TRADD	TNFR-associated death domain
TRAF2	TNFR-associated factor 2
Trx	Thioredoxin
TrxR	Thioredoxin reductase
VDAC2	Voltage-dependent anion-selective channel protein 2
VTI1A	Vesicle transport through interaction with t-SNAREs homolog 1A
WT	Wild-type
XIAP	X-linked inhibitor of apoptosis
zVAD.fmk	N-benzyloxycarbonyl-Val-Ala-Asp(O-Me)fluoromethylketone

List of figures

List of tables

1 Abstract

Acute lymphoblastic leukemia (ALL), a neoplastic disorder of blood cells of the lymphoid lineage, is the most frequent childhood cancer. In spite of increasing survival rates, the outcome for adults, infants or relapsed patients is still less favorable, highlighting the need for novel treatment options. Reactive oxygen species (ROS) are important signaling molecules that are involved in a variety of cellular pathways. As high ROS levels lead to oxidative stress and irreversible oxidation of cellular macromolecules, the production and elimination of ROS is tightly controlled. Therefore, cells express several antioxidant molecules and enzymes, including glutathione, catalase and the thioredoxin (Trx) system, to balance ROS levels. As cancer cells were found to have increased ROS levels that could contribute to tumor progression and metastasis, they rely strongly on these antioxidant systems to prevent oxidative damage, making cancer cells especially vulnerable to ROS-inducing treatments. ROS and oxidative stress have been shown to induce programmed cell death via different pathways, however the exact mechanisms that couples oxidative signaling and cell death is not completely understood.

As a disturbance of the cellular redox homeostasis was reported during leukemia development and progression, we wanted to determine the potential of Trx inhibitors for ALL therapy. Additionally, we aimed to further understand the role of ROS and subsequent protein oxidation in the induction and execution of programmed cell death.

First, we demonstrated that the Trx1 inhibitor PX-12 induced cell death in three ALL cell lines. Further analysis of the events leading to PX-12-induced cell death in FADD-deficient (FD) Jurkat cells revealed an increase in ROS levels and oxidation-mediated dimer formation of peroxiredoxin 3 (PRDX3). Interestingly cell death was inhibited by the thiol-containing antioxidant N-acetylcysteine (NAC), but not by non-thiol-containing ROS scavengers. PX-12 treatment further induced cleavage of caspase-9 and -3 and activation of the pro-apoptotic BCL-2 protein BAK, leading us to the conclusion that mitochondria-dependent apoptosis was induced. Interestingly, we could demonstrate an important role for the BH3-only protein NOXA in the mediation of PX-12-induced apoptosis as knock-down of NOXA prevented cell death induction and BAK activation. Our findings give novel insights into the mechanism of PX-12-induced cell death in ALL cell lines and underscores the potential of PX-12 for the treatment of ALL.

To further understand the processes leading to cell death upon inhibition of the Trx system, we analyzed global protein oxidation in Jurkat FD cells upon treatment with the Trx reductase inhibitor Auranofin. In line with previous results, Auranofin induced intrinsic apoptosis that was

dependent on BAK and accompanied by increased ROS levels. Using a BIAM Switch Assay followed by mass spectrometry, we demonstrated that Auranofin treatment induced oxidation of over 200 proteins. We identified several proteins whose oxidation upon Auranofin treatment was expected, like Trx1, Trx2 and several peroxiredoxins. Additionally, we verified oxidation of APAF1-interacting protein (APIP) and protein arginine N-methyltransferase (PRMT1) that are both implicated in the regulation of apoptosis. With this analysis we were able to demonstrate that Auranofin treatment leads to changes in global protein oxidation. Whether oxidation of the determined proteins changes their functionality and contributes to apoptosis induction remains to be elucidated.

As we identified BAK as an important player in PX-12- and Auranofin-induced cell death in the previous parts of this study, we wanted to further understand its involvement in ROS-mediated cell death. First analyses in wild-type (WT) and BAK$^{-/-}$ murine embryonic fibroblasts (MEFs) revealed that BAK was essential for Auranofin-induced cell death and that this cell death was caspase-independent in MEFs. Interestingly, BAK oxidation was induced upon treatment with Auranofin, but not upon stimulation with the apoptosis-inducing compound Etoposide. Expression of mutated BAK, with either one or both oxidation-sensitive cysteines mutated to oxidation-insensitive serines, revealed that mutating already one cysteine protected cells from Auranofin-, but not Etoposide-induced cell death. Of note, mutation of the BAK BH3 domain rescued MEFs from both, Auranofin- and Etoposide-mediated cell death. The presence of cysteine residues also altered BAK interactions as observed by a mass spectrometric analysis of Auranofin-treated MEFs expressing either WT or cysteine-less BAK. We identified interactions of WT BAK with proteins involved in mitochondrial fission and vesicle transport upon Auranofin treatment. Of note, interaction with proteins involved in apoptosis, like BAX or BCL-X$_L$, was not changed between WT and cysteine-less BAK. Our results demonstrate a critical role for BAK oxidation in Auranofin-induced cell death. Furthermore, we identified novel oxidation-dependent BAK interaction partners.

To conclude, this study highlights the potential of ROS-inducing treatments for ALL therapy and provides novel insights into the redox regulation of programmed cell death.

2 Introduction

2.1 Acute lymphoblastic leukemia

Leukemia is a neoplastic disorder of the blood and bone marrow and is the malignancy with the highest frequency in children. Acute lymphoblastic leukemia (ALL) accounts for approximately 75 % of all leukemia cases in children and has the highest prevalence between age three to five [1-3]. ALL is caused by changes in the proliferation and maturation of lymphoid progenitor cells that lead to the accumulation of leukemic blasts and disruption of normal hematopoiesis. Depending on the cell lineage giving rise to the disease, ALL can be subtyped into B-cell precursor, T-cell or mature B-cell types [4]. Only a small number of cases can be attributed to inherited genetic syndromes such as trisomy 21, Ataxia-telangiectasia (A-T) or Nijmegen breakage syndrome [1].

Mutations in genes regulating various cellular pathways are assumed to drive leukemogenic progression [1, 5]. Several chromosomal translocations have been identified in ALL. Approximately one quarter of B-cell precursor ALL cases express the *TEL-AML1* fusion gene that is generated by the t(12;21)(p13;q22) translocation [1, 6]. This translocation is thought to be a first-hit mutation that alters early B-lymphocyte development [1, 7]. The most common translocation in adult ALL, that is also found in chronic myelogenous leukemia (CML), is the Philadelphia chromosome or t(9;22)(q34;q11) translocation that generates the BCR-ABL fusion protein leading to constitutive activation of the tyrosine kinase ABL [8, 9]. A potent treatment option for Philadelphia chromosome-positive malignancies is the small molecule ABL kinase inhibitor imatinib mesylate (Glivec) [9, 10]. Additionally, genetic lesions such as hyper- and hypoploidy can be found in ALL, which are also involved in malignant transformation.

ALL patients usually receive intensive combination chemotherapy for up to 2.5 years that can be divided into three phases: remission-induction phase, consolidation phase and continuation phase. Chemotherapeutics commonly used include glucocorticoids, vinca alkaloids, asparaginase, anthracyclines, methotrexate and mercaptopurine. For high risk cases, allogeneic hematopoietic stem cell transplantation is an option, that is, however, associated with substantial morbiditiy and mortality [1, 4]. Besides classical chemotherapy, more targeted approaches are emerging, including tyrosine kinase inhibitors like imatinib, DNA methyltransferase inhibitors like decitabine and histone deacetylase inhibitors like vorinostat [1]. Another promising treatment option that has emerged in the last years, and was recently approved by the FDA, is chimeric antigen receptor (CAR) modified T cell therapy for B-cell ALL

[11]. Overall, 5-year survival rates have increased up to 80 – 90 % [2]. However, successful therapy for adults, young infants or relapsed patients is still challenging [11]. Furthermore, the toxicity of the current complex treatment regimens should not be disregarded. Therefore, further innovative approaches are needed to increase leukemia-free survival of all patients and alleviate the detrimental side-effects of the treatments.

2.2 Reactive oxygen species

Reactive oxygen species (ROS) are a group of molecules and radicals that are generated by the partial reduction of oxygen [12]. Under physiological conditions, ROS can act as signaling molecules in various cellular pathways, however, immoderate ROS production or insufficient ROS scavenging can lead to oxidative stress and detrimental oxidation of DNA, proteins and lipids [13].

2.2.1 ROS production

Cellular ROS production involves various enzymes and can take place at different cellular compartments. The most abundant cellular ROS are hydrogen peroxide (H_2O_2), superoxide anion ($O_2^{\bullet-}$) and hydroxyl radical ($HO\bullet$) [12, 14]. $O_2^{\bullet-}$ is generated by a one electron reduction of molecular oxygen (O_2) (equation 1). Nicotinamide adenine dinucleotide phosphate (NADPH) oxidase (NOX) complexes can catalyze this reaction with electrons provided by NADPH (equation 2) [14]:

$$O_2 + e^- \rightarrow O_2^{\bullet-} \ (1)$$

$$2O_2 + NADPH \rightarrow 2O_2^{\bullet-} + NADP^+ + H^+ \ (2)$$
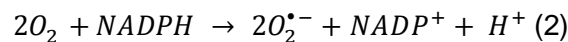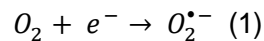
Further reduction of superoxide results in the formation of H_2O_2 (equation 3). This dismutation can take place spontaneously or can be catalyzed by the enzyme family of superoxide dismutases (SODs) [14].

$$2O_2^{\bullet-} + 2H^+ \rightarrow H_2O_2 + O_2 \ (3)$$
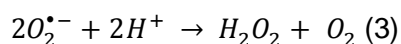
$HO\bullet$ can be generated from H_2O_2 through the Fenton reaction in the presence of metal ions (equation 4) [14, 15]:

$$Fe^{2+}/Cu^+ + H_2O_2 \rightarrow Fe^{3+}/Cu^{2+} + HO\bullet + OH^- \quad (4)$$
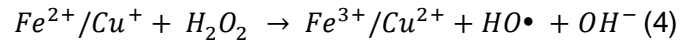
HO• is highly reactive and readily oxidizes a variety of biological macromolecules like lipids, DNA and proteins resulting in a short half-life, which limits its action to sites of production. $O_2^{\bullet-}$ favorably reacts with iron-sulphur ([Fe-S]) clusters but undergoes rapid dismutation to H_2O_2 [16]. Furthermore, its charge prevents it from diffusion through membranes weakening its fit as a signaling molecule. H_2O_2 is a weaker oxidant than HO• and $O_2^{\bullet-}$, but it has a longer cellular half-life and can cross membranes either by diffusion or by transport through aquaporins [16-18]. These properties and its selective reactivity make H_2O_2 a suitable signaling molecule [15, 16].

In the cell, the highest amount of ROS are thought to be produced in the mitochondria (Figure 1) [19, 20]. In the electron transport chain (ETC), electrons from nicotinamide adenine dinucleotide (NADH) and flavin adenine dinucleotide (FADH$_2$) are channeled through protein complexes in the inner mitochondrial membrane to reduce, in the final step, molecular oxygen to water. The energy that is released through this electron flow is used to generate a proton gradient across the inner mitochondrial membrane that drives adenosine triphosphate (ATP) production [15, 20]. However, electron leakage can result in the formation of $O_2^{\bullet-}$. This one electron reduction of molecular oxygen can take place at complex I of the ETC and results in $O_2^{\bullet-}$ formation in the mitochondrial intermembrane space. Additionally, $O_2^{\bullet-}$ can be generated at ETC complex III at which it can be released to both sides of the inner mitochondrial membrane (IMM) [19]. Dismutation of $O_2^{\bullet-}$ to H_2O_2 is catalyzed by mitochondrial manganese SOD (MnSOD) and contributes significantly to cellular H_2O_2 production [15].
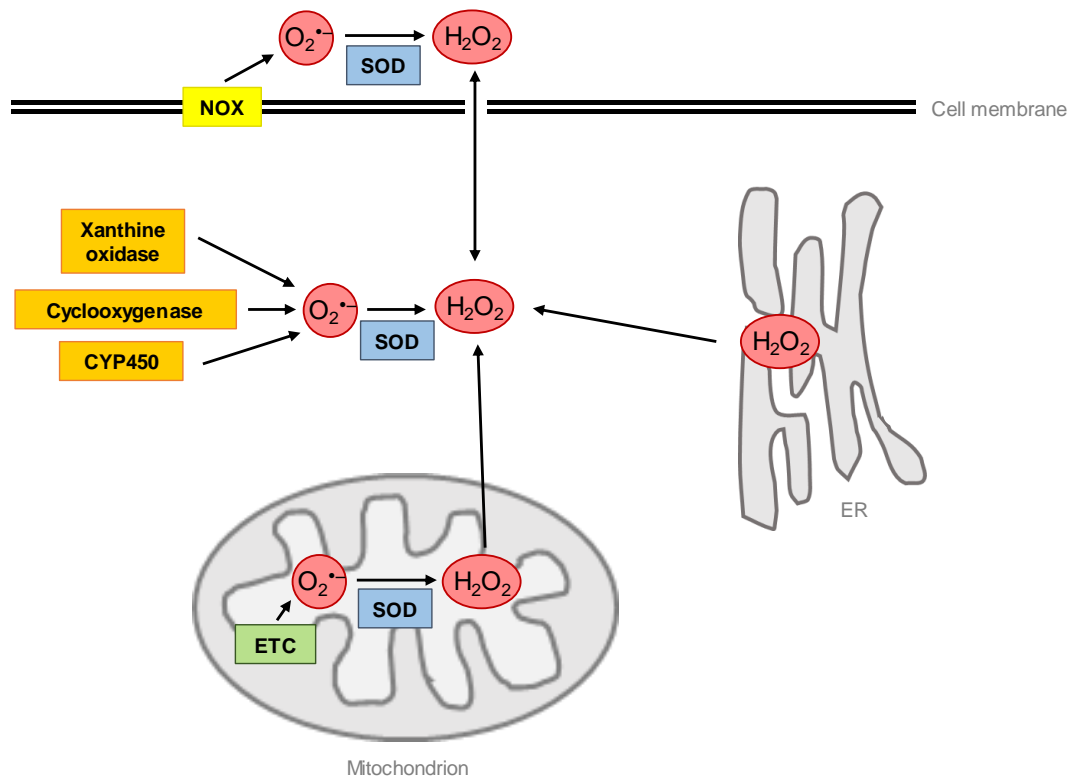
Figure 1: Schematic overview of ROS generation in the cell. Sites of ROS production include the mitochondria, in which electron leakage through the electron transport chain (ETC) leads to superoxide ($O_2^{\bullet-}$) production. ROS can also be produced at NADPH oxidase (NOX) complexes, the endoplasmic reticulum (ER) and through certain enzymes. Superoxide dismutases (SODs) can catalyze the conversion of $O_2^{\bullet-}$ to H_2O_2, which can pass through cellular membranes (Figure adapted from [21, 22]).

Another ROS source in the cell are NOX complexes [20]. These consist of a catalytic core unit and several coactivator proteins and cofactors that can be localized in the cytoplasm or at the membrane [15]. In humans, there are seven known NOX homologues, NOX1-5, dual oxidase 1 (DUOX1) and DUOX2, whose expression is tissue- and cell type-specific. Assembly of these complexes takes place at the plasma membrane or at intracellular membranes. Upon activation, an electron from NADPH is transferred from the cytosol across the membrane to molecular oxygen to produce $O_2^{\bullet-}$. $O_2^{\bullet-}$ can be dismutated to H_2O_2, which can then translocate across the membrane into the cytoplasm [15, 20].

The endoplasmic reticulum (ER) is the major site for protein folding in the cell. One important function is the formation of disulfide bonds that can be catalyzed by the enzyme protein disulfide isomerase (PDI). During oxidative protein folding and regeneration of PDI, ROS can be generated. Additionally, ROS can be produced through NOX4 which can be associated with the ER membrane. Moreover, electron leakage through the microsomal monooxygenase system contributes to ROS generation in the ER [23].

6

Furthermore, enzymes like xanthine oxidase, cyclooxygenases or cytochrome P450 (CYP450) enzymes can produce ROS. However, their contribution to redox signaling is yet to be determined [15, 20].

2.2.2 Antioxidant systems

Cells express various antioxidant molecules and enzymes to balance ROS levels. The most abundant non-enzymatic antioxidant is glutathione (GSH) [24, 25]. GSH is a tripeptide consisting of L-glutamate, L-cysteine and glycine. It is generated by a two-step mechanism that is catalyzed by γ-glutamyl-cysteine synthase and glutathione synthase [26]. GSH is synthesized in the cytoplasm, but can be transported across membranes and can also pass the plasma membrane [24, 27, 28]. GSH can act as a cofactor for antioxidant enzymes like glutathione peroxidases (GPXs) [25]. Furthermore, it can directly react with and thus scavenge free radicals and regenerate oxidized vitamin C and E [24, 25, 29]. Additionally, GSH can react with sulphenic acid groups in oxidized proteins and form S-glutathionylated proteins. These groups cannot be further oxidized, thus preventing irreversible protein oxidation. Reduction of S-glutathionylated proteins is achieved through glutathione reductase, glutaredoxin (Grx) and thioredoxin (Trx) [25]. Reduction of glutathione disulfide (GSSG) is catalyzed by glutathione reductase with NADPH as a cofactor [26].

Besides GSH, other non-enzymatic antioxidants are the free radical scavenger vitamin C (ascorbate) and fat-soluble vitamin E (α-Tocopherol) that is a lipid hydroperoxide scavenger [30, 31].

An important antioxidant enzyme is catalase that metabolizes H_2O_2 to water and molecular oxygen. Mammalian catalases are large homotetramers with each subunit containing heme as a prosthetic group [32]. The main cellular compartment that contains catalase is the peroxisome [33].

The Trx system is a major enzymatic antioxidant system in the cell. The thioredoxin superfamily shares a characteristic active site motif (Cys-Gly-Pro-Cys) that is conserved in all kingdoms of life [34, 35]. This motif is located in a well described thioredoxin fold and can be found in, but is not limited to, Trxs, Grxs, glutathione transferases and GPXs [36]. Trxs catalyze the reduction of protein disulfides via a dithiol-disulfide exchange reaction (Figure 2) [37, 38]. This reaction is thermodynamically favored as oxidized Trx is more stable than reduced Trx [37]. Furthermore, the pK_a value of the N-terminal cysteine of the active site motif is relatively low facilitating a nucleophilic attack on the target disulfide [37, 39]. There are two Trx isoforms expressed in mammals. These are Trx1, which is cytosolic, but can be translocated into the

nucleus and can also be secreted, and the mitochondrial isoform Trx2 [34]. Oxidized Trxs can be reduced in an NADPH-dependent reaction that is catalyzed by thioredoxin reductases (TrxRs).
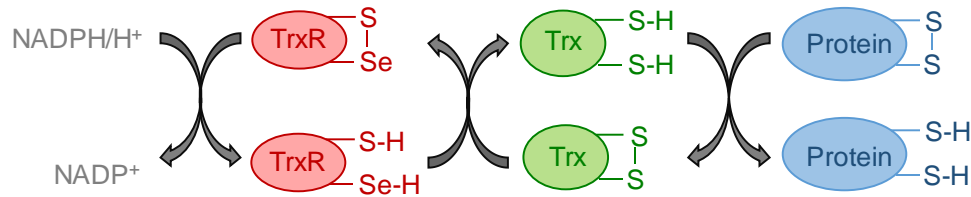
Figure 2: Schematic overview of the catalytic cycle of the thioredoxin (Trx) system. Trx can catalyze the reduction of oxidized proteins through a dithiol-disulfide exchange reaction. Oxidized Trx can be reduced by thioredoxin reductase (TrxR) in an NADPH-dependent reaction (Figure adapted from [40]).

Mammals express three TrxR isoforms: cytosolic and nuclear TrxR1, mitochondrial TrxR2 and testis-specific TrxR3 or thioredoxin glutathione reductase (TGR) [36, 38]. Human TrxRs are pyridine nucleotide-disulfide oxidoreductases that form homodimers and contain two redox active sites. The N-terminal catalytic site is located in the FAD binding domain, whereas the other active site is on the C-terminus of the enzyme and contains a selenocysteine [38]. The selenol group of selenocysteine is more reactive than the thiol group of cysteine due to its lower pK_a value making selenocysteine essential for TrxR function, as replacement with cysteine reduces TrxR activity [38, 41, 42]. Interestingly, knock-out of TrxR1 or TrxR2 in mice is embryonically lethal, further highlighting the importance of the Trx system [43, 44].

One function of the Trx system is the reduction of oxidized peroxiredoxins (PRDXs). PRDXs are thiol peroxidases that are widely expressed in the cell and react with H_2O_2, peroxynitrite and hydroperoxides [45]. PRDXs are actually thought to react with most of the H_2O_2 in the cell as their reactivity towards H_2O_2 is much higher compared to other thiol proteins [46, 47]. This makes PRDX a suitable candidate for relaying oxidizing equivalents from H_2O_2 to target proteins [47]. There are six different PRDXs expressed in mammals of which PRDX1-4 are the typical 2-Cys PRDXs that form disulfide linked homodimers upon oxidation. These have different cellular localizations with PRDX1 and PRDX2 residing in the cytoplasm, PRDX3 in the mitochondria and PRDX4 in the ER [45].

Glutaredoxins (Grxs) contain, as described above, a Trx motif in their active center and act as disulfide reductases that can even compensate for some functions of Trx [36, 48]. The main function of Grxs, however, is the reduction of S-glutathionylated proteins [48]. There are three Grxs expressed in mammalian cells with Grx1 being located in the cytoplasm and Grx2 and

8

Grx5 in the mitochondria [36]. In general, oxidized Grxs are reduced by GSH, but Grx2 can also be reduced by TrxR [36, 48].

GPXs, as mentioned above, are a family of enzymes that can reduce H_2O_2, lipid hydroperoxides and soluble hydroperoxides using GSH as a cofactor. Several of these enzymes have, like TrxRs, a selenocysteine in their active center. GPX1 is the most abundant GPX family member and is localized in the cytoplasm, mitochondria and, depending on the cell type, in peroxisomes [49]. Another isoform, GPX4, is also broadly expressed and can be found in several cellular compartments and also bound to membranes, where it preferentially reduces membrane-associated phospholipids [49, 50]. GPX4 is an essential enzyme to counter lipid peroxidation and ferroptosis [51, 52].

2.2.3 Redox signaling in healthy and malignant cells

ROS, although first thought to cause mainly harmful oxidation of cellular macromolecules, are now recognized as important signaling molecules that are important for several cellular pathways [25]. As described above, H_2O_2 has several properties that make it a good second messenger. These include its cellular half-life and its ability to cross membranes and to target specific amino acid residues in proteins.

2.2.3.1 Redox control of cellular signaling

The most sensitive residue for oxidation by H_2O_2 is cysteine [15]. Cysteine contains a thiol group with a polarizable sulfur atom, whose reactivity is increased in the deprotonated form [53]. The thiol can be oxidized to sulfenic acid which can undergo further reactions with either other cysteines, yielding an intra- or intermolecular disulfide, or with a nitrogen of a backbone amide forming a cyclic sulfonamide, or with GSH forming a glutathione disulfide. All these cysteine modifications are reversible and can be reduced by the GSH and Trx antioxidant systems [15]. Higher levels of H_2O_2, however, can further oxidize sulfenic acid to sulfinic and sulfonic acid, which cannot easily be reduced by the cellular reductants [15, 53]. Indeed, reduction of sulfinic acid can only be catalyzed by certain enzymes like sulphiredoxin in an ATP-dependent reaction, which is especially important for the reduction of higher-order oxidation of PRDXs [54, 55]. Not all cysteine residues are oxidized by H_2O_2, with the reactivity of the thiol depending on its pK_a as determined by nearby electron-withdrawing residues or

positive charges [56]. This makes thiol oxidation a specific and selective posttranslational modification [16].

Besides cysteine, the thioether group of methionine can be oxidized by H_2O_2 to methionine sulphoxide. The reaction kinetics for this oxidation however are less favorable and seem unlikely in the regulation of protein function *in vivo* [16].

Proteins that can be regulated by cysteine oxidation are certain phosphatases like protein tyrosine phosphatases (PTPs). Oxidation of cysteines in their active center can reversibly inhibit their activity [57]. This has been shown for different PTPs, one of which is PTP1B that dephosphorylates the epidermal growth factor (EGF) receptor (EGFR). Production of H_2O_2 is stimulated upon EGF signaling and subsequent inactivation of PTP1B increases EGFR phosphorylation and prolongs its activation [58, 59]. Another growth factor-associated phosphatase, SHP-2, is likewise inhibited by receptor-induced H_2O_2 signaling that leads to maintained platelet-derived growth factor (PDGF) receptor signaling and downstream mitogen-activated protein kinase (MAPK) activation [57]. Another phosphatase, the tumor suppressor phosphatase and tensin homolog (PTEN) can also be inhibited by oxidation, which subsequently leads to activation of phosphoinositide 3-kinase (PI3K) [60]. Therefore, redox signaling can maintain the activity of several signaling cascades that induce cellular growth, proliferation and survival.

Additionally, transcription factors can be activated by redox signaling. These are, for example, the forkhead box protein O (FOXO) family of transcription factors that regulate cellular homeostasis and can also upregulate the transcription of genes encoding antioxidant proteins. On the one hand, FOXO activity is regulated by upstream signaling, for example via PI3K that can be influenced by redox signaling. Furthermore, FOXOs themselves can be targets of oxidative modifications, e.g. through disulfide-linked covalent binding of co-regulators like CREB-binding protein (CBP) [61-63].

Another transcription factor that is activated upon oxidative stress is NF-E2-related factor 2 (NRF2), albeit not through direct oxidation. Under normoxic conditions, NRF2 is located in the cytosol in a complex with Kelch-like ECH-associated protein 1 (KEAP1) that together with Cullin 3 (CUL3) marks it for proteasomal degradation. Oxidation of KEAP1, however, reduces the E3 ubiquitin ligase activity of KEAP1/CUL3. This stabilizes NRF2, which can then translocate into the nucleus and induce transcription of genes under control of the Antioxidant Response Element (ARE) increasing antioxidant defenses. Thereby KEAP1/NRF2 acts as a redox sensor that plays an important role in balancing cellular ROS levels and protein oxidation [64-66].

Furthermore, stress signaling by p53 can be modified by oxidative stress, both via redox modifications of upstream effectors like Ataxia-telangiectasia mutated (ATM) and extracellular signal-regulated kinase (ERK), and by targeting p53 itself by S-glutathionylation of certain cysteine residues [67, 68]. How oxidative modifications alter the function of p53 is only incompletely understood, however, oxidation of cysteines in the DNA-binding region can affect binding to and regulation of certain target genes [69]. p53 can also induce antioxidant pathways by regulating the transcription of genes that are involved in redox homeostasis, e.g. TP53-inducible glycolysis and apoptosis regulator (TIGAR). TIGAR can promote glucose flux via the pentose phosphate pathway (PPP) thereby increasing NADPH levels and antioxidant capacity [70, 71]. Other antioxidant p53 target genes are GPX1, NRF2, aldehyde dehydrogenease 4 (ALDH4) and glutaminase 2 (GLS2) [72]. However, p53 also has pro-oxidant roles under conditions that favor apoptosis or senescence. p53 can induce the expression of p53-induced gene 3 (PIG3, quinone oxidoreductase) and PIG6 (proline oxidase) that promote ROS production [73-75]. Furthermore, p53 can inactivate glucose-6-phosphate dehydrogenase (G6PDH) and thereby limit flux through the PPP and NADPH production [76]. Overall, p53 has a dual role in ROS signaling that can either promote cell survival or cell death [72].

2.2.3.2 ROS in cancer development and progression

Interestingly, cancer cells were found to have increased ROS levels [13, 77, 78]. It is hypothesized that this increase in cellular ROS contributes to tumor progression and metastasis [78, 79]. High ROS levels can induce DNA damage that leads to cancer-promoting mutations and genetic instability [80]. Furthermore, high ROS levels were found to promote metastasis [81, 82] and can also act on the tumor microenvironment [83, 84].

Several characteristics of tumor cells contribute to the observed increase in ROS. For instance, activation of oncogenes like RAS or c-Myc could induce ROS levels [21, 85]. Oncogenic RAS signaling thereby induces superoxide production through NOXs [86, 87]. Loss of p53 function, as can be observed in many cancers, can alter cellular redox balance as expression of several antioxidant genes is controlled by p53 as outlined above [72]. Additionally, mutations in mitochondrial DNA have been correlated with higher ROS levels in cancer cells likely through increased electron leakage of the ETC [81, 88]. This could induce a vicious cycle with high ROS levels inducing further DNA damage leading to further ROS production [89]. There are also extrinsic factors that contribute to the increase in ROS levels in cancer cells. Inflammatory cytokines that are, for example, secreted by tumor-associated macrophages can also induce ROS production in cancer cells [90]. Another factor contributing to increased ROS levels is hypoxia. The cellular response to hypoxia includes superoxide production at mitochondrial

complex III that is needed for stabilization of hypoxia-inducible factor (HIF) [91]. Furthermore, HIF-mediated upregulation of growth factors and growth factor receptors can increase ROS levels through activation of NOXs [25].

Interestingly, protein levels of ROS scavenging enzymes like GPX, SOD or PRDXs are elevated in cancer cells, likely as an adaptive strategy to deal with the increase in ROS [21, 25]. Additionally, metabolic reprogramming of tumor cells induces NADPH production that increases cellular antioxidant capacity [92, 93]. Thereby cancer cells can maintain high ROS levels without the irreversible oxidation of macromolecules and induction of cell death. Furthermore, this increase in antioxidants is also associated with the development of resistance to chemotherapeutic treatments [94, 95].

2.2.4 Inhibitors of antioxidant systems

As outlined above, cancer cells show a disturbed redox homeostasis and benefit from increased ROS levels. However, due to their high amount of oxidants, they rely strongly on antioxidant enzymes. Treatments that inhibit those antioxidant systems and thereby increase ROS to harmful levels could be a way to target cancer cells specifically. The toxicity to healthy cells should be much lower due to their higher antioxidant capacity that keeps ROS levels below a harmful threshold (Figure 3) [13, 21].
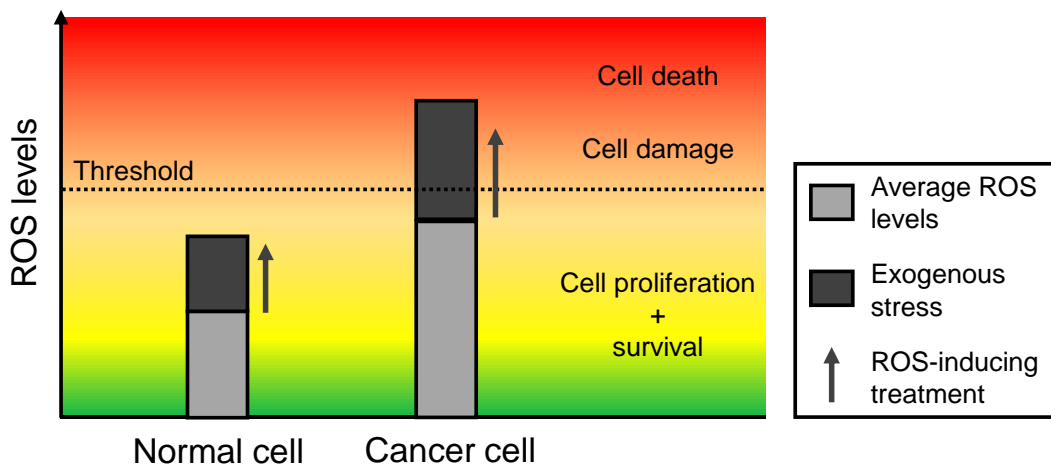
Figure 3: Schematic depiction of ROS levels in normal and malignant cells. Under physiological conditions normal cells maintain lower ROS levels than cancer cells. Upon ROS-inducing treatment, these ROS levels can be kept below a toxic threshold due to the cell's antioxidant capacity. Due to their higher basal ROS levels, cancer cells cannot cope with such exogenous stress as well, leading to an increase in ROS levels above a critical threshold and induction of cell death (Figure adapted from [13, 21]).

Several inhibitors of the GSH and the Trx antioxidant systems have been shown to limit growth and induce cell death in different cancer types [69]. In this study we focused on two inhibitors of the Trx system, Auranofin and PX-12, which will be described in more detail in the following.

2.2.4.1 Auranofin

Auranofin (2,3,4,6-tetra-*o*-acetyl-1-thio-β-D-glucopyranosato-S-(triethyl-phosphine) gold(I)) is an orally active, lipid soluble gold(I)-phosphine-thiolate complex that was initially employed as a treatment for rheumatoid arthritis [96, 97] (Figure 4). The phosphine and thiolate ligands stabilize the central gold(I) atom that shows high affinity for thiols and selenium ligands [96, 98]. The phosphine ligand additionally confers membrane permeability [99].
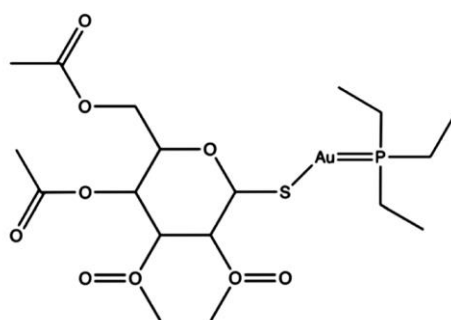
Figure 4. Chemical structure of Auranofin. Auranofin is an organic gold compound that is a potent TrxR inhibitor (Figure adapted from [100]).

Auranofin potently inhibits cytosolic and mitochondrial TrxR by targeting the selenocysteine in its active center [101, 102]. It was shown that Auranofin treatment induced a disturbance of the redox homoestasis, mitochondrial membrane permeabilization and apoptosis [103, 104]. Additionally, Auranofin was shown to inhibit proteasome-associated deubiquitinases [105]. Several studies could demonstrate anti-tumor activity of Auranofin *in vitro* and in *vivo* [106-111]. Furthermore, Auranofin has been examined in clinical trials for chronic lymphocytic leukemia, ovarian and lung cancer (NCT01419691, NCT01747798, NCT01737502).

2.2.4.2 PX-12

PX-12 (first described as Compound IV-2) is a 2-imidazolyl disulfide that irreversibly inhibits Trx1 by thioalkylating a critical cysteine residue [112] (Figure 5).
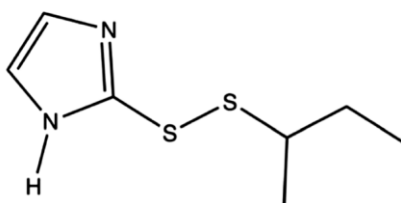
Figure 5. Chemical structure of PX-12. PX-12 is a small molecule inhibitor of Trx1 that induces cell death in several cancer cell lines (Figure adapted from [100]).

PX-12 treatment reduced the growth of several cancer cell lines, including hepatocellular carcinoma [113], colorectal carcinoma [114], multiple myeloma [115], cervical adenocarcinoma [116] and prostate cancer [117]. Additionally, PX-12 treatment impaired colony formation of primary T-cell ALL [118]. Treatment with PX-12 was shown to increase ROS levels and lead to GSH depletion *in vitro* [116]. PX-12 monotherapy has also been assessed in phase I and II clinical trials in patients with advanced solid tumors (NCT00736372, NCT00417287) [119-122]. In general, the toxicity profile of PX-12 was low and levels of circulating Trx1 were decreased, however, no significant antitumor activity was observed so far [119-121].

2.3 Programmed cell death

Programmed cell death can be found throughout the animal kingdom and plays important roles in the development of organisms, tissue homeostasis and in the response to intracellular or extracellular stresses [123]. Programmed cell death is different from accidental cell death upon physical damage or chemical insults as it is initiated upon certain molecular signaling events that lead the recruitment and activation of specialized enzymes. These pathways are tightly regulated to prevent accidental activation that could be harmful for the organism [123, 124]. However, these signaling cascades present interesting targets for pharmacological modulation in pathologies where programmed cell death is either inhibited (e.g. cancer, autoimmunity) or increased (e.g. diabetes, neurodegenerative diseases) [123, 125]. There are several types of programmed cell death that differ in their morphological, biochemical and functional properties. The most characterized form of programmed cell death is apoptosis that can be activated either extrinsically or intrinsically and will be described in more detail below. Common morphological features of apoptosis include chromatin condensation and DNA fragmentation, cytoplasmic shrinkage and blebbing of the plasma membrane and, finally, formation of "apoptotic bodies"

that can be taken up by phagocytic cells [123, 126, 127]. In the last years several other types of regulated cell death have been characterized that include, but are not limited to, necroptosis, ferroptosis, autophagic cell death and pyroptosis [123].

2.3.1 Extrinsic apoptosis

Extrinsic apoptosis is initiated when a ligand binds to its cognate receptor on the cell surface. These receptors include FAS (also known as CD95) and several members of the tumor necrosis factor (TNF) receptor family like TNF receptor 1 (TNFR1), TRAILR1 (also known as DR4) and TRAILR2 (also known as DR5) [123, 128]. Most death receptor ligands belong to the TNF superfamily and include, for example, TNFα, FAS ligand (CD95L) and TRAIL. Binding of these ligands to their respective receptors can induce apoptotic cell death in a matter of hours [128].

Signaling through FAS or TRAIL receptors induces receptor trimerization. The adaptor protein Fas-associated with death domain (FADD) can bind to these activated receptors via its death domain (DD) leading to the formation of the death inducing signaling complex (DISC) with the recruitment of caspase-8. Caspase-8 molecules can form homodimers via their death effector domain (DED) which leads to their activation through autoproteolytic cleavage [123].

Binding of TNFα to TNFR1, however, leads to the association of TNFR-associated death domain (TRADD) and formation of complex I that consists of TNFR-associated factor 2 (TRAF2), cellular inhibitor of apoptosis proteins (cIAP) 1 and 2 and receptor interacting protein kinase 1 (RIPK1) (Figure 6). Signaling through this complex can activate NF-κB and cellular survival. However, deubiquitination of RIPK1 by cylindromatosis (CYLD) leads to the formation of cytosolic complex II consisting of RIPK1, RIPK3, FADD, cFLIP and caspase-8. Subsequently caspase-8 is activated leading to cleavage of RIPK1 and RIPK3 [123, 129].
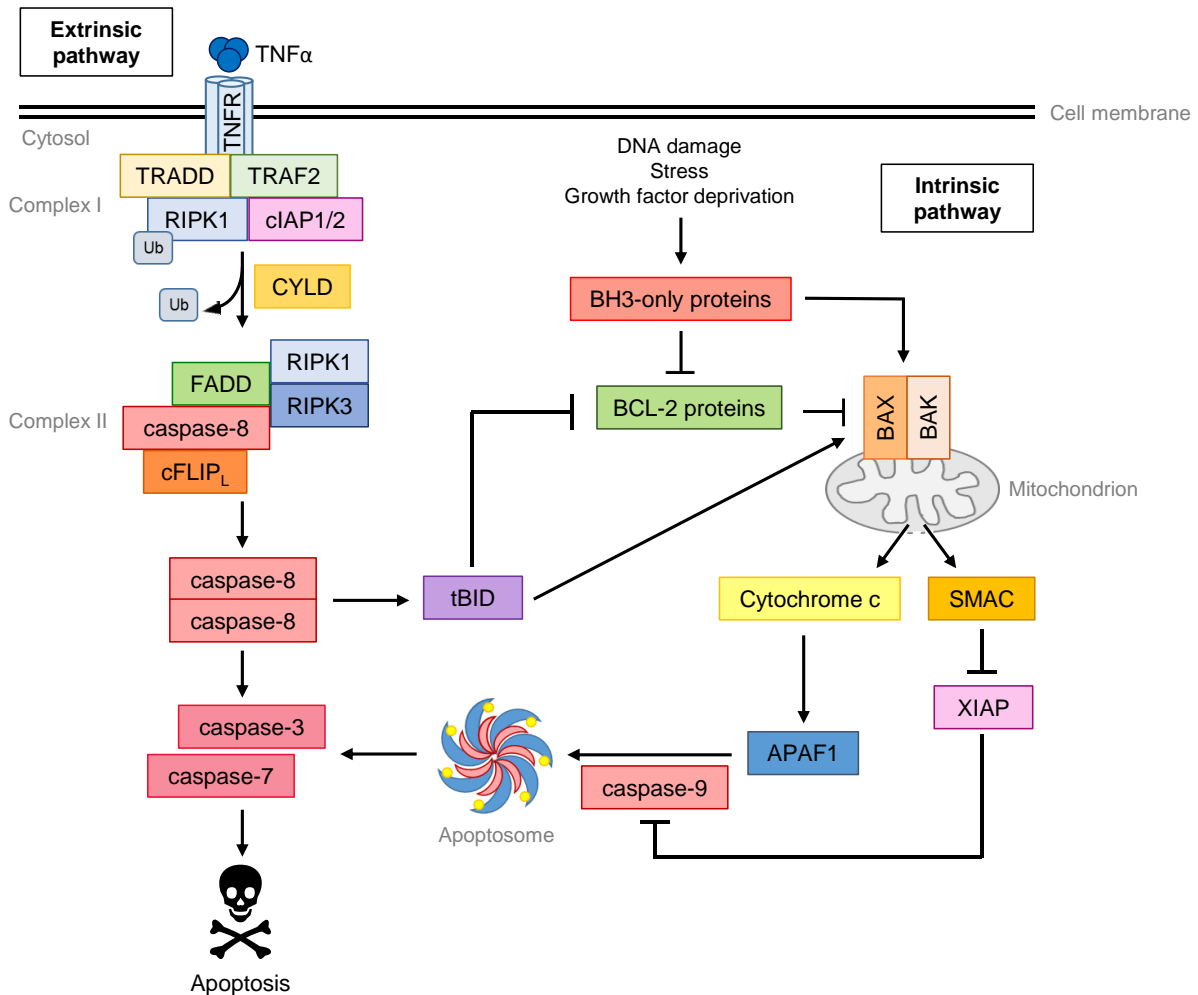
Figure 6. Schematic overview of the extrinsic and intrinsic pathway of apoptosis. Extrinsic apoptosis can be initiated by binding of TNFα to the TNF receptor which leads to the formation of complex I. Deubiquitination of RIPK1 can lead to the formation of complex II that acts as a platform for caspase-8 activation. Intracellular stresses can induce intrinsic apoptosis by shifting the balance between pro- and anti-apoptotic BCL-2 family proteins and activation of BAX and BAK. BAX and BAK can form oligomers at the outer mitochondrial membrane causing the release of the pro-apoptogenic factors cytochrome c and SMAC. Cytochrome c can interact with APAF1 and together with caspase-9 form the aptoptosome complex that induces caspase-9 activation. Activated caspase-8 or -9 can cleave and activate caspase-3 and -7 leading to apoptosis induction. Cross-talk between the extrinsic and the intrinsic pathway via tBID can amplify this signaling cascade (Figure modified from [130, 131]).

Activation of caspase-8, either via the DISC or complex II, leads to the cleavage and activation of the executioner caspases-3 and -7 that drive proteolytic cleavage of defined target proteins culminating in apoptotic cell death. Caspases are cysteine proteases that cleave proteins after Asp residues [132]. Caspase targets include inhibitor of caspase-activated DNase (ICAD) that inhibits caspase-activated DNase (CAD). Upon ICAD cleavage, CAD can dimerize and lead to internucleosomal DNA fragmentation [133, 134]. Another caspase target is poly(ADP-ribose) polymerase (PARP) that synthesizes poly(ADP-ribose) at sites of DNA damage [133, 135]. Furthermore, externalization of phosphatidylserine (PS) is promoted by caspases as they can activate scramblases that mediate PS exposure and inactivate flippases that induce PS

internalization [136, 137]. PS exposure on the plasma membrane can act as an "eat me" signal for phagocytic cells promoting the uptake of apoptotic cells [123, 127, 138]. There is also cross-talk between the extrinsic and the intrinsic pathway of apoptosis. Interestingly, caspase-8 can cleave the pro-apoptotic B cell lymphoma 2 (BCL-2) family protein BCL-2 homology (BH) 3-interacting domain death agonist (BID). This truncated BID (tBID) can activate BCL-2 antagonist/killer (BAK) and BCL-2-associated X protein (BAX) at the mitochondrial membrane or bind to anti-apoptotic BCL-2 family members, thus amplifying the death signal mediated by the extrinsic pathway [133, 139].

2.3.2 Intrinsic apoptosis

Intrinsic apoptosis can be initiated upon a variety of different stresses. These include, among others, DNA damage, growth factor withdrawal, ER stress, oxidative stress and cell cycle defects [123, 140-142]. An important feature of intrinsic apoptosis is mitochondrial outer membrane permeabilization (MOMP) that leads to the release of apoptogenic factors like cytochrome c and second mitochondrial activator of caspase (SMAC) into the cytosol (Figure 6). Cytosolic cytochrome c then binds to apoptotic peptidase activating factor 1 (APAF1) and pro-caspase-9 to form the apoptosome. This complex formation subsequently triggers autocatalytic cleavage and activation of caspase-9. Mature caspase-9 can cleave and activate effector caspases-3 and -7 leading to apoptosis as described in section 2.3.1. The release of SMAC from the mitochondrial intermembrane space further enhances apoptosis induction, as it can bind to X-linked inhibitor of apoptosis (XIAP). Free XIAP is a caspase-antagonist that inhibits caspase activity through direct sequestration. Therefore, SMAC release contributes to caspase activation [123, 143].

Initiation of intrinsic apoptosis is largely controlled by BCL-2 family proteins that can interact with each other via their BH domains. This protein family consists of anti-apoptotic BCL-2 proteins, pro-apoptotic effector BCL-2 proteins and pro-apoptotic BH3-only proteins. Under normal conditions anti-apoptotic BCL-2 proteins antagonize their pro-apoptotic family members and prevent apoptosis induction. However, when the cell faces various stresses, BH3-only proteins can be upregulated. These proteins can then sequester anti-apoptotic BCL-2 proteins leading to the release of pro-apoptotic effectors and MOMP [139].

Anti-apoptotic BCL-2 family members are BCL-2, BCL-2-like protein 1 (BCL-X_L), myeloid cell leukemia 1 (MCL-1), BCL-2-like protein 2 (BCL-W) and BCL-2-related protein A1 (BCL2A1). All of these pro-survival proteins, except BCL2A1, share four BH domains [123]. The pro-apoptotic effector proteins BAK and BAX also contain four BH domains and mediate MOMP

by forming pores in the outer mitochondrial membrane (OMM) [139]. BAK is predominantly localized in the OMM with its hydrophobic tail anchoring it in the membrane. BAX, however, mainly resides in the cytosol. Upon apoptotic signaling, its transmembrane domain becomes accessible and BAX inserts into the OMM [139, 144-146]. BAX, and to some extent also BAK, can be retro-translocated from the OMM to the cytosol by anti-apoptotic BCL-2 proteins, for example by BCL-X$_L$ [147, 148]. Anti-apoptotic BCL-2 proteins can bind to the BH3 domain of activated effector proteins. Activated BAX can be bound by all anti-apoptotic BCL-2 proteins, whereas binding of activated BAK is restricted to BCL-X$_L$ and MCL-1 [149, 150]. Pro-apoptotic BH3-only proteins include BCL-2-interacting mediator of cell death (BIM), BID, p53 upregulated modulator of apoptosis (PUMA), NOXA, BCL-2 antagonist of cell death (BAD) and BCL-2-modifying factor (BMF). These proteins only contain the BH3 domain. There is some selectivity concerning binding of the BH3-only proteins to the pro-survival BCL-2 proteins. BAD preferentially binds to BCL-2, BCL-X$_L$ and BCL-W, whereas NOXA favorably interacts with MCL-1 and BCL2A1. BIM, PUMA and tBID can sequester all pro-survival BCL-2 proteins [150, 151]. Some BH3-only proteins, like tBID and BIM, so called "activators", can directly bind and activate BAK and BAX, whereas other members, like BAD or BMF, only interact with anti-apoptotic BCL-2 proteins. These proteins are therefore referred to as "sensitizers", as they block anti-apoptotic proteins, which can inhibit the activation of BAK and BAX [123, 152, 153]. Binding of the BH3-only activators induces conformational changes in BAK and BAX, leading to their unfolding, release of the pro-apoptotic activators and exposure of the BH3 domain [154-156]. Binding of pro-survival BCL-2 proteins to this exposed BH3 domain inhibits apoptosis. However, if the pro-survival proteins are sequestered by BH3-only proteins, BAK and BAX can form homodimers, which are essential for the formation of higher order oligomers that induce MOMP [139, 157-159]. Interestingly, BH3-only proteins are not essential for activation of BAK and BAX, as cells that do not express BH3-only proteins can die via intrinsic apoptosis. In the absence of pro-survival BCL-2 proteins, BAX and BAK can self-activate, albeit with slow kinetics [160, 161].

Higher order oligomer and pore formation of BAK and BAX is still incompletely understood. Several pore forming models exist that suggest complicated oligomeric structures and also the involvement of lipids. Super-resolution microscopy could recently demonstrate rings and arc-like structures of activated BAX in mitochondria [139, 162-164].

The role of BCL2-related ovarian killer (BOK), a protein that shares its domain structure with the BCL-2 effector proteins BAK and BAX, in apoptosis is not clear [143]. BOK can induce MOMP in the absence of BAK and BAX, however, BAK and BAX can compensate for its loss [165-167].

2.3.3 ROS and programmed cell death

Low ROS levels, as described above, can play important roles in cellular signaling, but also in the regulation of programmed cell death. ROS and oxidative stress can lead to the induction, mediation or execution of different cell death programs in the cell.

ROS play a major role in ferroptosis, an iron-dependent form of programmed cell death [168]. The main feature of ferroptosis is the accumulation of toxic lipid peroxides that can be inhibited by ROS scavengers like vitamin E. Ferroptosis can be triggered by GSH depleting agents or inhibitors of GPX4, which reduces lipid peroxides in a GSH-dependent reaction [169].

Moreover, oxidative stress can induce intrinsic apoptosis, for example by inducing mtDNA damage [170, 171]. Loss of cytochrome c after MOMP can further increase ROS levels as it disrupts the ETC [172]. Additionally, ROS can activate apoptosis signal-regulating kinase 1 (ASK-1), which is usually kept in its inactive conformation by binding to Trx1. Upon increased ROS, Trx1 is oxidized and ASK-1 is released resulting in the activation of its targets c-Jun N-terminal kinase (JNK) and MAPK p38 [173, 174]. JNK can induce an inhibitory phosphorylation of anti-apoptotic BCL-2 which favors induction of intrinsic apoptosis [175, 176]. Activation of death receptor signaling and apoptosis can also be promoted by NOX-mediated ROS formation, which is triggered upon binding of FAS or TNFα to their receptors [177-179]. Additionally, ROS can lead to the upregulation of death receptors like TRAILR2 [180].

Severe oxidative stress can also lead to mitochondrial permeability transition (MPT)-driven necrosis [123]. MPT-driven necrosis is induced upon opening of the MPT pore (MPTP) complex that is formed at junctions between the IMM and the OMM. Its structure, composition and mode of action is still under debate with cyclophilin D (CYPD) being the only protein whose involvement in the MPTP is widely accepted. Opening of the MPTP leads to rapid loss of the mitochondrial membrane potential, osmotic swelling and breakdown of mitochondrial membranes and cell death [123, 130]. Interestingly, BCL-2 proteins can also interact with the MPTP [181, 182]

Necroptosis induction and execution can also be influenced by ROS. Necroptosis can be initiated by certain death receptors or pathogen recognition receptors that lead to the activation of RIPK1, which under circumstances of caspase inhibition, can activate RIPK3 upon formation of the necrosome complex. Activated RIPK3 can then phosphorylate the pseudokinase mixed lineage kinase domain-like (MLKL) leading to its oligomerization and translocation to the plasma membrane, where it can trigger plasma membrane permeabilization [123, 130, 183]. Interestingly, mitochondrial ROS have been shown to promote necroptosis through the stabilization of the necrosome complex [184, 185]. Indeed, oxidation of three cysteine residues

in RIPK1 has been shown to promote RIPK1 autophosphorylation and necroptosis induction [186].

Furthermore, ROS have been implicated in the induction of parthanatos and lysosome-dependent cell death [123].

3 Aim of the study

ALL is the most common malignancy in children and adolescents under the age of 20 [2]. The overall survival rate has improved favorably over the last years, however, novel treatment options are still needed to limit toxicity and improve outcome for high risk groups and patients with recurrent disease [3].

The aim of this study was to determine the potential of compounds that increase oxidative stress for ALL therapy. Additionally, we aimed to explore the role of ROS and subsequent protein oxidation in the regulation of programmed cell death. We focused on inhibitors of the thioredoxin system as it has been shown that Trx1 is upregulated in ALL [118] and that Auranofin could sensitize ALL cell lines to SMAC mimetic-induced cell death [187].

In the first part of the study, we wanted to analyze whether the Trx1 inhibitor PX-12 could induce cell death in ALL cell lines. We aimed to further characterize the events leading to cell death induction and we were especially interested to understand the role of ROS and protein oxidation in this treatment.

Next, we wanted to analyze global protein oxidation upon inhibition of the Trx system and used Auranofin, an inhibitor of TrxR that was previously shown to induce ROS and cell death in different cancer entities including ALL [109, 187-189]. After characterizing cell death and ROS induction in our system, we wanted to employ an unbiased, mass spectrometry-based approach to identify novel target proteins whose oxidation state is influenced by Auranofin treatment and that could potentially contribute to cell death induction.

In the third part of the study, we aimed to further understand the contribution of BAK in ROS-mediated cell death as we could demonstrate the importance of BAK in PX-12- and Auranofin-induced cell death in the previous parts. We were especially interested whether BAK is oxidized upon Auranofin treatment, as earlier findings of our group could show BAK oxidation upon necroptosis induction [190]. Next, we wanted to analyze if BAK oxidation is critical for cell death induction upon oxidative stress and whether changes in its oxidation state could influence its function or its protein-protein interactions.

4 Materials and Methods

4.1 Materials

4.1.1 Cell lines

All human cell lines were authenticated by STR profiling at Leibniz Institute, German Collection of Microorganisms and Cell culture (Deutsche Sammlung von Mikroorganismen und Zellkulturen (DSMZ)). All cell lines were continuously monitored for mycoplasma contamination using polymerase chain reaction (PCR).

4.1.1.1 Human cell lines

Table 1: Human cell lines

Cell line	Type	Source
Jurkat FADD$^{-/-}$ (Jurkat FD)	Human T-cell leukemia	kindly provided by J. Blenis [191]
KOPN-8	Human B-cell precursor leukemia	DSMZ
Phoenix-AMPHO	2nd generation retrovirus-producing cell line	ATCC
REH	Human B-cell precursor leukemia	DSMZ

4.1.1.2 Murine cell lines

Table 2: Murine cell lines

Cell line	Type	Source
MEF WT	Murine embryonic fibroblasts	kindly provided by A. Letai
MEF BAK$^{-/-}$	Murine embryonic fibroblasts	kindly provided by A. Letai

MEF BAK$^{-/-}$ cell lines expressing mRuby2-BAK were generated by retroviral transduction and selection using Hygromycin B for 14 days after which monoclonal cell lines were established.

Transgene expression was regularly monitored by Western blotting and fluorescence microscopy.

4.1.1.3 Stable overexpression cell lines

Table 3: Stable overexpression cell lines

Cell line	Transgene	Vector source
MEF BAK$^{-/-}$	mRuby2-BAK-WT	kindly provided by B. T. Kile [192]
MEF BAK$^{-/-}$	mRuby2-BAK-C14S	Site-directed mutagenesis
MEF BAK$^{-/-}$	mRuby2-BAK-C154S	Site-directed mutagenesis
MEF BAK$^{-/-}$	mRuby2-BAK-C14S-C154S	Site-directed mutagenesis
MEF BAK$^{-/-}$	mRuby2-BAK-I79T	Site-directed mutagenesis
MEF BAK$^{-/-}$	mRuby2-BAK-D81G	Site-directed mutagenesis

4.1.2 Cell culture reagents

Table 4: Cell culture reagents

Reagent	Supplier
4-(2-hydroxyethyl)-1-piperazineethanesulfonic acid (HEPES)	Life Technologies, Darmstadt, Germany
Dulbecco's Modified Eagle Medium (DMEM) GlutaMAX^{TM}	Life Technologies, Darmstadt, Germany
Fetal calf serum (FCS)	Life Technologies, Darmstadt, Germany
Hygromycin B	Carl Roth, Karlsruhe, Germany
Penicillin/Streptomycin (10000 U/ml)	Life Technologies, Darmstadt, Germany
Roswell Park Memorial Institute Medium (RPMI) 1640 GlutaMAX^{TM}	Life Technologies, Darmstadt, Germany
RPMI 1640 [-] Phenol Red	Life Technologies, Darmstadt, Germany
Sodium Pyruvate	Life Technologies, Darmstadt, Germany
Trypan blue solution, 0.4 %	Life Technologies, Darmstadt, Germany
Trypsin/EDTA solution (0.05 %), phenol red	Life Technologies, Darmstadt, Germany

4.1.3 Drugs, inhibitors and ROS scavengers

Table 5: Drugs

Reagent	Supplier
Auranofin	Santa Cruz Biotechnology, Santa Cruz, CA, USA
Etoposide	TEVA GmbH, Ulm, Germany
PX-12	Sigma Aldrich, Darmstadt, Germany

Table 6: Inhibitors

Reagent	Supplier
Dabrafenib (Dab)	Selleckchem, Houston, TX, USA
GSK'872 (GSK)	Merck, Darmstadt, Germany
N-benzyloxycarbonyl-Val-Ala-Asp(O-Me)fluoromethylketone (zVAD.fmk)	Bachem, Heidelberg, Germany
Necrostatin-1s (Nec-1s)	Calbiochem, Darmstadt, Germany

Table 7: Antioxidants and ROS scavengers

Reagent	Supplier
α-Tocopherol (α-Toc)	Sigma-Aldrich, Darmstadt, Germany
Butylated hydroyanisole (BHA)	Sigma-Aldrich, Darmstadt, Germany
N-acetylcysteine (NAC)	Sigma-Aldrich, Darmstadt, Germany
Mn(III)tetrakis(4-benzoic acid)porphyrin chloride (MnTBAP)	Calbiochem, Darmstadt, Germany
tert-Butylhydroquinone (Tbhq)	Sigma-Aldrich, Darmstadt, Germany

4.1.4 Fluorescent dyes

Table 8: Fluorescent dyes

Reagent	Supplier
BODIPY 581/591-C11 (BODIPY)	Thermo Fisher Scientfic, Waltham, MA, USA
CM-H2DCFDA (H2DCF)	Thermo Fisher Scientfic, Waltham, MA, USA
Hoechst 33342	Thermo Fisher Scientfic, Waltham, MA, USA

Reagent	Supplier
MitoSOX™ Red	Thermo Fisher Scientfic, Waltham, MA, USA
Propidium iodide (PI)	Sigma-Aldrich, Darmstadt, Germany
SYTOX™ Green Nucleic Acid Stain	Thermo Fisher Scientfic, Waltham, MA, USA

4.1.5 Antibodies

4.1.5.1 Primary antibodies for Western blotting

Primary antibodies for Western blotting were diluted in 2 % BSA in PBS-T.

Table 9: Primary antibodies for Western blotting

Antibody	Species	Dilution	Supplier
anti-APIP	rabbit	1:1000	Thermo Fisher Scientific, Waltham, MA, USA
anti-β-Actin	mouse	1:5000	Sigma-Aldrich, Darmstadt, Germany
anti-BAK (NT)	rabbit	1:1000	Merck, Darmstadt, Germany
anti-BAX (NT)	rabbit	1:1000	Cell Signaling, Beverly, MA, USA
anti-caspase-3	rabbit	1:1000	Cell Signaling, Beverly, MA, USA
anti-caspase-9	rabbit	1:1000	Cell Signaling, Beverly, MA, USA
anti-GAPDH	mouse	1:5000	Hytest, Turku, Finland
anti-MFF	rabbit	1:1000	Cell Signaling, Beverly, MA, USA
anti-NOXA	mouse	1:1000	Enzo, Lörrach, Germany
anti-PRDX3	rabbit	1:1000	Abfrontier, Seoul, South Korea
anti-PRMT1	mouse	1:1000	Santa Cruz Biotechnology, Santa Cruz, CA, USA
anti-Vinculin	mouse	1:2000	Merck, Darmstadt, Germany
anti-VTI1A	mouse	1:1000	Santa Cruz Biotechnology, Santa Cruz, CA, USA

4.1.5.2 Secondary antibodies for Western blotting

Secondary antibodies for Western blotting were diluted in 5 % milk in PBS-T.

Table 10: Secondary antibodies for Western blotting

Antibody	Species	Dilution	Supplier
HRP-conjugated anti-mouse-IgG	goat	1:10000	Abcam, Cambridge, UK
HRP-conjugated anti-rabbit-IgG	goat	1:10000	Abcam, Cambridge, UK

4.1.5.3 Antibodies for immunoprecipitation

Table 11: Antibodies for immunoprecipitation

Antibody	Species	Amount	Supplier
anti-BAK clone AB-1	mouse	4 µg	Calbiochem, Darmstadt, Germany

4.1.5.4 Antibodies for immunofluorescence

Antibodies for immunofluorescence were diluted in 5 % BSA in PBS.

Table 12: Antibodies for immunofluorescence

Antibody	Species	Dilution	Supplier
anti-TOMM20	rabbit	1:200	Proteintech, Manchester, UK
Cy2 anti-rabbit	donkey	1:500	Jackson ImmunoResearch, Baltimore, PA, USA

4.1.6 Plasmids

Table 13: Plasmids

Vector backbone	Transgene	Source
pMSCV-Hygromycin	mRuby2-BAK-WT	kindly provided by B. T. Kile [192]
pMSCV-Hygromycin	mRuby2-BAK-C14S	Site-directed mutagenesis
pMSCV-Hygromycin	mRuby2-BAK-C154S	Site-directed mutagenesis
pMSCV-Hygromycin	mRuby2-BAK-C14S-C154S	Site-directed mutagenesis
pMSCV-Hygromycin	mRuby2-BAK-I79T	Site-directed mutagenesis
pMSCV-Hygromycin	mRuby2-BAK-D81G	Site-directed mutagenesis

4.1.7 Primer

4.1.7.1 Mutagenesis Primer

Table 14: Mutagenesis Primer

Primer	Sequence (5' → 3')
BAK-C14S-fwd	CCGAAGGTGGGCAGCGATGAGTCCC
BAK-C14S-rev	GGGACTCATCGCTGCCCACCTTCGG
BAK-C154S-fwd	CCTGGGCCAGGTGACCAGCTTTTTGGCTGATATC
BAK-C154S-rev	GATATCAGCCAAAAAGCTGGTCACCTGGCCCAGG
BAK-I79T-fwd	GGCAGCTTGCTCTCACCGGAGATGATATTAAC
BAK-I79T-rev	GTTAATATCATCTCCGGTGAGAGCAAGCTGCC
BAK-D81G-fwd	GCTCTCATCGGAGGCGATATTAACCGGCG
BAK-D81G-rev	CGCCGGTTAATATCGCCTCCGATGAGAGC

4.1.7.2 Sequencing Primer

Table 15: Sequencing Primer

Primer	Sequence (5' → 3')
IRES-rev	GCTCGTCAAGAAGACAGG
mRuby2-fwd	GTATCCATGCCGTTGATCACCG
MSCV-fwd	GAACCTCCTCGTTCGAC

4.1.8 Small-interfering RNAs

All small-interfering RNAs (siRNAs) were purchased from Thermo Fisher Scientific (Waltham, MA, USA) as Silencer® Select siRNA.

Table 16: Small-interfering RNAs (siRNAs)

siRNA	Sequence code	Target	Concentration
siBAK #1	s18880	BAK	100 nM
siBAK #2	s1881	BAK	100 nM
siCtrl	4390843	non-targeting control	80-100 nM

siRNA	Sequence code	Target	Concentration
siNOXA #1	s10708	NOXA	80 nM
siNOXA #2	s10709	NOXA	80 nM
siNOXA #3	s10710	NOXA	80 nM

4.1.9 Reagents and kits

Table 17: Reagents and kits

Reagents/Kits	Supplier
Ampicillin	Carl Roth, Karlsruhe, Germany
CellTiterGlo® Luminescent Cell Viability Assay	Promega, Mannheim, Germany
cOmplete Protease Inhibitor Cocktail (PIC, 25x)	Roche Diagnostics, Mannheim, Germany
cOmplete Protease Inhibitor Cocktail (PIC), EDTA free (25x)	Roche Diagnostics, Mannheim, Germany
DH5α competent E.coli	Thermo Fisher Scientfic, Waltham, MA, USA
DMSO (for PCR)	New England Biolabs, Frankfurt, Germany
Dynabeads™ anti-mouse IgG	Life Technologies, Darmstadt, Germany
EZ-Link™ Iodoacetyl-PEG2-Biotin (BIAM)	Thermo Fisher Scientfic, Waltham, MA, USA
FACS Clean/Rinse Solution	BD Bioscience, Heidelberg, Germany
FACS Flow Sheath Fluid	BD Bioscience, Heidelberg, Germany
FACS Shutdown Solution	BD Bioscience, Heidelberg, Germany
FastDigest™ DpnI	Thermo Fisher Scientfic, Waltham, MA, USA
GeneElute PCR clean-up Kit	Sigma-Aldrich, Darmstadt, Germany
GeneJet Plasmid Miniprep Kit	Thermo Fisher Scientfic, Waltham, MA, USA
Glycerol	Carl Roth, Karlsruhe, Germany
Lipofectamine 2000	Life Technologies, Darmstadt, Germany
Neon® Transfection System 100 μl Kit	Thermo Fisher Scientfic, Waltham, MA, USA
Nuclease-free water	Thermo Fisher Scientfic, Waltham, MA, USA
OptiMEM transfection medium	Thermo Fisher Scientfic, Waltham, MA, USA
PageRuler™ Plus Prestained Protein Ladder	Thermo Fisher Scientfic, Waltham, MA, USA
peqGOLD Gel Extraction Kit	Peqlab, Erlangen, Germany
Phusion polymerase Kit	New England Biolabs, Frankfurt, Germany
Pierce™ BCA Protein Assay	Thermo Fisher Scientfic, Waltham, MA, USA

Reagents/Kits	Supplier
Pierce™ ECL Western Blotting Substrate	Thermo Fisher Scientfic, Waltham, MA, USA
Pierce™ High Capacity Streptavidin Agarose	Thermo Fisher Scientfic, Waltham, MA, USA
PureLink™ HiPure Plasmid Maxiprep Kit	Thermo Fisher Scientfic, Waltham, MA, USA
RFP-Trap® Magnetic Agarose	Chromotek, Planegg-Martinsried, Germany
ROENTEROLL HC X-Ray Developer	Tetenal, Norderstadt, Germany
S.O.C Medium	Life Technologies, Darmstadt, Germany
SUPERFIX MRP X-Ray Fixer	Tetenal, Norderstadt, Germany
TE Buffer	Thermo Fisher Scientfic, Waltham, MA, USA
Thioredoxin Activity Fluorescent Assay Kit	IMCO, Stockholm, Sweden

4.1.10 Chemicals

Table 18: Chemicals

Reagent	Supplier
2-propanol	Carl Roth, Karlsruhe, Germany
Acetone	Carl Roth, Karlsruhe, Germany
Acetonitrile	Sigma-Aldrich, Darmstadt, Germany
Acrylamide mix, 30 % (Rotiphorese)	Carl Roth, Karlsruhe, Germany
Agar	Carl Roth, Karlsruhe, Germany
Albumin fraction V (BSA)	Carl Roth, Karlsruhe, Germany
Ammonium persulfate (APS)	Carl Roth, Karlsruhe, Germany
Ampicillin	Carl Roth, Karlsruhe, Germany
β-Glycerophosphate	Sigma-Aldrich, Darmstadt, Germany
Bromophenolblue	Carl Roth, Karlsruhe, Germany
Chloroacetamide	Sigma-Aldrich, Darmstadt, Germany
Cholamidopropyldimethyl ammonio propane sulfonate (CHAPS)	Sigma-Aldrich, Darmstadt, Germany
Dithiothreitol (DTT)	Millipore, Darmstadt, Germany
Dimethyl sulfoxide (DMSO)	Sigma-Aldrich, Darmstadt, Germany
Disodium phosphate (Na_2HPO_4)	Carl Roth, Karlsruhe, Germany
Ethanol	Carl Roth, Karlsruhe, Germany
Ethylene diamine tetraacetic acid (EDTA)	Carl Roth, Karlsruhe, Germany
Formic acid	Sigma-Aldrich, Darmstadt, Germany

Reagent	Supplier
Guanidinium chloride (GdmCl)	Sigma-Aldrich, Darmstadt, Germany
Glycerol	Carl Roth, Karlsruhe, Germany
Glycine	Carl Roth, Karlsruhe, Germany
HEPES	Carl Roth, Karlsruhe, Germany
Hexadimethrine bromide (polybrene)	Carl Roth, Karlsruhe, Germany
Hydrochloric acid (HCl)	Carl Roth, Karlsruhe, Germany
Hydrogen peroxide (H_2O_2, 30 %)	Carl Roth, Karlsruhe, Germany
LB medium	Carl Roth, Karlsruhe, Germany
Magnesium chloride ($MgCl_2$)	Carl Roth, Karlsruhe, Germany
Methanol	Carl Roth, Karlsruhe, Germany
Milk powder	Carl Roth, Karlsruhe, Germany
N-ethylmaleimide (NEM)	Sigma-Aldrich, Darmstadt, Germany
NP-40	Carl Roth, Karlsruhe, Germany
Paraformaldehyde	Sigma-Aldrich, Darmstadt, Germany
Phenylmethylsulfonyl fluoride (PMSF)	Carl Roth, Karlsruhe, Germany
Potassium chloride (KCl)	Carl Roth, Karlsruhe, Germany
Potassium dihydrogen phosphate (KH_2PO_4)	Carl Roth, Karlsruhe, Germany
ReproSil C18 resin	Dr. Maisch HPLC GmbH, Ammerbruch-Entringen, Germany
Sodium chloride (NaCl)	Carl Roth, Karlsruhe, Germany
Sodium dodecyl sulfate (SDS)	Carl Roth, Karlsruhe, Germany
Sodium fluoride	Sigma-Aldrich, Darmstadt, Germany
Sodium hydroxide (NaOH)	Carl Roth, Karlsruhe, Germany
Sodium orthovanadate	Sigma-Aldrich, Darmstadt, Germany
Urea	Carl Roth, Karlsruhe, Germany
Tetramethylethylendiamine (TEMED)	Carl Roth, Karlsruhe, Germany
Trichloroacetic acid (TCA)	Carl Roth, Karlsruhe Germany
Triethanolamine	Carl Roth, Karlsruhe, Germany
Trifluoroacetic acid	Sigma-Aldrich, Darmstadt, Germany
Tris(2-carboxyethyl)phosphine (TCEP)	Sigma-Aldrich, Darmstadt, Germany
Tris Base	Carl Roth, Karlsruhe, Germany
Tris HCl	Carl Roth, Karlsruhe, Germany
Triton X-100	Carl Roth, Karlsruhe, Germany

Reagent	Supplier
Trypsin (sequencing grade)	Promega, Mannheim, Germany
Tween20	Carl Roth, Karlsruhe, Germany

4.1.11 Buffers

Table 19: Buffers

Buffer	Ingredients
BIAM-resolution buffer (pH 8.5)	50 mM Tris HCl, 8 M Urea, 5 mM EDTA, 0.5 % SDS, 20 mg/ml BIAM
Blocking buffer	5 % milk powder in PBS-T
Blotting buffer	5.8 g/l Tris Base, 2.9 g/l glycine, 0.04 % SDS, 20 % methanol
CHAPS lysis buffer (pH 7.4)	10 mM HEPES, 150 mM NaCl, 1 % CHAPS, 1x PIC
DTT-resolution buffer (pH 8.5)	50 mM Tris HCl, 8 M Urea, 5 mM EDTA, 0.5 % SDS, 4 mM DTT
NEM-resolution buffer (pH 8.5)	50 mM Tris HCl, 8 M Urea, 5 mM EDTA, 0.5 % SDS, 25 mM NEM
NP-40 lysis buffer (pH 7.5)	10 mM Tris HCl, 150 mM NaCl, 0.5 mM EDTA, 0.5 % NP-40, 0.5 mM PMSF, 1x PIC
Phosphate buffered saline (PBS, 10x, pH 7.4)	80 g/l NaCl, 2 g/l KCl, 2 g/l KH_2PO_4, 14.4 g/l Na_2HPO_4
PBS-Tween (PBS-T)	1x PBS, 0.1 % Tween20
Resuspension buffer (pH 8.5)	50 mM Tris HCl, 5 mM EDTA, 1 % Triton X-100, 1 % SDS, 1x PIC

Buffer	Ingredients
RFP-Trap® washing buffer (pH 7.5)	10 mM Tris HCl, 150 mM NaCl, 0.5 mM EDTA
SDS Loading buffer (6x) (pH 6.8)	350 mM Tris Base, 3.8 % glycerol, 10 % SDS, 0.093 g/ml DTT, 0.12 mg/ml bromophenolblue
SDS Loading buffer, non-reducing (6x) (pH 6.8)	350 mM Tris Base, 3.8 % glycerol, 10 % SDS, 0.12 mg/ml bromophenolblue
SDS Running buffer (5x)	15.1 g/l Tris Base, 94 g/l glycine, 0.5 % SDS
Triethanolamine (TEA) buffer (pH 8.2)	0.2 M Triethanolamine in ddH$_2$O
Triton X-100 lysis buffer	30 mM TrisHCl, 150 mM NaCl, 10 % glycerol, 1 % Triton X-100, 0.5 mM PMSF, 2 mM DTT, 1x PIC

4.1.12 Consumables

Table 20: Consumables

Consumable	Supplier
Aluminium foil	Carl Roth, Karlsruhe, Germany
Cell culture dishes (6 cm, 10 cm, 14.5 cm)	Greiner Bio-One, Frickenhausen, Germany
Cell culture flasks (25 cm^2, 75 cm^2, 175 cm^2)	Greiner Bio-One, Frickenhausen, Germany
Cell culture plates, transparent (96-well, 48-well, 24-well, 6-well)	Greiner Bio-One, Frickenhausen, Germany
Cell culture plates, black, clear bottom (96-well)	Greiner Bio-One, Frickenhausen, Germany
Cell culture plates, white (96-well)	Greiner Bio-One, Frickenhausen, Germany
Cell scraper	BD Bioscience, Heidelberg, Germany
Combitips, all sizes	Eppendorf, Hamburg, Germany
Centrifuge tubes (15 ml, 50 ml)	Greiner Bio-One, Frickenhausen, Germany
Cryogenic vials (1.8 ml)	Starlab, Hamburg, Germany
Disposal bags	Carl Roth, Karlsruhe, Germany
Filter tips, all sizes	Starlab, Hamburg, Germany

Consumable	Supplier
Filters, sterile (0.45 µM)	Merck Millipore, Darmstadt, Germany
Hybond ECL nitrocellulose membrane	GE Healthcare, Buckinghamshire, UK
Hyperfilm ECL	GE Healthcare, Buckinghamshire, UK
Microcentrifuge tubes (0.5 ml, 1.5 ml, 2 ml)	Starlab, Hamburg, Germany
Nitrile gloves	Starlab, Hamburg, Germany
Parafilm	VWE, Deisenhofen, Germany
Pasteur pipettes (15 cm, 30 cm)	Carl Roth, Karlsruhe, Germany
PCR tubes	Starlab, Hamburg, Germany
Picotip Emitter Tip (Ø 100 µm, 15 cm)	New Objective, Woburn, MA, USA
Pipette tips, all sizes	Starlab, Hamburg, Germany
Round-bottom tubes	BD Bioscience, Heidelberg, Germany
Scalpels	B. Braun, Melsungen, Germany
Syringes (2 ml, 5 ml, 10 ml)	B. Braun, Melsungen, Germany
Whatman paper	Thermo Fisher Scientific, Waltham, MA, USA

4.1.13 Equipment

Table 21: Equipment

Equipment	Supplier
Autoclave V-15	Systec, Pforzheim, Germany
Avanti J-26 XP ultracentrifuge	Beckman Coulter, Krefeld, Germany
C18 reversed-phase precolumn	Thermo Fisher Scientific, Waltham, MA, USA
Centrifuge MIKRO 200 R	Hettich, Baden-Baden, Germany
Centrifuge ROTIXA 50 RS	Hettich, Baden-Baden, Germany
Centrifuge ROTANTA 460 R	Hettich, Baden-Baden, Germany
CO_2 incubator MCO-19AIC	Sanyo, Wehr, Germany
Dionex™ UltiMate™ 3000	Thermo Fisher Scientific, Waltham, MA, USA
Easypet© 3	Eppendorf, Hamburg, Germany
Electronic analytical balance EW	Kern, Balingen, Germany
Electronic analytical balance 770	Kern, Balingen, Germany
FACS Canto II	BD Bioscience, Heidelberg, Germany
Freezer (-20°C)	Ewald Innovationstechnik, Bad Nenndorf, Germany

Equipment	Supplier
Freezer (-80°C)	Sanyo, Wehr, Germany
Fridge (4°C)	Ewald Innovationstechnik, Bad Nenndorf, Germany
Glass plates for SDS-PAGE	Bio-Rad, München, Germany
Heating block	Eppendorf, Hamburg, Germany
Heating magnetic stirrer ARE	VELP scientifica, Usmate, Italy
HeraSafe class II biological safety cabinet	Kendro, Langenselbold, Germany
ImageXpress micro XLS system	Molecular devices, Sunnyvale, CA, USA
Infinite M100 microplate reader	Tecan, Crailsheim, Germany
Innova 4230 bacteria shaker	New Bruinswick Scientific, Edison, NJ, USA
Inolab© pH7310 pH meter	WTW, Weilheim, Germany
Magnetic rack	AMS Biotechnology, Abington, UK
Mastercycler® pro	Eppendorf, Hamburg, Germany
Microcentrifuge	Benning, Bocholt, Germany
Microscope CKX41	Olympus, Hamburg, Germany
Mini-PROTEAN Tetra cell electrophoresis system	Bio-Rad, München, Germany
Multipipette© plus	Eppendorf, Hamburg, Germany
Nalgene® Mr Frosty freezing container	Sigma-Aldrich, Darmstadt, Germany
NanoDrop 1000 spectrophotometer	Peqlab, Erlangen, Germany
Nanospray Flex™ Ion source	Thermo Fisher Scientific, Waltham, MA, USA
Neon Transfection System	Thermo Fisher Scientific, Waltham, MA, USA
Neubauer improved counting chamber	Carl Roth, Karlsruhe, Germany
Pipette Research plus (2.5 µl, 10 µl, 100 µl, 200 µl, 1000 µl)	Eppendorf, Hamburg, Germany
PerfectBlue™ Dual Gel Twin L electrophoresis system	Peqlab, Erlangen, Germany
PowerPac™ Universal power supply	Bio-Rad, München, Germany
Q Exactive™ Plus Mass Spectrometer	Thermo Fisher Scientific, Waltham, MA, USA
Rocking Shaker	MS-L, Wiesloch, Germany
Roller mixer	Ratek, Victoria, Australia
Spinning wheel	MS-L, Wiesloch, Germany
Thermomixer comfort	Eppendorf, Hamburg, Germany
Trans-Blot© SD Semi-Dry Transfer Cell	Bio-Rad, München, Germany

Equipment	Supplier
Vacuum Pump HLC	Ditabis, Pforzheim, Germany
Vortex mixer ZX classic	VELP scientifica, Usmate, Italy
Water bath SWB20	Medingen, Arnsdorf, Germany
X-Ray cassette type G	Rego X-Ray, Augsburg, Germany

4.1.14 Software

Table 22: Software

Software	Company/Institute
Benchling	Benchling, San Francisco, CA, USA
EndNote (X7.4)	Thomson Reuters, Toronto, Canada
FACSDiva™ (6.1.3)	BD Bioscience, Heidelberg, Germany
Gorilla Gene Ontology Enrichment Analysis and Visualization Tool	Multi Knowledge Project [193]
GraphPad Prism® (8.3.1)	GraphPad Software, San Diego, CA, USA
ImageJ (1.52e)	National Institute of Health, Bethesda, MD, USA
Magellan Data Analysis (7.2)	Tecan, Crailsheim, Germany
MaxQuant (1.5.3.30/1.6.1.0)	Max-Planck-Institute of Biochemistry [194]
MetaXpress© (6.5.1.347)	Molecular Devices, Sunnyvale, CA, USA
Microsoft Office 2013	Microsoft, Redmond, WA, USA
NanoDrop Software (3.8.1)	Peqlab, Erlangen, Germany
Perseus (1.5.6.0/1.6.1.3)	Max-Planck-Institute of Biochemistry [195]
REVIGO	Rudjer Boskovic Institute, Zagreb, Croatia [196]
Tecan i-control™ (1.10)	Tecan, Crailsheim, Germany
Xcalibur™ Software	Thermo Fisher Scientific, Waltham, MA, USA

4.2 Methods

4.2.1 Cell culture

4.2.1.1 Cultivation of cells

All cell lines were cultivated in a humidified atmosphere at 37 °C with 5 % carbon dioxide (CO_2) in recommended medium. Cells were cultured for 30 passages.

Human ALL cell lines (Jurkat FD, KOPN-8, REH) were cultured in RPMI 1640 GlutaMAX™ supplemented with 10 % FCS, 1 mM sodium pyruvate, 25 mM HEPES and 1 % penicillin/streptomycin. Cells were passaged twice weekly at a ratio of 1:3 to 1:8 depending on the cell line. For passaging, the appropriate amount of cell suspension was added to a new flask with fresh medium.

MEF cell lines were cultured in DMEM GlutaMAX™ supplemented with 10 % FCS, 1 mM sodium pyruvate and 1 % penicillin/streptomycin. Cells were passaged three times per week at a ratio of 1:15. For passaging, the medium was aspirated and the cells were washed with pre-warmed PBS. For detachment, Trypsin/EDTA was added and the cells were incubated for 5 min at 37 °C and 5 % CO_2. After cells were detached, Trypsin/EDTA activity was blocked by addition of medium and the appropriate amount of cell suspension was added to a new flask with fresh medium.

Phoenix-AMPHO cells were cultured in DMEM GlutaMAX™ supplemented with 10 % FCS and 1 % penicillin/streptomycin. Cells were passaged twice weekly at a ratio of 1:10. For passaging, the medium was aspirated, cells were washed with pre-warmed PBS and Trypsin/EDTA was added. Cells were then incubated at 37 °C and 5 % CO_2 for 5 min. After detachment of the cells, medium was added to block Trypsin/EDTA activity and the appropriate amount of cell suspension was added to a new flask containing fresh medium.

4.2.1.2 Freezing and thawing of cells

For freezing, cells were centrifuged for 5 min at 1800 rpm at room temperature (RT). The medium was discarded and cells were resuspended in FCS supplemented with 10 % DMSO. The cell suspension was transferred into cryogenic vials and frozen overnight in a Mr. Frosty

freezing container at -80 °C. For long-term storage, cells were kept in a liquid nitrogen tank at -196 °C.

For thawing, vials were quickly defrosted in a water bath at 37 °C. The cell suspension was transferred into 10 ml pre-warmed medium and centrifuged for 5 min at 1800 rpm at RT to remove residual DMSO. Cells were then resuspended in fresh medium and transferred into culture flasks.

4.2.1.3 Seeding and treatment of cells

For all experiments, cells were seeded in an appropriate density for treatment that would not lead to overgrowth by the end of the experiment. To ensure comparable cell numbers, cells were counted prior to seeding. ALL cells were resuspended and MEFs and Phoenix-AMPHO cells were detached using Trypsin/EDTA as described above and resuspended in 10 ml medium. For counting, 20 µl cell suspension was added to 60 µl Trypan Blue solution. Cells were counted using a Neubauer improved cell counting chamber, dead cells were excluded and the number of cells/ml was calculated. The appropriate volume of cell suspension was then added to fresh medium and seeded in the desired culture plates or flasks.

ALL cells were seeded in 96-well plates (100 µl), 48-well plates (250 µl), 24-well plates (500 µl), 6-well plates (3 ml) or 25 cm^2 flasks (10 ml) at a density of 2×10^5/ml (Jurkat FD, KOPN-8) or 3×10^5/ml (REH) depending on the experiment and treated on the day of seeding. For pre-treatment with cell death inhibitors or ROS scavengers, the substances were added to the cells 1 h before the treatment substances were added.

MEFs were seeded at a density of 0.1×10^5/cm^2 one day before treatment in 96-well plates, 24-well plates, 6-well plates, 10 cm dishes or 15 cm dishes. On the day of treatment, the medium was discarded and fresh medium containing the pre-treatment or the treatment was added to the cells. Pre-treatment was performed for 1 h before the treatment substances were added.

Phoenix-AMPHO cells were seeded at a density of 0.5×10^5/cm^2 in 6-well plates one day before transfection.

4.2.2 Generation of stable cell lines by retroviral transduction

4.2.2.1 Site-directed mutagenesis of pMSCV-Hygromycin-mRuby2-BAK-WT

Point mutations in the mRuby2-BAK-WT sequence encoded on the retroviral expression plasmid pMSCV-Hygromycin were introduced using site-directed mutagenesis. For double mutants, the mutations were performed successively. First, the plasmid DNA was amplified in a PCR with the mutagenesis primers listed in Table 14 containing the target mutation. The PCR was performed using the Phusion polymerase Kit according to manufacturer's instruction with the following settings (Table 23):

Table 23: PCR cycle settings for site-directed mutagenesis of pMSCV-Hygromycin-mRuby2-BAK-WT

Step	Temperature	Time	Number of cycles
Initial denaturation	98 °C	2 min	1
Denaturation	98 °C	10 sec	
Annealing	72 °C	5 min	25
Extension			
Final Extension	72 °C	10 min	1
Hold	4 °C	∞	

Afterwards, the template plasmid was digested using the FastDigest™ DpnI restriction enzyme for 20 min at 37 °C. The PCR product was purified using the GeneElute PCR clean-up Kit according to manufacturer's instructions. Subsequently, DNA concentration of the purified PCR product was determined using a NanoDrop 100 spectrophotometer. The PCR product was then transformed into DH5α competent E.coli using heat shock. In brief, cells were thawed on ice, 100-200 ng of the PCR product was added to the bacteria and incubated for 30 min on ice. Afterwards, the heat shock was performed for 30 sec at 42 °C after which the bacteria were incubated on ice for 2 min. 200 µl pre-warmed S.O.C medium was added and the bacteria were grown for 1 h at 37 °C with shaking. Subsequently, 50 µl of the bacteria solution were plated onto LB plates containing 100 µg/ml Ampicillin and grown overnight at 37 °C. On the next day, single colonies were picked and grown overnight in 3 ml LB medium containing 100 µg/ml Ampicillin in a shaking incubator at 37 °C. Plasmid DNA was extracted from 1 ml of the pre-culture using the GeneJet Plasmid Miniprep Kit according to manufacturer's instructions. To ensure successful mutation, purified plasmid DNA was sequenced using Sanger sequencing. The appropriate primers are listed in Table 15. Sanger sequencing was performed by LGC Genomics, Berlin, Germany. Bacterial cultures expressing the correct

plasmid were expanded by addition of 1 ml pre-culture to 250 ml LB medium containing 100 µg/ml Ampicillin and incubated in a shaking incubator overnight at 37 °C. Plasmid DNA was extracted using the PureLink™ HiPure Plasmid Maxiprep Kit according to manufacturer's instructions.

4.2.2.2 Production of retroviral particles

For production of retroviral particles, the packaging cell line Phoenix-AMPHO was transfected with plasmid DNA using Lipofectamine 2000 transfection reagent according to manufacturer's instructions. In short, 3 µg of plasmid DNA was diluted in 150 µl OptiMEM and mixed with 12 µl Lipofectamine in 150 µl OptiMEM and incubated for 5 min at RT. The DNA-Lipofectamine mix was added drop-wise to the cells, which were then incubated for 24 h at 37 °C and 5 % CO_2, after which the medium was changed. Medium containing retroviral particles was harvested 48 and 72 h post transfection, sterile-filtered and either used directly for transduction or snap frozen in liquid nitrogen and stored at -80 °C.

4.2.2.3 Retroviral transduction, selection and single clone expansion

Stable cell lines expressing mRuby2-BAK-WT and mutant BAK were generated by transduction with retroviral particles. MEF BAK$^{-/-}$ cells were seeded in 6-well plates 24 h before transduction. On the day of transduction, the growth medium was discarded and replaced with 1 ml viral supernatant, 1 ml serum-free medium and 8 µg/ml polybrene. Cells were incubated for 2 h at 37 °C and 5 % CO_2, after which 2 ml medium with FCS was added. Three days after transduction, cells were transferred into a 10 cm dish with fresh medium containing 500 µg/ml Hygromycin B. Selection of cells was performed for 2 weeks with the parental cell line as selection control. For establishment of monoclonal cell lines, transduced and selected cells were detached from the plate, serial diluted and single cells seeded in 96-well plates. Cell lines were expanded and expression of the transgene was confirmed by Western blotting and immunofluorescence microscopy.

4.2.3 RNA interference

Silencer® Select siRNAs and the Neon® Transfection system were used for transient gene silencing in Jurkat FD cells. For each siRNA, 2 x 10^6 cells were washed with pre-warmed PBS and resuspended in 120 µl Resuspension Buffer. 80 or 100 nM siRNA was added and electroporation was performed according to manufacturer's instruction with 1200 V, 2 ms, 2 pulses. After electroporation, cells were transferred into a 6-well plate with 3 ml antibiotic-free medium. 24 h after electroporation 5 ml full medium was added. Cells were seeded for experiments 48 h after transduction and knock-down (KD) efficiency was analyzed by Western blotting.

4.2.4 Determination of cell death

4.2.4.1 Forward/Side scatter analysis

Cell death of ALL cells was determined by forward scatter (FSC) and side scatter (SSC) analysis using flow cytometry. FSC measures the size of the cell, while SSC determines their granularity. Dying cells can be distinguished from the living population as they become smaller and more granular resulting in a lower FSC and higher SSC. For FSC/SSC analysis cells were treated, transferred into round bottom tubes and directly analyzed by flow cytometry.

4.2.4.2 Microscope-based determination of cell death

Cell death of MEFs was analyzed using PI/Hoechst 33342 or Sytox^{TM} Green/Hoechst 33342 co-staining and fluorescence microscopy. PI and Sytox^{TM} Green dyes are not membrane-permeable and therefore do not stain living cells, in contrast to Hoechst 33342. Therefore, co-staining can be used to analyze the percentage of PI positive cells or Sytox^{TM} Green-positive cells (i.e. dead cells) to Hoechst 33342 positive cells (i.e. all cells). Treated cells were stained with 1 µg/ml PI, Sytox^{TM} Green or Hoechst 33342 diluted in PBS and incubated for 5 min at 37 °C and 5 % CO_2. PI, Sytox^{TM} Green and Hoechst 33342 signal was measured using the ImageXpress® Micro XLS system with the 4x objective and the TRITC, FITC or DAPI channel, respectively, according to manufacturer's instructions. To quantify PI, Sytox^{TM} Green or Hoechst 33342 positive cells, the "Cell Scoring" tool of the MetaXpress® software was employed.

4.2.5 Determination of cell viability

Cell viability was assessed using the CellTiterGlo® Luminescent Cell Viability Assay according to manufacturer's instructions. In brief, cells were seeded in white 96-well plates and treated as specified. 5 µl CellTiterGlo® reagent was added to each well and the cells were incubated for 10 min at RT. Absorbance at 490 nm was measured using the Infinite M100 microplate reader. Absorbance was normalized to control samples and shown as percentage of control.

4.2.6 Determination of ROS production and lipid peroxidation

For determination of ROS levels, cells were stained with the fluorescent dyes H_2DCF, a general oxidative stress indicator, MitoSOX^{TM}, a mitochondrial superoxide indicator and BODIPY, an indicator for lipid peroxidation, according to manufacturer's instructions using the FACSCanto II flow cytometer. Detection of ROS was performed at time points at which cell death did not exceed 30 % as determined by FSC/SSC analysis. In brief, cells were seeded in 24-well plates and treated as specified.

For detection of ROS in ALL cells, cells were transferred into round bottom tubes and centrifuged for 5 min at 1800 rpm at RT. Medium was discarded and the cells resuspended in 100 µl Phenol Red-free RPMI with 5 µM H_2DCF or BODIPY for 30 min or 5 µM MitoSOX for 10 min at 37 °C in the dark. Afterwards, cells were stored on ice and immediately analyzed by flow cytometry using the FITC (H_2DCF) or PE channel (MitoSOX) gating on the living population using the FSC and SSC.

For detection of ROS in MEFs, medium was discarded and cells were incubated with 100 µl Phenol Red-free RPMI with 5 µM H_2DCF or BODIPY for 30 min or 5 µM MitoSOX for 10 min at 37 °C in the dark. Cells were detached using Trypsin/EDTA, washed once with PBS and resuspended in Phenol Red-free RPMI before immediate analysis by flow cytometry using the FITC (H_2DCF, BODIPY) or PE channel (MitoSOX) gating on the living population using the FSC and SSC.

4.2.7 Determination of Trx activity

Trx activity was analyzed using the Thioredoxin Activity Fluorescent Assay Kit according to manufacturer's instructions. In brief, cells were treated as specified and harvested by

centrifugation for 5 min at 1800 rpm and 4 °C. Cells were washed once with PBS, resuspended in TE Buffer supplemented with EDTA-free PIC and lysed by sonication. Cell debris was removed by centrifugation for 25 min at 14,000 rpm and 4 °C. The supernatants were collected and protein concentration was determined using the Pierce™ BCA Protein Assay Kit according to manufacturer's instructions. 30 µg protein was incubated with 10 µl eosin-labeled insulin and fluorescence intensity was recorded at 545 nm after excitation at 520 nm for 60 min at RT using the Infinite M100 fluorescence plate reader. Increase in fluorescence over time (Δfluorescence/time) was calculated from the linear range of the curves and background corrected.

4.2.8 Immunofluorescence microscopy

For immunofluorescence staining, cells were seeded in black, clear bottom 96-well plates. Medium was discarded and cells were washed with PBS and fixed with 3.7 % paraformaldehyde for 5 min. Cells were washed three times with PBS and permeabilized with 0.1 % Triton X-100 in PBS for 10 min. Cells were incubated with primary antibodies in 5 % BSA in PBS for 2 h at RT. After washing three times with PBS, cells were incubated with fluorescently-labeled secondary antibodies and DAPI (1:5000) in 5 % BSA in PBS for 1 h at RT. Cells were washed three times with PBS and imaged using the ImageXpress® Micro XLS system with the 60x objective and the DAPI, FITC (Cy2) or Texas Red (mRuby2) channel. Image formatting was performed using ImageJ.

4.2.9 Western Blot analysis

4.2.9.1 Protein extraction

For protein extraction of ALL cells, cells were treated as specified and the cell suspension was centrifuged for 5 min at 1800 rpm and 4 °C after which cells were washed twice with ice-cold PBS. For harvesting of MEFs, cells were treated as indicated, the medium was discarded and ice-cold PBS was added. Cells were scraped off the plate using a cell scraper and centrifuged for 5 min at 1800 rpm and 4 °C.

Lysis of ALL cells and MEFs was performed similarly by washing them with PBS and resuspending the cell pellet in Triton X-100 lysis buffer supplemented with phosphatase inhibitors sodium orthovanadate (1 mM), β-glycerophosphate (1 mM) and sodium fluoride

(5 mM). Cells were incubated on ice for 25 min. Cell debris was removed by centrifugation for 25 min at 14,000 rpm and 4 °C. Protein-containing supernatants were collected and protein concentration was determined using the Pierce™ BCA Protein Assay Kit according to manufacturer's instructions. Lysates were either used directly for SDS-polyacrylamide gel electrophoresis (PAGE) or stored at -20 °C. 50 µg protein was diluted in 1x SDS loading buffer and denatured for 5 min at 96 °C.

For analysis of PRDX3 dimers, cells were washed twice with PBS supplemented with 50 mM NEM and lysed under non-reducing conditions using CHAPS buffer supplemented with 100 mM NEM. For non-reducing conditions, lysates were boiled in 1x non-reducing SDS-loading buffer, whereas lysates were boiled in 1x SDS loading buffer for reducing conditions.

4.2.9.2 SDS-PAGE and Western blotting

For protein separation according to size, SDS-PAGE was performed. Prepared samples were loaded onto handcast gels. Gels consisted of a 5 % stacking gel (5 % acrylamide, 125 mM TrisHCl (pH 6.8), 0.1 % SDS, 0.1 % APS, 0.1 % TEMED) and a resolving gel containing 10 %, 12 % and 15 % acrylamide depending on the expected protein size (10/12/15 % acrylamide, 250 mM TrisHCl (pH 8.8), 0.1 % SDS, 0.1 % APS, 0.04 % TEMED). Electrophoresis was performed in 1x SDS running buffer at initially 80 V until the samples passed through the stacking gel and at 120 V until proteins were separated as desired. A visible protein ladder was employed to monitor protein separation. Proteins were transferred onto a nitrocellulose membrane using a semi-dry blotting system. The membrane, Whatman papers and gels were soaked in 1x Blotting buffer. The nitrocellulose membrane was placed onto two Whatman papers, after which the gel was transferred onto the membrane and air bubbles were removed. Two Whatman papers were placed onto the gel and excess buffer was removed. Protein transfer was performed for 70 – 90 min with a constant current of 1 mA/cm^2 of nitrocellulose membrane.

4.2.9.3 Protein detection

After blotting, the nitrocellulose membrane was blocked in Blocking buffer for 1 h at RT to reduce unspecific antibody binding. The membrane was subsequently washed three times with PBS-T and incubated with primary antibodies in 5 % BSA in PBS-T overnight at 4 °C. On the next day, the membrane was washed three times with PBS-T and incubated with secondary

antibodies conjugated with horseradish peroxidase (HRP) in 5 % milk in PBS-T for 1 h at RT. After three washing steps with PBS-T, the membrane was incubated with Pierce™ ECL Western Blotting Substrate according to manufacturer's instructions to detect HRP-conjugated antibodies by enhanced chemiluminescence. Membranes were placed in an X-ray cassette and ECL Hyperfilms were exposed for 30 sec – 1 h in a darkroom. Films were developed according to manufacturer's instructions.

4.2.10 Immunoprecipitation

4.2.10.1 Active BAK immunoprecipitation

For analysis of BAK activity, cells were treated as specified and lysed in CHAPS lysis buffer. 200 – 500 µg protein lysate (in a total volume of 400 µl CHAPS) was incubated with 10 µl anti-mouse Dynabeads™ and 2 µl anti-BAK AB-1 antibody that recognizes only the active conformation of BAK. Lysates were incubated overnight at 4 °C on a rotating wheel. On the next day, beads were washed four times using CHAPS buffer. Bound protein was eluted by boiling with 1x SDS loading buffer and analyzed by SDS-PAGE and Western blotting.

4.2.10.2 mRuby2-BAK Co-Immunoprecipitation (Co-IP)

For pull-down of mRuby2-tagged BAK and bound proteins, RFP-Trap® Magnetic Agarose was used according to manufacturer's instructions. Cells were washed twice with PBS supplemented with 50 mM NEM and lysed in NP-40 lysis buffer supplemented with 70 mM NEM. 500 µg protein was incubated with 50 µl bead slurry overnight at 4 °C on a rotating wheel. Beads were washed five times with RFP-Trap® washing buffer before elution of bound proteins with 1x SDS loading buffer. Bound proteins were analyzed by SDS-PAGE and Western blotting.

For analysis of bound proteins by mass spectrometry, beads were washed 4 times with RFP-Trap® washing buffer and then transferred into a new microcentrifuge tube with 10 mM Tris HCl (ph 7.5) and stored at -80 °C until further sample preparation as described below.

4.2.11 BIAM Switch Assay

For analysis of protein oxidation, a BIAM Switch Assay was performed. Jurkat FD cells were treated as specified and harvested by centrifugation for 5 min at 1800 rpm and 4 °C. For blocking of free thiols, medium was discarded and cells were incubated with PBS supplemented with 50 mM NEM for 5 min at RT in the dark, after which cells were centrifuged for 5 min at 1800 rpm and 4 °C. Cells were washed once with PBS supplemented with 50 mM NEM. MEFs were treated as specified. At the indicated time point, the medium was discarded and cells were incubated with PBS supplemented with 50 mM NEM for 5 min at RT in the dark after which cells were scraped from the plate and harvested by centrifugation. Proteins were precipitated in ice-cold 20 % TCA. Pellets were subsequently washed once with 10 % TCA, 5 % TCA and twice with ice-cold acetone. Pellets were resolved in 400 µl NEM-resolution buffer for 1-2 h at 37 °C on a shaker at 1400 rpm. 1 ml acetone was added to stop the reaction and proteins were precipitated at -20 °C overnight, after which proteins were collected by centrifugation and washed twice with ice-cold acetone. For reduction of oxidized thiols, proteins were resuspended in 200 µl DTT-resolution buffer for 10 min at 37 °C on a shaker at 1400 rpm. Reduced thiols were then labeled with EZ-Link™ Iodoacetyl-PEG2-Biotin (BIAM) in 200 µl BIAM-resolution buffer for 1 h at 37 °C on a shaker at 1400 rpm. Proteins were precipitated by addition of 1 ml ice-cold acetone and incubation at -20 °C for 4 h after which proteins were collected by centrifugation and washed twice with ice-cold acetone. Protein pellets were resuspended in 200 µl resuspension buffer and broken up by sonication. For the pull-down of biotinylated proteins, 500-1000 µg protein was incubated with 50 µl Pierce™ High Capacity Streptavidin Agarose overnight at 4 °C on a rotating wheel. To remove unbound proteins, beads were washed 5 times with Resuspension buffer after which bound proteins were eluted by boiling in sample buffer and analyzed by SDS-PAGE and Western blotting. For quantification of oxidized proteins, ImageJ was used. High resolution digital scans of Western blot films were utilized for analysis. In brief, the signal intensity of each band was determined using the area under the curve. Signal intensities of BIAM-labeled proteins were normalized to the respective input signal. Three independent experiments were used for quantification.

For analysis of global protein oxidation by mass spectrometry, cells were treated as specified and harvested by centrifugation for 2 min at 1800 rpm and RT. Cells were washed twice with PBS and precipitated in 20 % TCA. Samples were stored at -80 °C until further sample preparation as described below.

4.2.12 Mass Spectrometry

Sample preparation for liquid chromatography/mass spectrometry (LC/MS), LC/MS and data analysis was performed by Dr. Ilka Wittig, Functional Proteomics, Faculty of Medicine, Goethe-University Frankfurt.

4.2.12.1 Mass spectrometric analysis of global protein oxidation in Jurkat FD cells

Samples were prepared as described in section 4.2.11.

BIAM Switch Assay, LC/MS and data analysis was performed as described in [197]. 750 µg protein was used for affinity purification. Proteins were identified using the human reference proteome set (UniProt, December 2016, 70947 entries).

4.2.12.2 Mass spectrometric analysis of mRuby2-BAK Co-IP

Samples were prepared as described in section 4.2.10.2.

Sample preparation for LC/MS, LC/MS and data analysis was performed as described in [198]. Proteins were identified using the reviewed mouse reference proteome database (UniProt, February 2018, 52538 entries, supplemented with the sequence of fluorescent protein Ruby). Acetylation (+42.01) at N-terminus and oxidation of methionine (+15.99), N-ethylmaleimide (+) or carbamidomethylation (+57.02) on cysteines were selected as variable modifications.

4.2.13 Cluster analysis

Enriched GO terms were analyzed with GOrilla using two unranked lists (significantly enriched in mRuby2-BAK-WT versus significantly enriched in mRuby2-BAK-SS) and a p-value threshold of 10^{-3}. The GO term "cellular process" was summarized and visualized using REVIGO.

4.2.14 Statistical analysis

47

Results are presented as mean + standard deviation (SD). GraphPad Prism was employed to calculate statistical significance using Student's t-test or ANOVA as indicated. p-values were assigned as follows: * $p < 0.5$; ** $p < 0.01$; *** $p < 0.001$.

5 Results

5.1 PX-12 treatment triggers intrinsic apoptosis in ALL cell lines

Parts of this work were published in the international peer-reviewed journal *Biological Chemistry* in 2019 with the title *"Thioredoxin inhibitor PX-12 induces mitochondria-mediated apoptosis in acute lymphoblastic leukemia cells"* [199].

Novel treatment options are needed to increase survival of ALL patients that have developed resistance to chemotherapy. Since redox homeostasis was found to be disturbed during leukemia development, progression and relapse [200], we wanted to evaluate the mechanism of action and therapeutic potential of PX-12, an irreversible inhibitor of Trx1 [112], in ALL cell lines.

5.1.1 PX-12 diminishes cell viability and induces cell death in ALL cell lines

To investigate the vulnerability of ALL cell lines to Trx1 inhibition, we treated three ALL cell lines (Jurkat-FD, KOPN-8 and REH cells) with PX-12. We used increasing concentrations (1-20 µM) of PX-12 and quantified cell viability after 24 h (Figure 7 A-C). All three cell lines showed a significant decrease in cell viability in a dose-dependent manner. As this method cannot distinguish between alterations in cell proliferation or actual cell death, a flow cytometric FSC/SSC analysis was performed to determine cell death induction. PX-12 treatment triggered cell death in all three cell lines in a dose-dependent manner that corresponds with the observed decrease in cell viability (Figure 7 D-F).

These results highlight that inhibition of the Trx system using PX-12 diminishes cell viability and induces cell death in ALL cell lines. Next, we wanted to elucidate the molecular mechanisms of PX-12-induced cell death. The successful treatment of ALL is often challenging due to the development of resistance to apoptosis-inducing treatments (Fulda 2009). Therefore, in the following experiments, Jurkat FD ALL cells were used since these cells are resistant to extrinsic apoptotic stimuli as FADD is essential for the formation of the signaling complex downstream of death receptors [201]. We chose 15 µM PX-12 as our standard treatment as it decreased cell viability to less than 15 % and induced cell death to up to 50 % after 24 h in Jurkat FD cells.
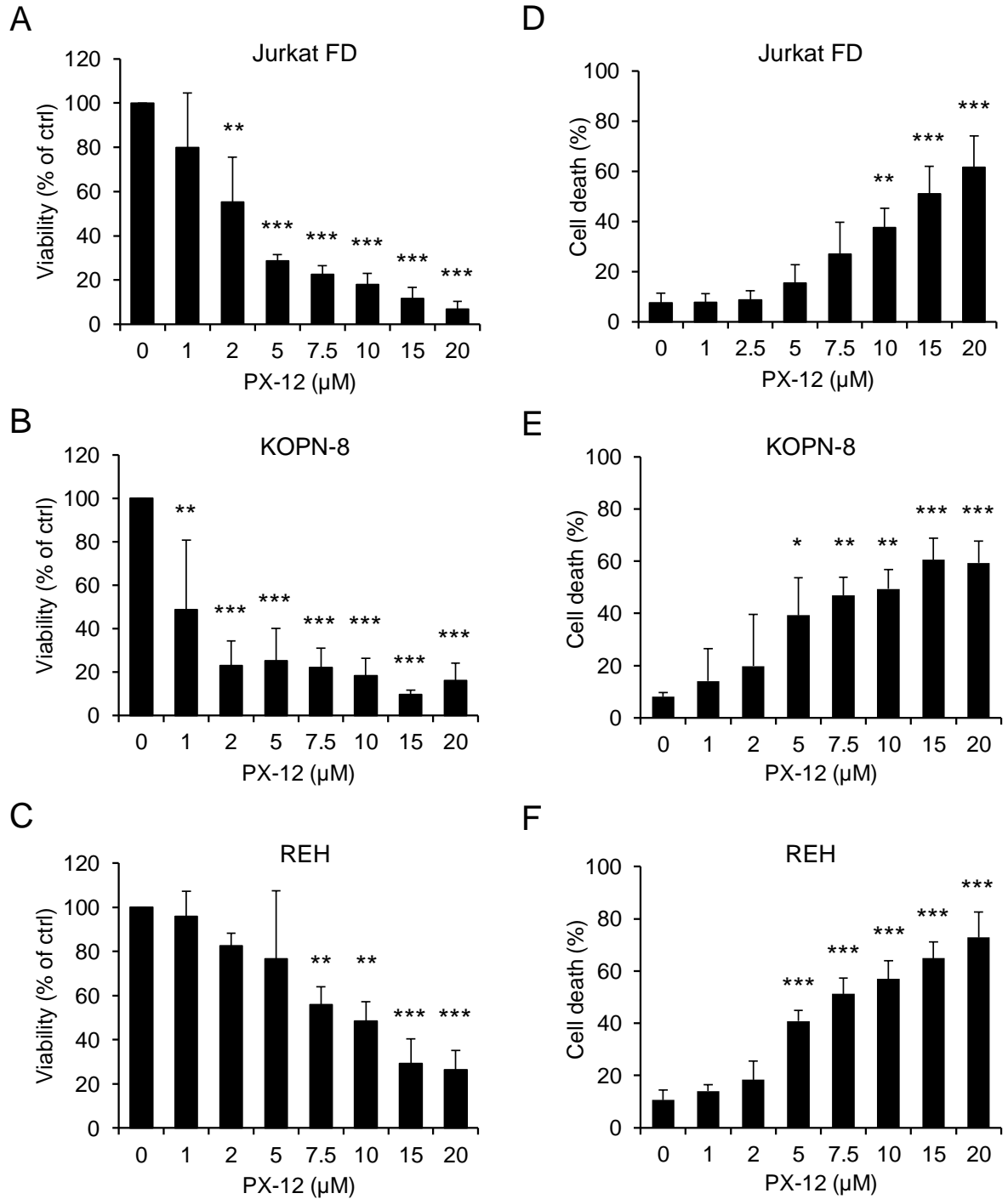
Figure 7. PX-12 decreases cell viability and causes cell death in ALL cell lines. Jurkat FD (A, D), KOPN-8 (B, E) and REH cells (C, F) were treated with PX-12 for 24 h as indicated after which cell viability was measured using CellTiterGlo®assay (A-C) or cell death was assessed using flow cytometry and FSC/SSC analysis (D-E). Mean and SD of three independent experiments performed in triplicate are shown. Significances were assessed using one-way ANOVA followed by Dunnett's post-hoc test. Significances are shown compared to untreated cells, * $p < 0.5$; ** $p < 0.01$; *** $p < 0.001$.

Next, we analyzed the kinetics of PX-12-induced cell death in Jurkat FD cells (Figure 8). Significant differences in cell death induction could be observed as early as 6 h after PX-12 treatment, followed by a steady increase in cell death induction.
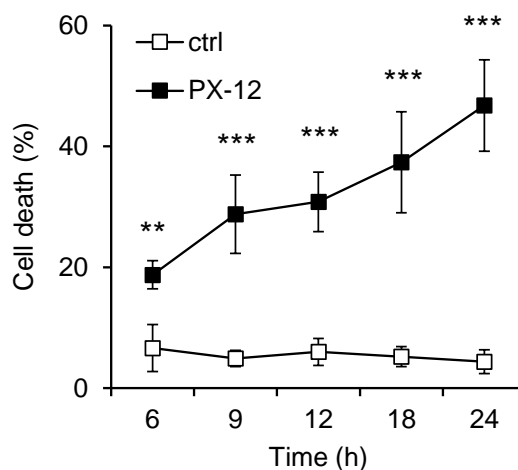
Figure 8. PX-12 induces cell death in a time-dependent manner in Jurkat FD cells. Cells were treated with 15 µM PX-12 or left untreated (ctrl). At the indicated time-points, cell death was measured using flow cytometry and FSC/SSC analysis. Mean and SD of three experiments performed in triplicate are shown. Significances were calculated using one-way ANOVA followed by Tukey's post-hoc test and are indicated compared to ctrl, ** $p < 0.01$; *** $p < 0.001$.

5.1.2 PX-12 reduces Trx activity and increases ROS levels and PRDX3 oxidation

PX-12 was described to increase ROS levels in various cell lines [113, 115, 116, 202], but its efficacy in ALL cell lines has not been reported yet. As PX-12 was developed as an inhibitor of Trx1, we first aimed to verify its functionality in Jurkat FD cells by subjecting them to 15 µM PX-12 for 6 h, followed by determination of Trx activity. Notably, PX-12 treatment significantly reduced Trx activity in Jurkat FD cells (Figure 9 A).

Next, we investigated the effect of PX-12 on cellular and mitochondrial ROS levels using the fluorescent dyes H₂DCF and MitoSOX, respectively, measured by flow cytometry. Interestingly, both cellular and mitochondrial ROS levels were significantly elevated after PX-12 treatment in Jurkat FD cells (Figure 9 B, C).
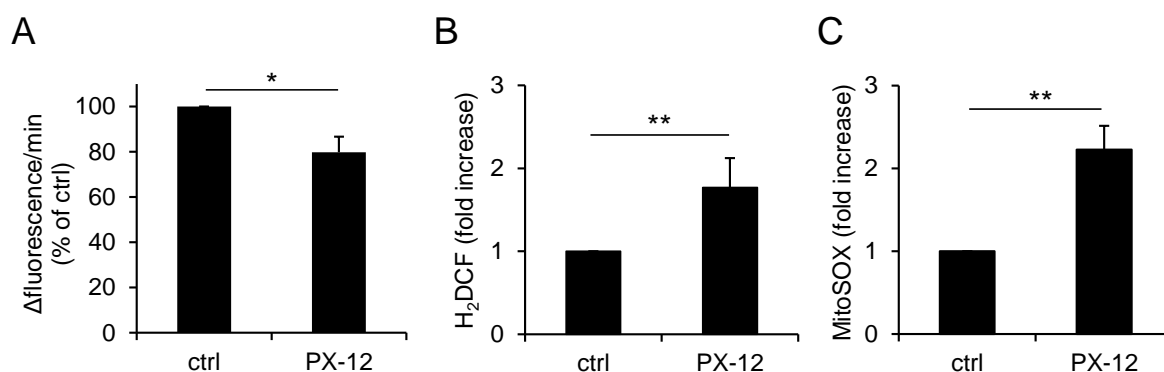
Figure 9. PX-12 decreases Trx activity that is accompanied by ROS formation in Jurkat FD cells. (A) Cells were treated with 15 µM PX-12 or left untreated. Cells were harvested after 6 h and lysed by sonication. Reduction of eosin-labeled insulin was measured for 1 h and the increase in fluorescence over time (Δfluorescence/min) was determined. Results are shown as percentage of untreated control (ctrl). Mean and SD of three experiments performed in duplicate are shown. (B, C) Cells were treated with 15 µM PX-12 for 7 h followed by measurement of ROS levels using the fluorescent dye H_2DCF (B) or MitoSOX (C) and flow cytometry. Data was normalized to ctrl. Mean and SD of three experiments performed in triplicate are shown. Significances were assessed using Student's t-test (unpaired, two-tailed), * $p < 0.05$; ** $p < 0.01$.

Additionally, we wanted to determine whether PX-12 treatment increases protein oxidation. Therefore, we examined the oxidation state of the mitochondrial protein PRDX3 that becomes easily oxidized upon oxidative stress and forms disulfide-linked dimers that can be detected using Western blotting. These dimers are expected to migrate as two separate bands under non-reducing conditions as was shown previously for PRDX2 [203]. Importantly, the migration behavior reflects the amount of disulfide bonds present in the dimer, with the dimer containing two disulfide bonds being more compact and migrating more easily through the gel compared to the dimer with just one disulfide bond [203]. Interestingly, we observed two bands at the expected size for the PRDX3 dimer (48 kDa) under non-reducing conditions upon PX-12 treatment, which were not apparent under reducing conditions (Figure 10). Intriguingly, the lower, more oxidized PRDX3 dimer band increased upon treatment with PX-12. After 6 h the lower dimer band was comparable to that induced upon treatment with the well-described TrxR inhibitor Auranofin [104]. These experiments confirm that PX-12 treatment increases ROS levels and stimulates PRDX3 dimer formation, which is highly indicative for increased protein oxidation, in Jurkat FD cells.
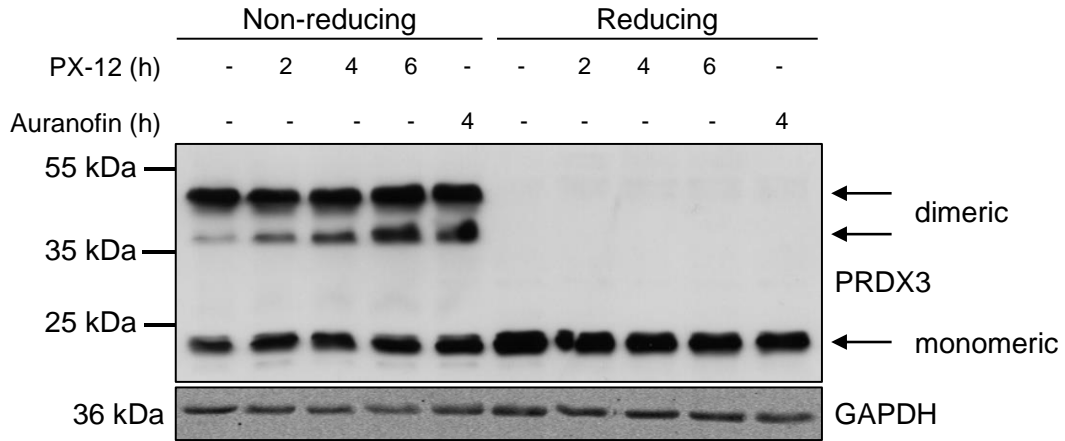
Figure 10. PRDX3 dimer formation is increased upon PX-12 treatment. Jurkat FD cells were treated with 15 µM PX-12 or 2 µM Auranofin for the indicated time-points followed by lysis of cells and preparation for SDS-PAGE under non-reducing or reducing conditions and Western blotting with GAPDH as loading control. Representative blot of two independent experiments is shown.

5.1.3 PX-12-induced cell death and ROS increase is inhibited by NAC

To further assess the role of ROS upon PX-12 treatment, we evaluated if ROS scavengers could affect PX-12-induced cell death and ROS levels in Jurkat FD. To scavenge different types of ROS, we pre-treated cells with the GSH precursor NAC, the vitamin E derivate α-Toc or the superoxide dismutase mimetic MnTBAP for 1 h before addition of PX-12 and measured cell death and ROS formation (Figure 11). Importantly, cell death was significantly decreased after 7 and 24 h of PX-12 treatment upon NAC pre-treatment (Figure 11 A, B). In contrast, pre-treatment with α-Toc or MnTBAP did not alter cell death induction upon PX-12 treatment. Moreover, addition of NAC, but not α-Toc or MnTBAP, significantly diminished the increase in mitochondrial ROS levels that was triggered upon PX-12 treatment, a trend that was also apparent, albeit not significant, when measuring cellular ROS levels (Figure 11 C, D). Interestingly, only the thiol-containing antioxidant NAC, but not the non-thiol containing compounds α-Toc and MnTBAP, were effective in counteracting PX-12 treatment in Jurkat FD cells.

A

B

C

D
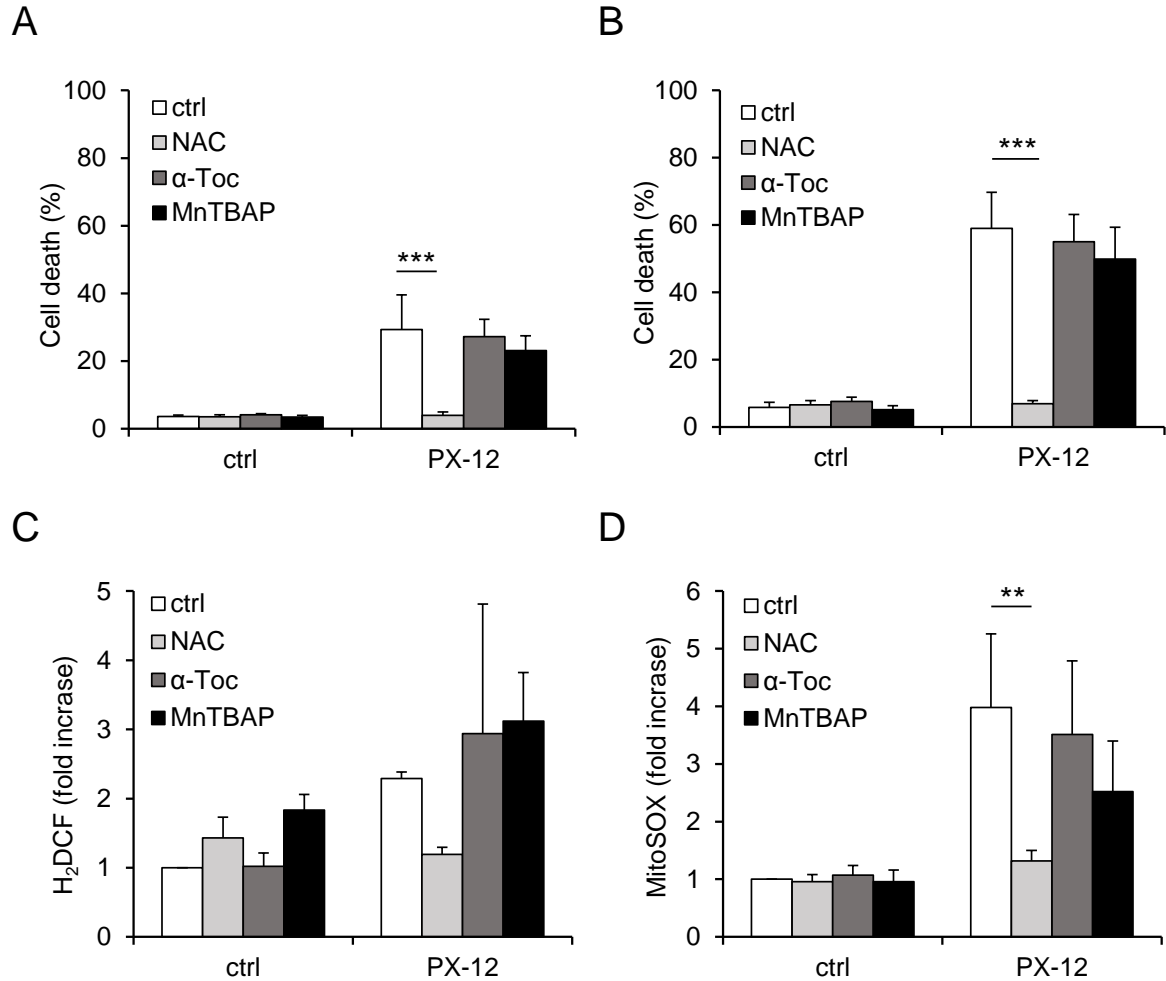
Figure 11. NAC rescues PX-12-induced cell death and ROS increase. Jurkat FD cells were pre-treated for 1 h with NAC (10 mM), α-Toc (200 µM) or MnTBAP (300 µM) before treatment with 15 µM PX-12. Cell death was analyzed with flow cytometry and FSC/SSC analysis after 7 h (A) or 24 h (B). (C, D) Cellular (C) or mitochondrial (D) ROS levels were measured using the fluorescent dye H_2DCF (C) or MitoSOX (D) and flow cytometry 7 h after addition of PX-12. Data was normalized to control (ctrl). (A-D) Mean and SD of three experiments performed in triplicate are shown. Significances were calculated using one-way ANOVA followed by Tukey's post-hoc test, ** $p < 0.01$; *** $p < 0.001$.

5.1.4 PX-12 triggers activation of caspases

Since ROS appeared to only partially contribute to PX-12-induced cell death, the type of cell death that is triggered upon PX-12 treatment was further analyzed. For that, the effect of pre-treatment with the pan-caspase inhibitor zVAD.fmk, an inhibitor of apoptosis, or the RIPK1 inhibitor Nec-1s that prevents necroptosis, on PX-12-induced cell death was tested. Notably, only pre-treatment with zVAD.fmk could significantly decrease cell death induction after PX-12 treatment in Jurkat FD cells (Figure 12 A). As addition of Nec-1s did not alter the level of cell death upon PX-12 treatment, we concluded that PX-12 does not trigger necroptotic cell death in Jurkat FD cells.

To further confirm the involvement of caspases in PX-12-induced cell death, we analyzed caspase cleavage using Western blotting, since these are cleaved and thereby activated upon induction of apoptosis [143]. Indeed, cleavage products of caspase-3 and -9 could be detected as early as 2 h after addition of PX-12 (Figure 12 B). Initiator caspase-9 is recruited and activated after the onset of intrinsic apoptosis and subsequently cleaves and activates executioner caspase-3 [143]. Thus, we concluded that PX-12 treatment induces caspase-dependent apoptosis in Jurkat FD cells.
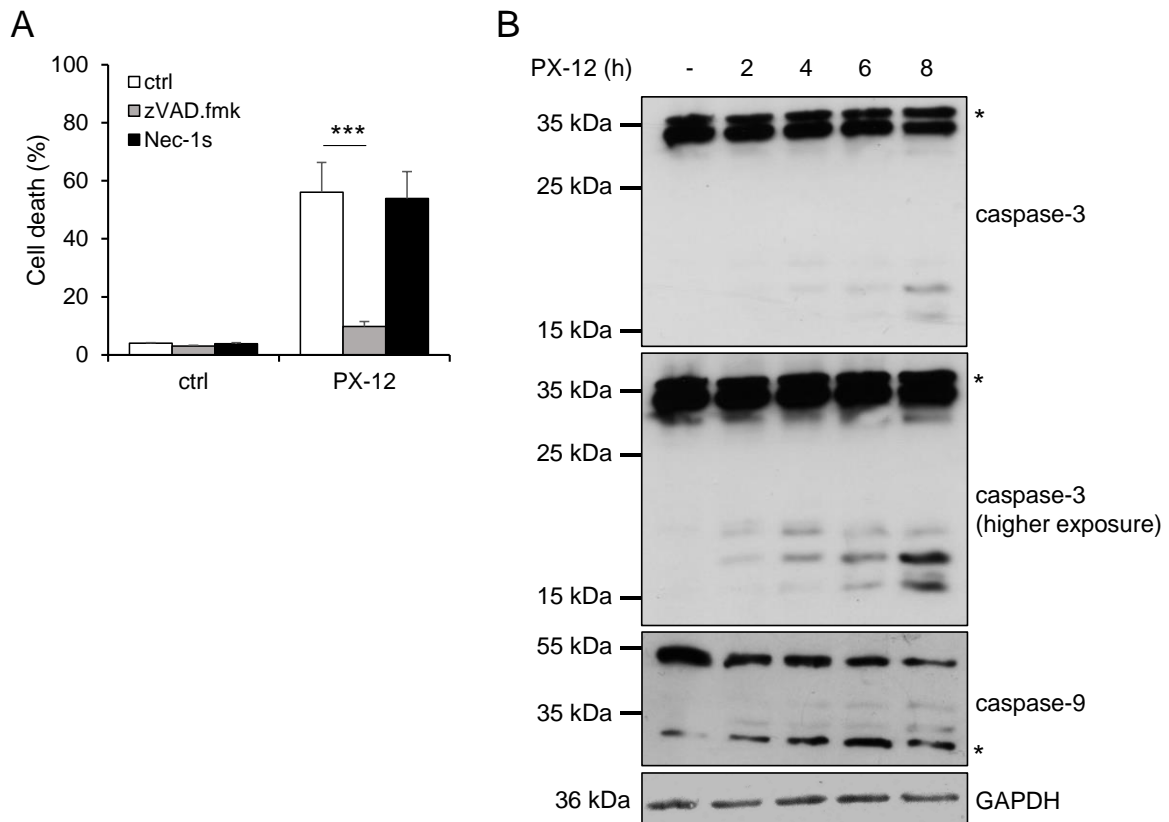
Figure 12. PX-12 induces caspase-dependent cell death. (A) Jurkat FD cells were pre-treated with 20 µM zVAD.fmk or 10 µM Nec-1s for 1 h before addition of 15 µM PX-12. 24 h later, cell death was measured with flow cytometry and FSC/SSC analysis. Mean and SD of three experiments performed in triplicate are shown. Significances were assessed using one-way ANOVA followed by Tukey's post-hoc test, *** $p < 0.001$. (B) Jurkat FD cells were treated with 15 µM PX-12 for the indicated time-points. Cleavage of caspase-3 and -9 was analyzed by SDS-PAGE and Western blotting with GAPDH as loading control. Unspecific bands are labeled with an asterisk (*). Representative blot of two independent experiments is shown.

5.1.5 PX-12-induced cell death and ROS accumulation is dependent on BAK

As we could demonstrate the involvement of caspase-9 in PX-12-stimulated cell death and Jurkat FD cells cannot undergo extrinsic apoptosis due to the absence of FADD, we focused our next experiments on proteins involved in mediating intrinsic apoptosis. For this, we analyzed activation of BAK, the pro-apoptotic BCL-2 family protein that is an integral part of the mitochondrial membrane and important in inducing mitochondrial membrane permeabilization upon stimuli that induce intrinsic apoptosis [204]. We focused our studies on BAK, as Jurkat cells do not express BAX due to frameshift mutations in the BAX gene [205, 206]. Using immunoprecipitation with a conformation-specific antibody that only recognizes the active conformation of BAK, we could demonstrate that BAK activation occurred upon PX-12 treatment in a time-dependent manner (Figure 13 A).

Next, we wanted to evaluate the relevance of BAK for PX-12-mediated cell death. Therefore, we used RNA interference (RNAi) to diminish BAK protein expression. Knock-down of BAK significantly reduced cell death upon PX-12 treatment (Figure 13 B). Successful knock-down of BAK was verified by Western blotting (Figure 13 C).

Additionally, we assessed the role of BAK and caspases on the increased ROS levels triggered by PX-12 treatment. For this, cellular and mitochondrial ROS levels were quantified in cells treated with PX-12 that were either transfected with siRNA against BAK or pre-treated with zVAD.fmk. Interestingly, the increase in cellular and mitochondrial ROS levels induced by PX-12 treatment was diminished upon either BAK knock-down or caspase inhibition (Figure 13 D, E).

These results highlight the importance of BAK and mitochondrial apoptosis in PX-12-stimulated cell death in Jurkat FD cells. Furthermore, BAK and caspases seem to be important in increasing ROS levels after PX-12 treatment.
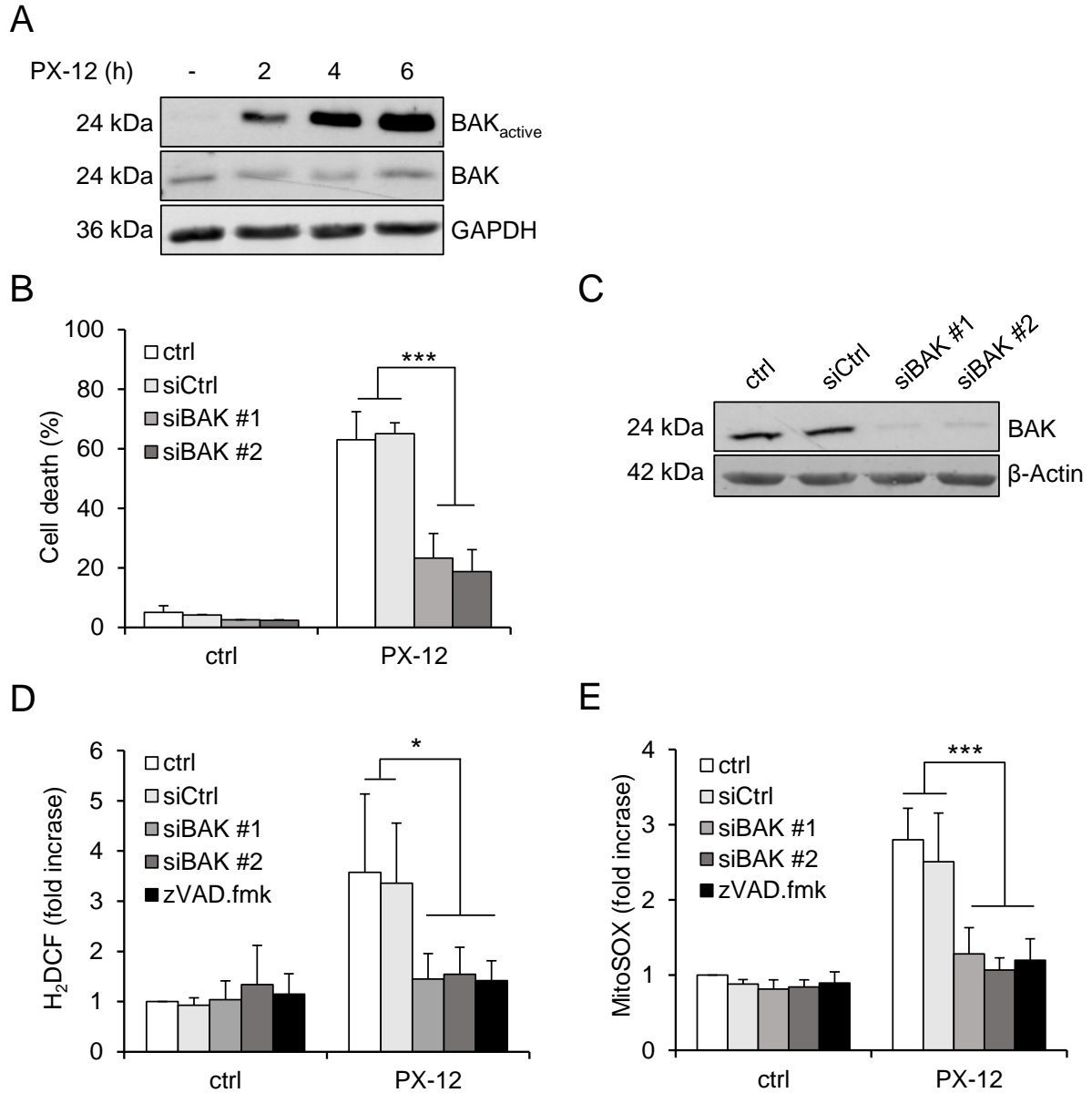
Figure 13. BAK is activated upon PX-12 treatment and involved in cell death induction and ROS increase. (A) BAK activation was determined in Jurkat FD cells treated with 15 µM PX-12 after the indicated time-points by immunoprecipitation with a conformation specific antibody against active BAK followed by SDS-PAGE and Western blotting with GAPDH as loading control. Representative blot of two independent experiments is shown. (B-E) Jurkat FD were transiently transfected with siRNA against BAK (siBAK) or non-targeting siRNA (siCtrl) for 48 h or left untreated (ctrl). (B) Cells were treated with 15 µM PX-12 for 24 h followed by cell death measurements using flow cytometry and FSC/SSC analysis. Mean and SD of three experiments performed in triplicate are shown. (C) BAK protein expression was analyzed by SDS-PAGE and Western blotting with β-Actin as loading control. Representative blot of three independent experiments is shown. (D, E) Transiently transfected cells or cells pre-treated with 20 µM zVAD.fmk were treated with 15 µM PX-12 for 7 h. Cellular (D) or mitochondrial (E) ROS levels were measured using the fluorescent dye H_2DCF (D) or MitoSOX (E) and flow cytometry. Data was normalized to ctrl. Mean and SD of three experiments performed in triplicate are shown. (B, D, E) Significances were assessed using one-way ANOVA followed by Dunnett's post-hoc test, * $p < 0.5$; *** $p < 0.001$.

5.1.6 NOXA mediates cell death and BAK activation upon PX-12 treatment

To further elucidate the role of BCL-2 proteins in PX-12-mediated cell death, the involvement of NOXA, a pro-apoptotic BH3-only protein that acts upstream of BAK, was analyzed [207]. RNAi was used to reduce NOXA protein expression levels in Jurkat FD cells, after which these cells were treated with PX-12. Knock-down of NOXA significantly lowered cell death induction upon PX-12 treatment (Figure 14 A). Successful knock-down of NOXA was validated by Western blotting (Figure 14 B).

To verify that NOXA acts upstream of BAK, we assessed PX-12-induced BAK activation in cells after siRNA-mediated NOXA knock-down. Interestingly, NOXA silencing prevented activation of BAK after PX-12 treatment (Figure 14 C). Additionally, we observed an increase in NOXA protein levels in the PX-12-treated control cells compared to untreated cells. These results emphasize the role of NOXA in inducing mitochondria-mediated apoptosis through activation of BAK in Jurkat FD cells upon PX-12 treatment.

In summary, we could demonstrate that PX-12 induces loss of cell viability and cell death in three ALL cell lines. We could show that PX-12 triggered mitochondria-mediated apoptosis in Jurkat FD cells that could be rescued by caspase-inhibition or silencing of BAK or NOXA. Additionally, PX-12 treatment led to increased protein oxidation as seen by PRDX3 dimer formation and elevated ROS levels in Jurkat FD cells.
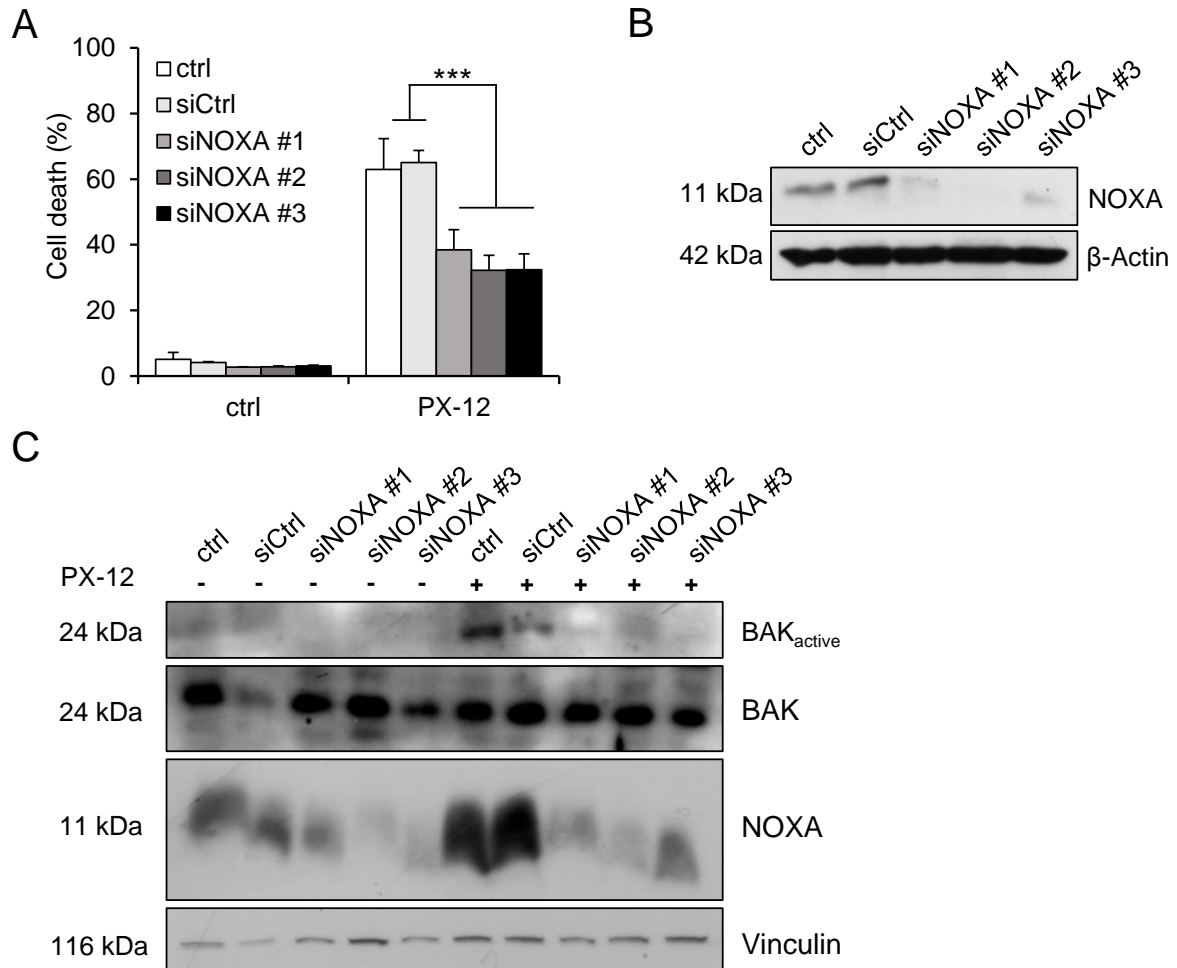
Figure 14. NOXA is involved in PX-12-mediated cell death and BAK activation. Jurkat FD cells were transiently transfected with siRNA against NOXA (siNOXA) or non-targeting siRNA (siCtrl) for 48 h or left untreated (ctrl). (A) Cells were treated with 15 µM PX-12 for 24 h after which cell death was measured using flow cytometry and FSC/SSC analysis. Mean and SD of three experiments performed in triplicate are shown. Significances were assessed using one-way ANOVA followed by Dunnett's post-hoc test, *** $p < 0.001$. (B) NOXA protein expression was analyzed by SDS-PAGE and Western blotting with β-Actin as loading control. Representative blot of three independent experiments is shown. (C) Cells were treated with 15 µM PX-12 for 4 h after which BAK activation was determined with a conformation-specific antibody against active BAK followed by SDS-PAGE and Western blotting with Vinculin as loading control. NOXA protein levels were assessed to ensure the success of the knock-down. Representative blot of two independent experiments is shown.

5.2 TrxR inhibition by Auranofin changes the redox proteome in Jurkat FD cells

To further understand the processes that underlie Trx-inhibition-mediated oxidative stress and cell death, global protein oxidation states were analyzed. For this, Jurkat FD ALL cells were used, since our previous findings highlighted their vulnerability to Trx1 inhibitor PX-12. For induction of oxidative stress, we used the well described TrxR inhibitor Auranofin [101].

5.2.1 Auranofin causes dose-dependent cell death in Jurkat FD cells

To evaluate and characterize Auranofin-induced cell death, Jurkat FD ALL cells were treated with increasing concentrations of Auranofin followed by quantification of cell death after 24 h. Notably, Auranofin-mediated cell death was dose-dependent and led to approximately 70 % cell death (Figure 15). We determined 2 µM as our standard treatment as higher concentrations did not induce more cell death.
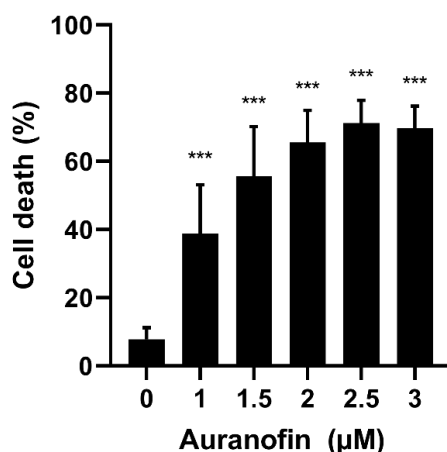
Figure 15. Auranofin-induced cell death is dose-dependent. Jurkat FD cells were treated with the indicated concentrations of Auranofin for 24 h followed by measuring cell death using flow cytometry and FSC/SSC analysis. Mean and SD of five experiments performed in triplicate are shown. Significances are shown compared to untreated cells and were assessed using one-way ANOVA followed by Dunnett's post-hoc test, *** $p < 0.001$.

5.2.2 Auranofin-induced cell death is caspase-dependent

To elucidate the type of cell death induced by Auranofin in Jurkat FD cells, the effects of the necroptosis inhibitors Nec-1s, GSK and Dab and the pan-caspase inhibitor zVAD.fmk were evaluated. Importantly, Auranofin-induced cell death could only be inhibited by zVAD.fmk and not by the necroptosis inhibitors (Figure 16 A, B).

Furthermore, we examined caspase activation upon Auranofin treatment by assessing caspase cleavage using SDS-PAGE and Western blotting. Indeed, cleavage products of caspase-3 and -9 were visible 4 h after Auranofin treatment (Figure 16 C). These results indicate that Auranofin induces caspase-mediated apoptosis in Jurkat FD cells, similar to PX-12.
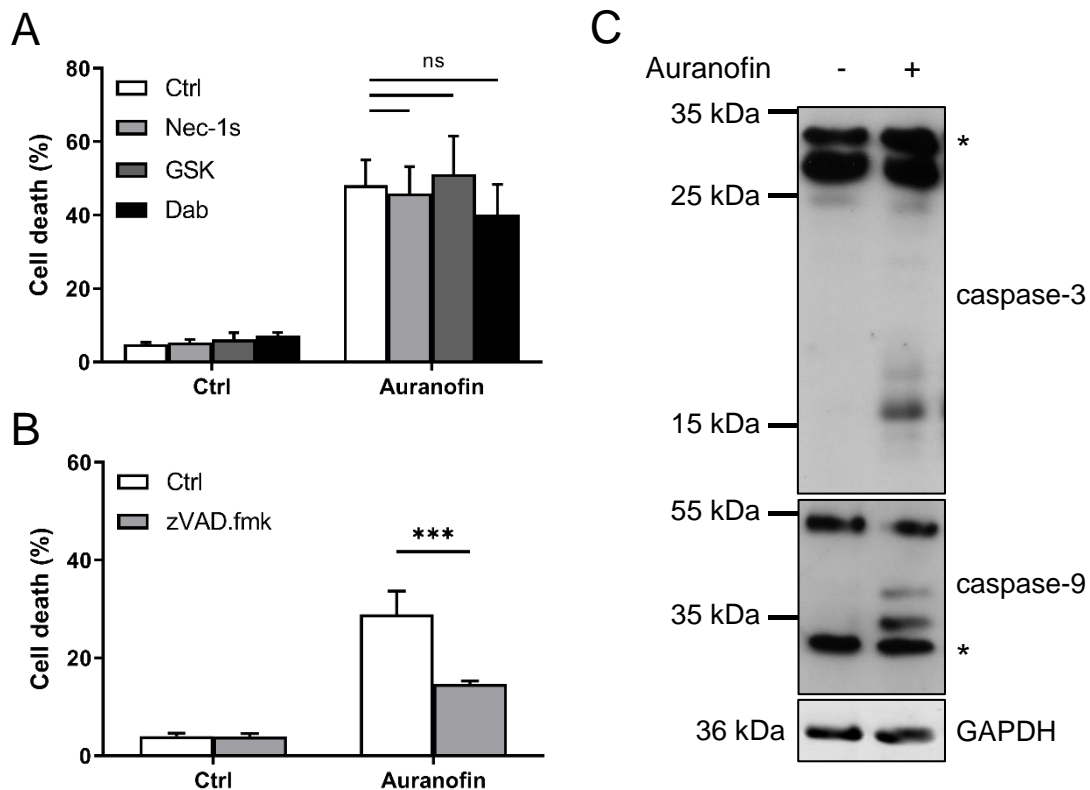
Figure 16. Cell death triggered by Auranofin is not necroptosis, but caspase-mediated apoptosis. (A, B) Jurkat FD cells were treated with 10 µM Nec-1s, 10 µM GSK, 1 µM Dab (A) or 20 µM zVAD.fmk (B) for 1 h before treatment with 2 µM Auranofin for 8 h. Flow cytometry and FSC/SSC analysis was employed to measure cell death. Mean and SD of three experiments performed in triplicate are shown. Significances were assessed using one-way ANOVA followed by Tukey's post-hoc test, ns: not significant; *** $p < 0.001$. (C) Jurkat FD cells were treated with 2 µM Auranofin for 4 h after which cells were harvested and cleavage of caspase-3 and -9 was analyzed by SDS-PAGE and Western blotting with GAPDH as loading control. Unspecific bands are labeled with an asterisk (*). Representative blot of two independent experiments is shown.

5.2.3 BAK is essential for cell death caused by Auranofin treatment

Since BAK was crucial for PX-12-induced apoptosis in Jurkat FD cells, we also analyzed the role of BAK in Auranofin-mediated cell death. BAK activation, as measured by immunoprecipitation using an active conformation-specific antibody, could already be detected after 3 h of Auranofin treatment and further increased over time (Figure 17 A).

Additionally, we performed RNAi to reduce BAK protein levels to determine the relevance of BAK for Auranofin-induced cell death. Knock-down of BAK significantly reduced cell death induction by Auranofin (Figure 17 B). Successful reduction of BAK protein expression levels was verified by Western blotting (Figure 17 C). These results emphasize the importance of BAK in Auranofin-induced cell death and highlight the similarities between Auranofin- and PX-12-mediated intrinsic apoptosis in Jurkat FD cells.
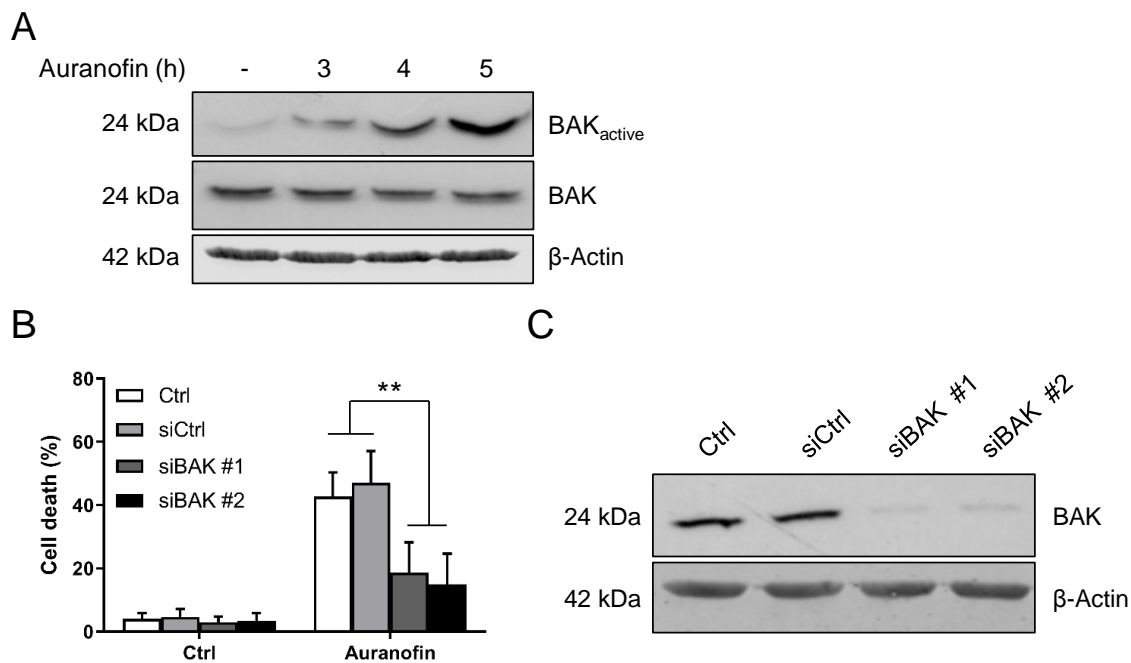
Figure 17. Auranofin-induced cell death is dependent on BAK. (A) Jurkat FD cells were treated with 2 µM Auranofin for the indicated time-points. Activation of BAK was analyzed using an active conformation-specific antibody and immunoprecipitation followed by SDS-PAGE and Western blotting. β-Actin served as loading control. Representative blot of two independent experiments is shown. (B, C) Jurkat FD cells were transiently transfected with siRNA against BAK (siBAK) or non-targeting siRNA (siCtrl) for 48 h or left untreated (Ctrl). (B) 2 µM Auranofin was applied for 24 h and cell death was determined using flow cytometry and FSC/SSC analysis. Mean and SD of three experiments performed in triplicate are shown. Significance was calculated using one-way ANOVA followed by Tukey's post-hoc test, ** $p < 0.01$. (C) BAK knock-down efficiency was assessed using SDS-PAGE and Western blotting with β-Actin as loading control. Representative blot of three independent experiments is shown.

5.2.4 Auranofin increases ROS levels in Jurkat FD

Intrigued by potential changes in protein oxidation induced by Auranofin, induction of ROS upon Auranofin treatment was quantified by measuring fluorescence intensities of the fluorescent dyes H_2DCF and MitoSOX. Both cellular and mitochondrial ROS levels were significantly elevated upon treatment of cells with Auranofin (Figure 18) underscoring the suitability of Auranofin in Jurkat FD cells for a redox proteomics screen.
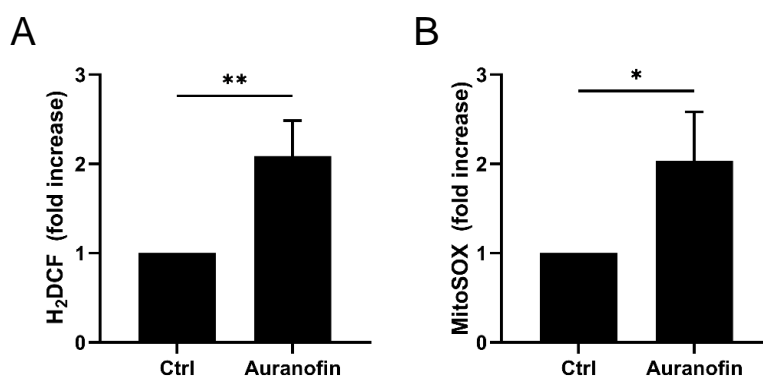
Figure 18. ROS levels are elevated upon Auranofin treatment. Jurkat FD cells were treated with 2 μM Auranofin for 4 h after which cellular (A) and mitochondrial (B) ROS levels were measured with the fluorescent dyes H_2DCF (A) and MitoSOX (B) and flow cytometry. Data was normalized to control (Ctrl). Mean and SD of three experiments performed in triplicate are shown. Significances were assessed using Student's t-test (unpaired, two-tailed), * $p < 0.05$; ** $p < 0.01$.

5.2.5 BIAM Switch Assay coupled to LC/MS uncovers changes in the redox proteome after Auranofin treatment

Since our earlier experiments demonstrated the profound effects of Auranofin on cell death and ROS production in Jurkat FD cells, a BIAM Switch Assay was established for these settings. This assay has been described previously as a method to detect S-nitrosylated proteins [208] but can be adjusted to detect global redox modifications by using DTT that reduces disulfide bonds and sulfenic acid [209]. Oxidized proteins can be enriched by a sequential protocol in which free thiols are blocked by NEM, followed by reduction of oxidized cysteine thiols with DTT and subsequent labeling of the newly reduced thiols with BIAM. These labeled proteins are enriched using immobilized streptavidin, followed by LC/MS analysis (Figure 19 A). Using this unbiased approach, global protein oxidation patterns can be analyzed and differentially oxidized proteins can be identified.

To identify differentially oxidized proteins upon Auranofin treatment, Jurkat FD cells were treated for 4 h with Auranofin or left untreated, followed by a BIAM Switch Assay and LC/MS analysis. By doing so, 204 proteins were significantly oxidized upon Auranofin treatment in Jurkat FD (Figure 19 B, Table 24). Of note, several previously identified target proteins of TrxR were detected, such as Trx1 (TXN), Trx2 (TXN2) and Thioredoxin domain-containing protein 17 (TXNDC17) [210], which provide a first validation of the method. Furthermore, several peroxiredoxins, i.e. PRDX1, PRDX2 and PRDX3, were found to be oxidized upon Auranofin treatment. This further validates the functionality of the screen and the inhibition of the Trx system by Auranofin as peroxiredoxins are targets of thioredoxins [210].

Among the 204 proteins identified, the 25 most significantly enriched proteins upon Auranofin treatment were determined, sorted by significance and displayed in a heat-map according to fold change ($\log_2$(Auranofin/Ctrl)) (Figure 19 C). These candidates contained several proteins involved in posttranslational modifications, like phosphohistidine phosphatase 1 (PHPT1), protein tyrosine phosphatase type IVA 2 (PTP4A2), protein arginine N-methyltransferase 1 (PRMT1) and N-alpha-acetyltransferase 40 (NAA40). Furthermore, proteins involved in cytoskeletal organization (profilin-2 (PFN2), PDZ and LIM domain protein 1 (PDLIM1)), membrane trafficking (Ras-related protein Rab-11A and Rab-11B (RAB11A, RAB11B)) and amino acid metabolism (Branched-chain aminotransferase (BCAT1), APAF1-interacting protein (APIP)) were identified as well.
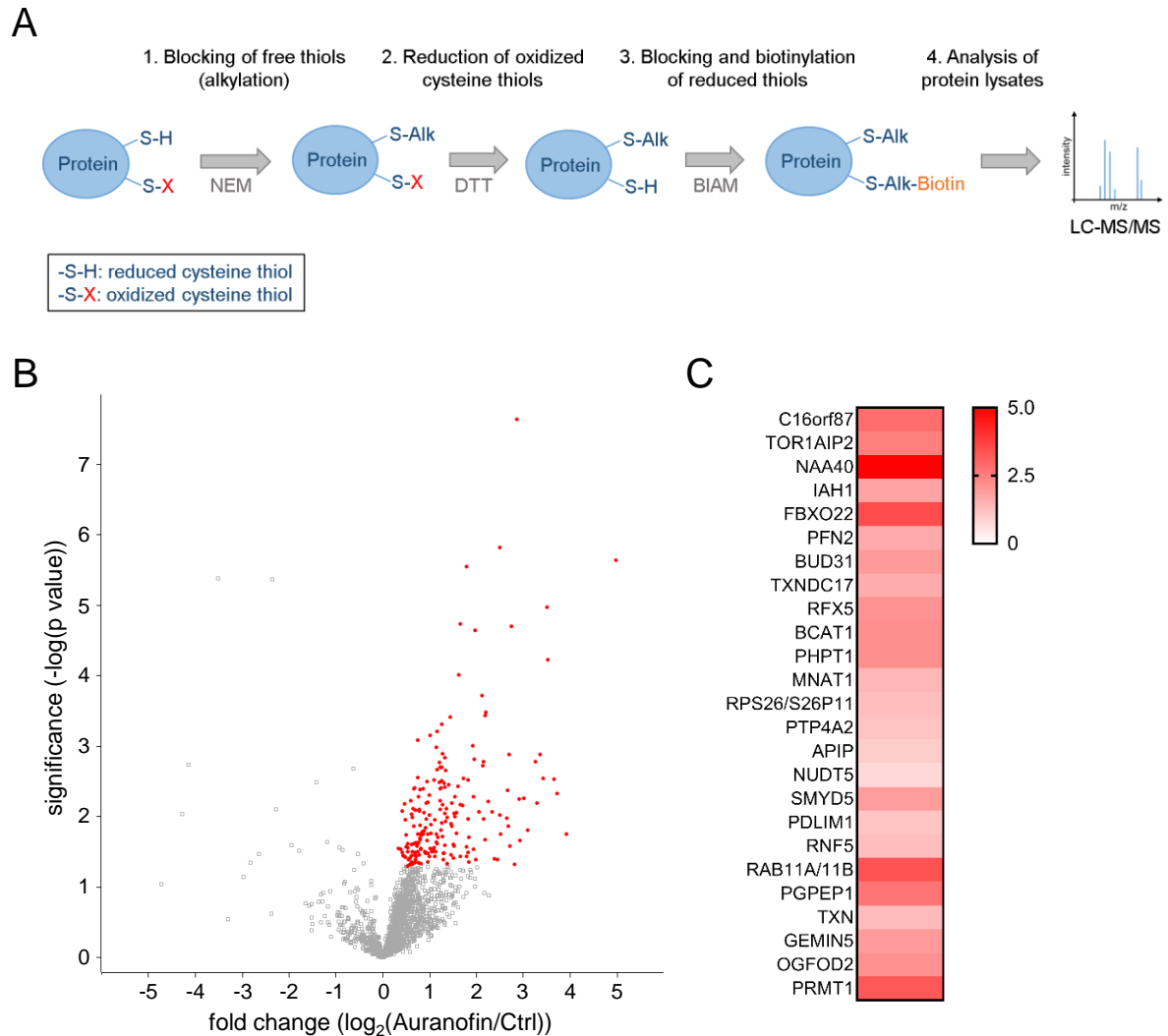
Figure 19. Auranofin treatment induces changes in global protein oxidation in Jurkat FD cells.
(A) Schematic overview of the workflow of the BIAM Switch Assay. (Figure adapted from [211]). (B) Jurkat FD cells were treated with 2 µM Auranofin for 4 h or left untreated (Ctrl). BIAM Switch Assay coupled to LC/MS was performed. Auranofin-treated samples were compared to Ctrl. Significant differentially oxidized proteins are indicated in red (p < 0.05, fold change > 1). Figure was generated by I. Wittig. (C) Top 25 differentially oxidized proteins in response to Auranofin are shown (gene names). The list was sorted by significance and colors assigned according to fold change (log2(Auranofin/Ctrl)).

Of those 25 most significantly upregulated proteins, APIP and PRMT1 were further validated by BIAM Switch Assay, SDS-PAGE and Western blotting. Importantly, both proteins were significantly more oxidized upon Auranofin treatment in Jurkat FD cells as determined by Western blot quantification (Figure 20). The increase in APIP and PRMT1 oxidation was in the same range as determined by MS analysis further validating the functionality of the redox screen.
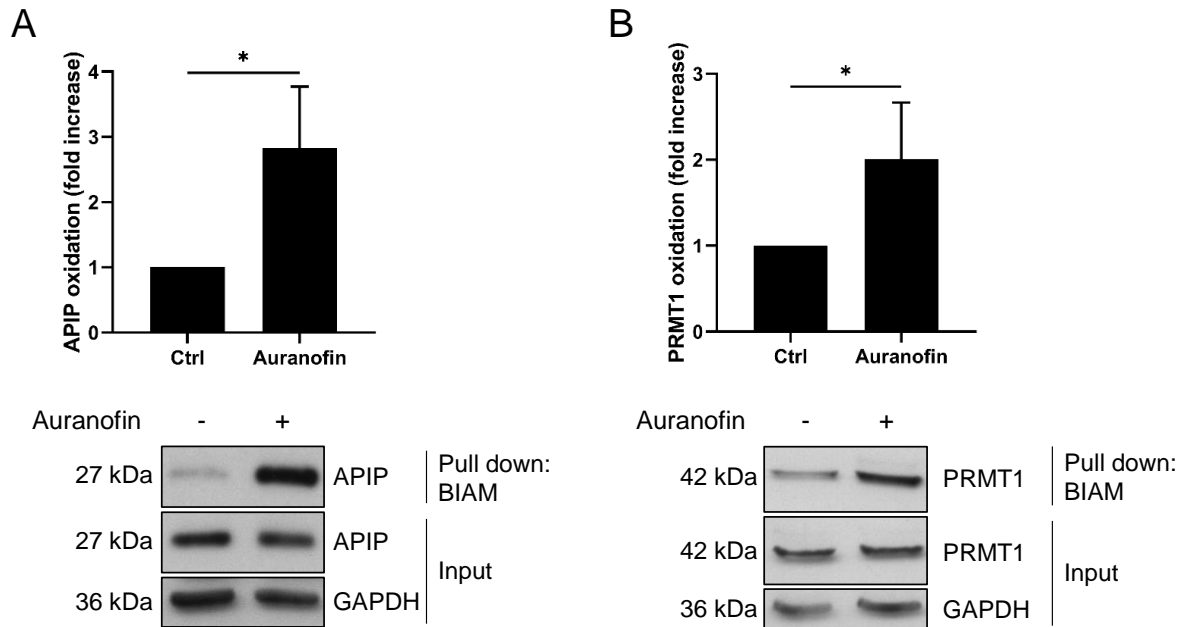
Figure 20. Auranofin-treatment induces oxidation of APIP and PRMT1. Jurkat FD cells were treated with 2 μM Auranofin for 4 h. BIAM Switch Assay followed by SDS-PAGE and Western blotting was used to determine APIP (A) and PRMT1 (B) oxidation status. GAPDH was used as loading control. Oxidation was assessed compared to untreated cells (Ctrl) and shown as fold increase. Mean and SD of three experiments are shown. Significances were assessed using Student's t-test (unpaired, two-tailed), * $p < 0.05$. Representative blots of three experiments are shown.

In summary, using the BIAM Switch Assay coupled to LC/MS enabled us to detect global changes in the redox proteome of Jurkat FD cells upon Auranofin treatment. Furthermore, several known targets of TrxR could be identified with this approach, as well as novel redox targets that could be direct or indirect targets of Auranofin treatment in Jurkat FD cells.

5.3 BAK oxidation is critical for Auranofin-induced cell death in MEFs

Given the central role of BAK in mediating PX-12- and Auranofin-induced apoptosis in Jurkat FD cells, we aimed to further analyze the role of BAK in ROS-mediated cell death. As BAK oxidation was previously demonstrated upon necroptotic stimuli [190], we were interested whether it was also oxidized upon Auranofin-treatment and whether oxidation affects BAK activity or its interaction.

5.3.1 BAK$^{-/-}$ MEFs are less sensitive to Auranofin-induced cell death

To analyze the role of BAK in ROS-induced cell death, we employed wild-type (WT) and BAK$^{-/-}$ MEFs. BAK deficiency was confirmed using Western blotting (Figure 21 A) and BAX protein levels were not affected by BAK knock-out.

Next, WT and BAK$^{-/-}$ MEFs were subjected to Auranofin, followed by quantification of cell death induction after 24 h. Indeed, Auranofin treatment induced cell death in WT MEFs, but BAK$^{-/-}$ MEFs were protected from Auranofin-induced cell death (Figure 21 B). These results are in line with our previous findings demonstrating that BAK is necessary for Auranofin-induced cell death in Jurkat FD cells.

Since Auranofin-treatment induced intrinsic apoptosis in Jurkat FD cells, we next wanted to determine the type of cell death that is triggered upon Auranofin treatment in MEFs. We pre-treated WT MEFs with the pan-caspase inhibitor zVAD.fmk or the RIPK1 inhibitor Nec-1s or both prior to treatment with Auranofin. Interestingly, neither zVAD.fmk, nor Nec-1s rescued Auranofin-induced cell death (Figure 21 C). We concluded that Auranofin induces BAK-dependent cell death in MEFs, which is neither caspase-dependent apoptosis nor RIPK1-dependent necroptosis.

A

B

C
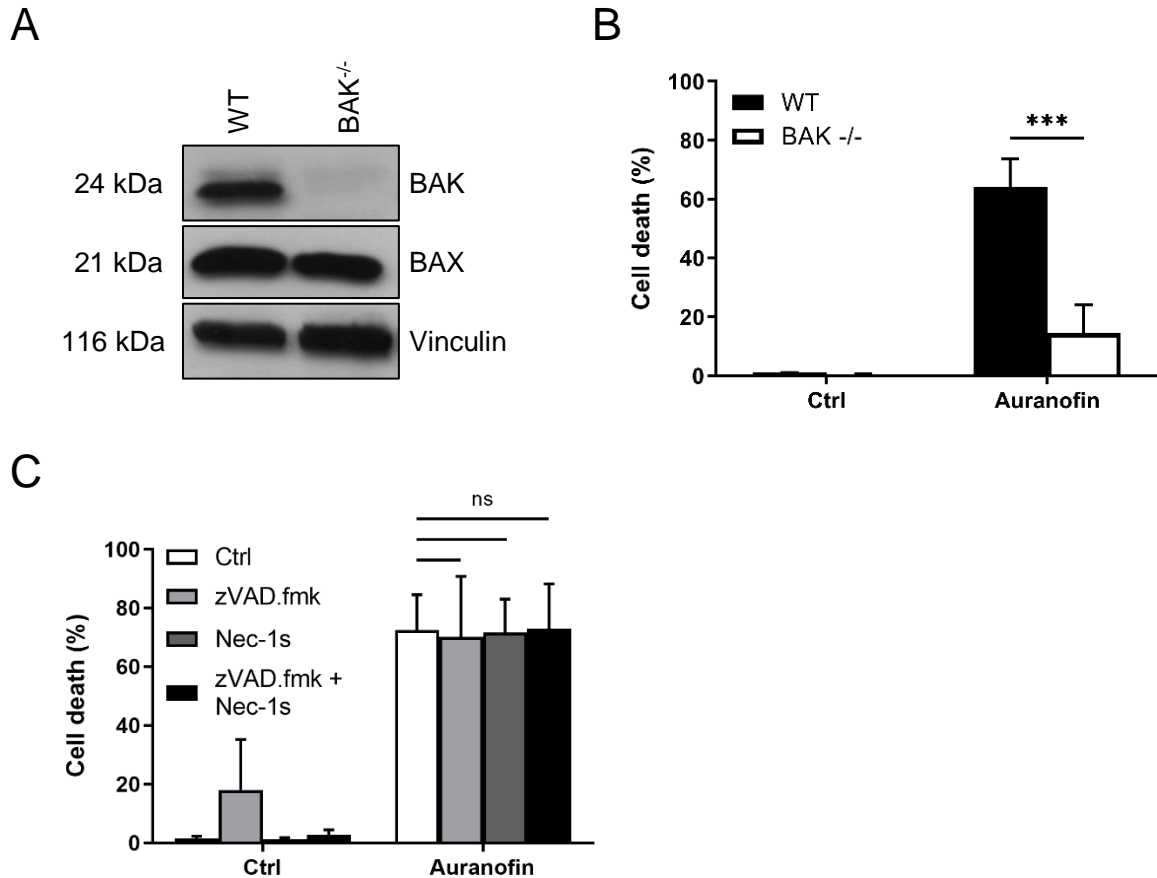
Figure 21. Auranofin induces cell death in WT, but not BAK-/- MEFs that is not dependent on caspases or RIPK1. (A) Lysates of WT and BAK-/- MEFs were analyzed for expression of BAK and BAX by Western blotting with Vinculin as loading control. Representative blot of two independent experiments is shown. (B) WT and BAK-/- MEFs were treated with 4 µM Auranofin for 24 h. (C) WT MEFs were treated with 40 µM zVAD.fmk, 10 µM Nec-1s or both for 1 h, prior to treatment with 4 µm Auranofin for 24 h. (B, C) Cell death was determined by PI/Hoechst staining and fluorescence microscopy. Mean and SD of three experiments performed in triplicate are shown. Significance was analyzed by one-way ANOVA followed by Tukey's post-hoc test, ns: not significant; *** p < 0.001.

5.3.2 Etoposide induces BAK-dependent apoptosis in MEFs

Since Auranofin treatment induced intrinsic apoptosis in Jurkat FD cells, we wanted to ensure that the MEFs we used were able to execute apoptosis. Therefore, we treated WT and BAK-/- MEFs with Etoposide, an inhibitor of topoisomerase II that triggers intrinsic apoptosis [212]. Etoposide treatment induced cell death in WT MEFs after 24 h (Figure 22 A). As expected, BAK-/- MEFs were significantly less sensitive to Etoposide treatment. Of note, pre-treatment with caspase inhibitor zVAD.fmk significantly reduced Etoposide-induced cell death in WT MEFs (Figure 22 B). These results indicate that Etoposide indeed induces BAK-dependent apoptosis in WT MEFs.
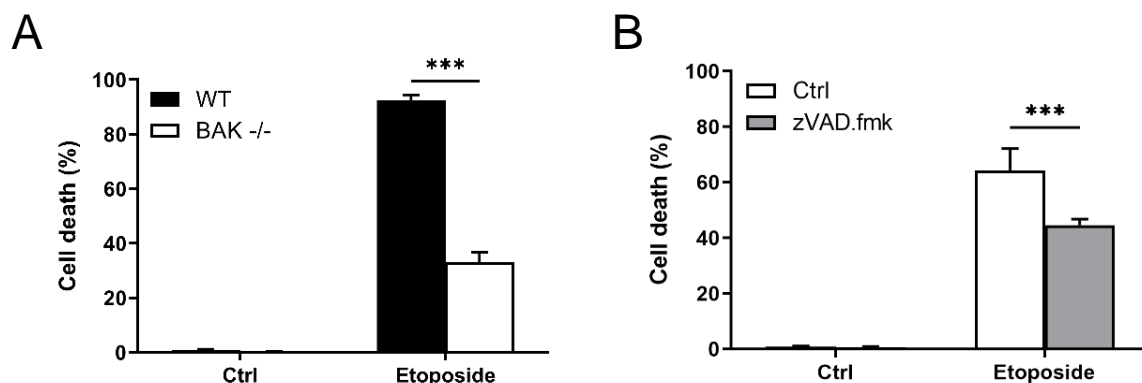
Figure 22. Etoposide-mediated cell death in MEFs is BAK- and caspase-dependent. (A) WT and BAK$^{-/-}$ MEFs were treated with 10 µM Etoposide for 24 h after which cell death was determined by PI/Hoechst staining and fluorescence microscopy. (B) WT MEFs were treated with 40 µM zVAD.fmk for 1 h before treatment with 10 µM Etoposide. Cell death was measured using PI/Hoechst staining and fluorescence microscopy. (A, B) Mean and SD of four experiments performed in triplicate are shown. Significances were determined using one-way ANOVA followed by Tukey's post-hoc test, *** p < 0.001.

5.3.3 BAK$^{-/-}$ MEFs are protected from Auranofin-induced ROS increase and ROS scavengers rescue WT MEFs from Auranofin-induced cell death

Since ROS levels were increased in Jurkat FD cells upon Auranofin treatment, we wanted to further determine the role of ROS in Auranofin-treated MEFs. Therefore, we measured cellular and mitochondrial ROS levels and lipid peroxidation with the fluorescent dyes H$_2$DCF, MitoSOX and BODIPY, respectively, in WT and BAK$^{-/-}$ MEFs. Cellular ROS levels were almost 4-fold increased upon Auranofin treatment in WT MEFs (Figure 23 A). This increase was significantly higher in WT MEFs compared to BAK$^{-/-}$ MEFs. The same effects could be observed for mitochondrial ROS levels with an increase in WT MEFs compared to BAK$^{-/-}$ MEFs (Figure 23 B). Interestingly, Auranofin treatment also led to increased lipid peroxidation that was significantly higher in WT MEFs compared to BAK$^{-/-}$ MEFs (Figure 23 C). These results emphasize the importance of BAK, not only for Auranofin-induced cell death, but also ROS induction.

Next, we tested whether the ROS scavengers α-Toc, BHA or Tbhq could attenuate cell death upon Auranofin treatment. Notably, pre-treatment with either of the three tested ROS scavengers significantly reduced Auranofin-induced cell death in WT MEFs (Figure 23 D). These results highlight the importance of ROS in Auranofin-induced cell death in MEFs.
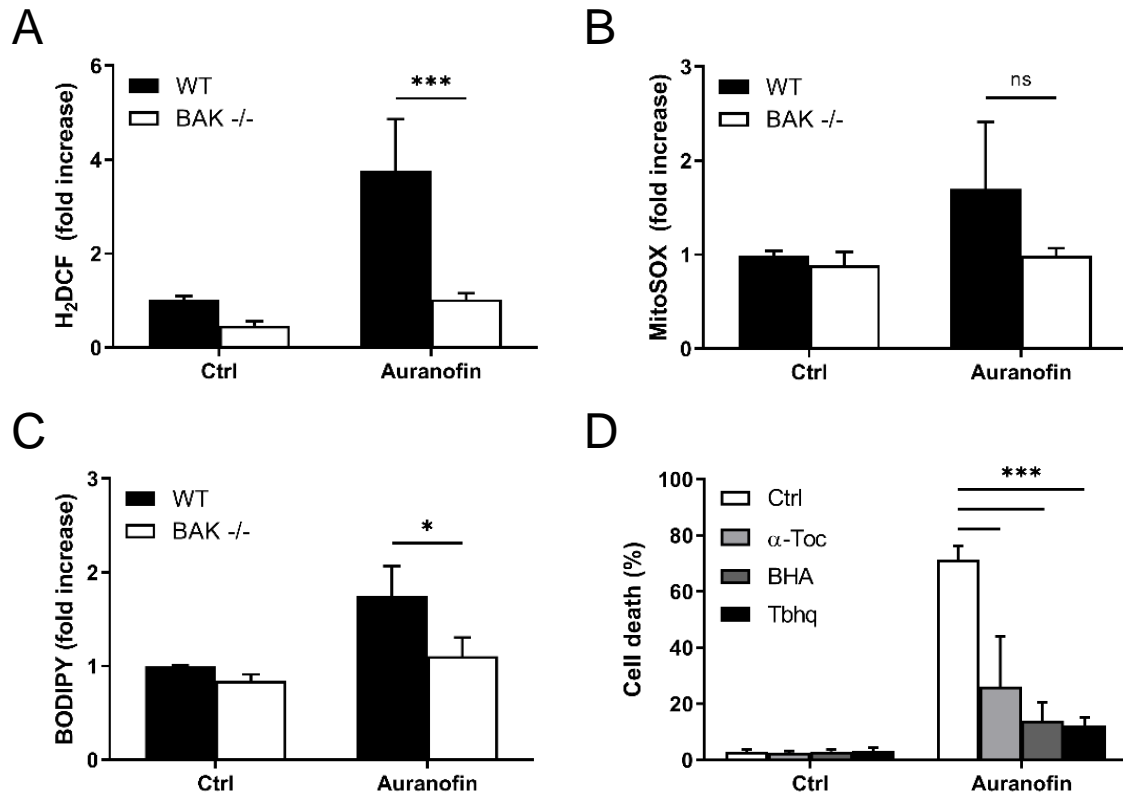
Figure 23. ROS and lipid peroxidation are increased upon Auranofin treatment in WT MEFs and ROS scavengers rescue WT MEFs from Auranofin-induced cell death. WT and BAK^{-/-} MEFs were treated with 4 µM Auranofin for 1.5 h after which cellular (A) and mitochondrial ROS (B) and lipid peroxidation (C) were measured with the fluorescent dyes H_2DCF (A), MitoSOX (B) or BODIPY (C) and flow cytometry. Data was normalized to untreated WT control (ctrl). (D) WT MEFs were treated with 50 µM α-Toc, 50 µM BHA or 10 µM Tbhq for 1 h, before treatment with 4 µm Auranofin. Cell death was measured after 6 h using PI/Hoechst staining and fluorescence microscopy. (A-D) Mean and SD of at least three independent experiments performed in triplicate are shown. Significances were determined using one-way ANOVA followed by Tukey's post-hoc test, ns: not significant; * $p < 0.05$; *** $p < 0.001$.

5.3.4 BAK is oxidized upon Auranofin, but not Etoposide treatment

As we could demonstrate an increase in ROS levels upon Auranofin treatment in WT MEFs and ROS scavengers attenuated Auranofin-induced cell death, we wanted to analyze whether BAK itself was oxidized upon Auranofin treatment. Using the BIAM Switch Assay and Western blotting we could clearly see increased pull-down of BAK after 2 and 3 h of Auranofin treatment or 15 min of H_2O_2 treatment that served as a positive control, suggesting increased oxidation of BAK (Figure 24 A). In contrast, Etoposide treatment did not lead to increased BAK oxidation (Figure 24 B).

A

Auranofin (2h)	-	+	-	-
Auranofin (3h)	-	-	+	-
H_2O_2	-	-	-	+

24 kDa .... BAK ⌉ Pull down: BIAM

24 kDa .... BAK ⌉

42 kDa .... β-Actin ⌋ Input

B

Etoposide	-	+	-
H_2O_2	-	-	+

24 kDa .... BAK ⌉ Pull down: BIAM

24 kDa .... BAK ⌉

116 kDa .... Vinculin ⌋ Input
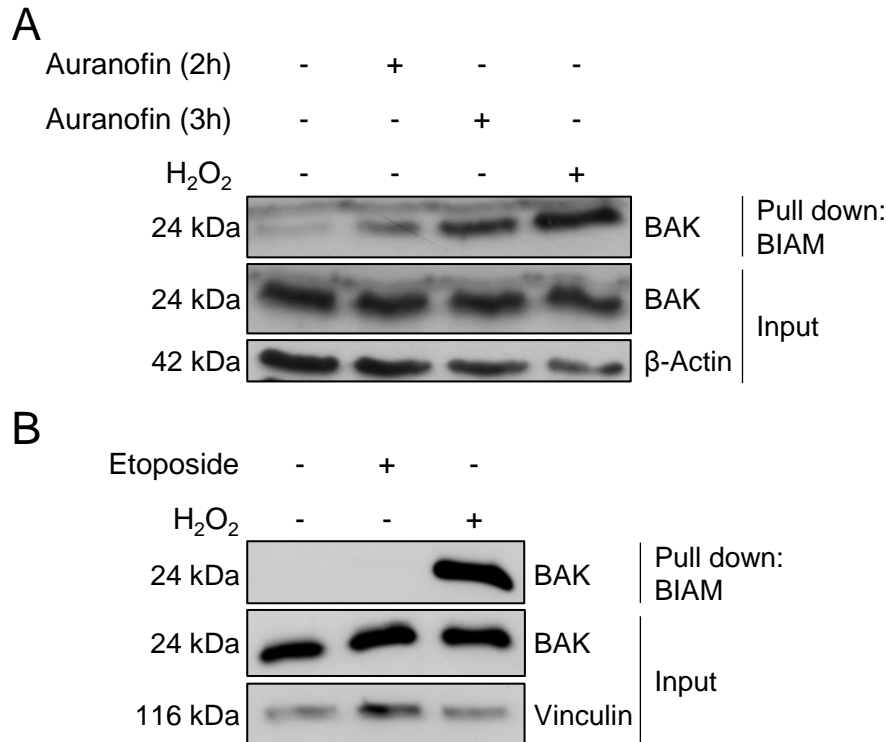
Figure 24. Auranofin, but not Etoposide, induces oxidation of BAK in WT MEFs. WT MEFs were treated with 4 µM Auranofin for 2 or 3 h (A), 10 µM Etoposide for 4 h (B) or 10 mM H_2O_2 for 15 min (A, B) after which a BIAM Switch Assay was performed. Enrichment of BAK was analyzed by SDS-PAGE and Western blotting with β-Actin (A) or Vinculin (B) as loading controls. Blots shown are representative of two independent experiments.

5.3.5 BAK cysteine residues do not influence BAK localization to mitochondria

To understand the relevance of Auranofin-induced BAK oxidation for Auranofin-induced cell death, BAK^{-/-} MEFs were reconstituted with BAK fused to a red fluorescent tag (mRuby2). As cysteine residues are most sensitive to oxidation [15], we mutated either one or both cysteine residues in BAK to oxidation-insensitive serine (C14S/C154S) (Figure 25 A).

Next, we determined the expression levels of these mutants using Western blotting. The mRuby2-tagged BAK protein has a molecular weight of approximately 50 kDa. The expression levels of all mutants were comparable and similar to that of endogenous BAK in WT MEFs (Figure 25 B).

To ensure that all mutants still localize to mitochondria, we performed fluorescence microscopy and stained cells for protein translocase of outer mitochondrial membrane (TOMM20). Indeed, co-localization with TOMM20 could be demonstrated for WT BAK and all cysteine mutants (Figure 25 C).
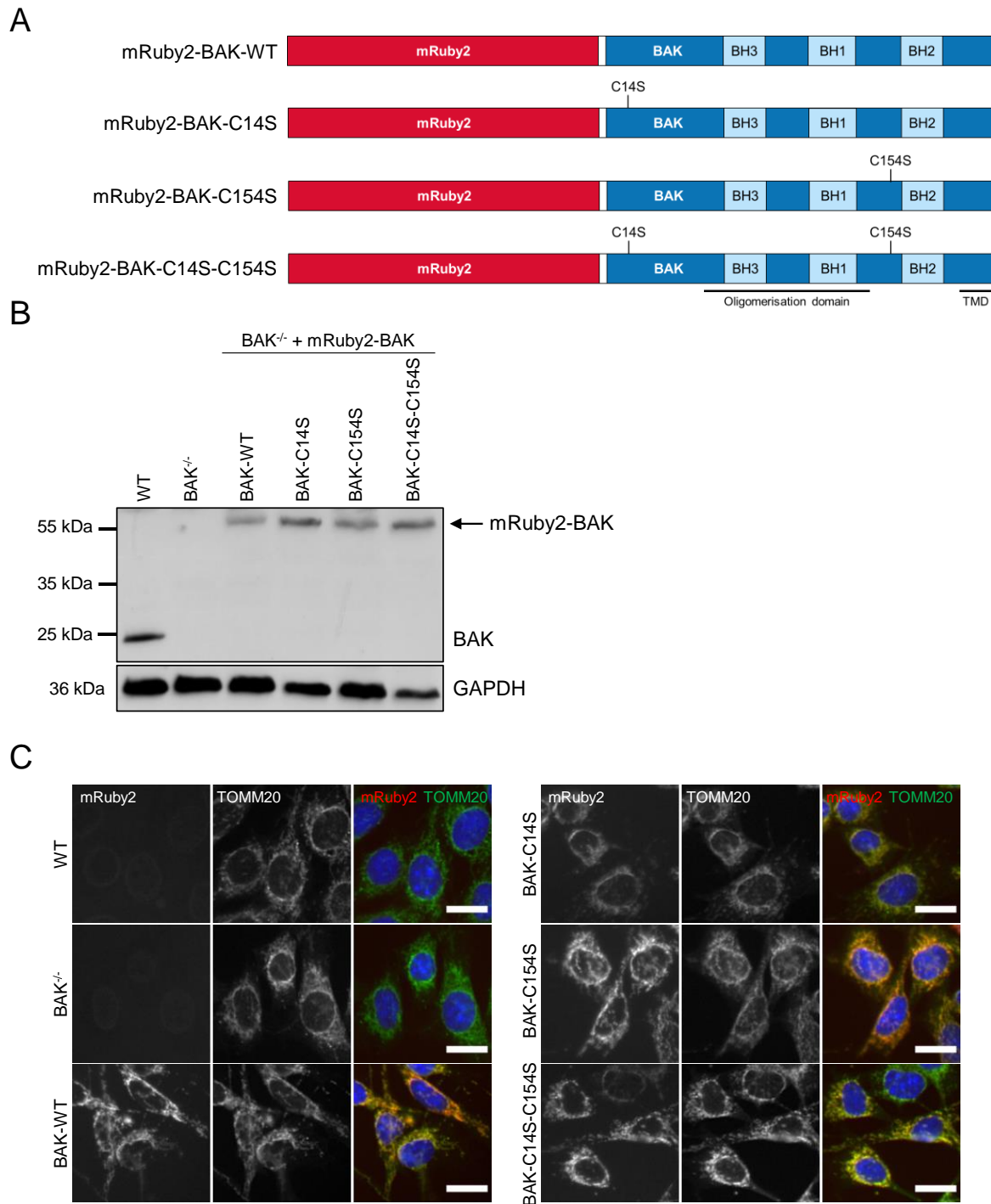
Figure 25. BAK cysteine mutants are expressed and co-localize with TOMM20 in BAK^{-/-} MEFs. (A) Schematic depiction of BAK fused to the fluorescent protein mRuby2 that was expressed in BAK$^{-/-}$ MEFs. Mutation of BAK cysteine residues C14 and C154 is indicated. BH1-3: BCL-2 homology domain 1-3, TMD: transmembrane domain. (B) Lysates of WT and BAK$^{-/-}$ MEFs and BAK$^{-/-}$ MEFs reconstituted with mRuby2-BAK-WT and BAK cysteine mutants were analyzed by Western blotting for expression of BAK. GAPDH was used as loading control. Representative blot of two experiments is shown. (C) Immunofluorescence imaging of WT and BAK$^{-/-}$ MEFs and BAK$^{-/-}$ MEFs reconstituted with mRuby2-BAK-WT and BAK cysteine mutants stained against TOMM20. Scale bar = 20 μm. Representative images of three independent experiments are shown.

5.3.6 Cysteine residues in BAK are crucial for Auranofin-, but not Etoposide-induced cell death

To evaluate if the reconstituted mRuby2-BAK MEFs are susceptible to cell death, these cells were treated with Etoposide and Auranofin. Intriguingly, expression of WT BAK in BAK^{-/-} MEFs resensitized cells to Etoposide treatment (Figure 26 A). Interestingly, BAK^{-/-} MEFs expressing the BAK cysteine mutants were more sensitive to Etoposide-induced cell death compared to BAK^{-/-} MEFs. MEFs expressing the double cysteine mutant BAK-C14S-C154S were equally sensitive to Etoposide treatment as MEFs expressing WT BAK. Together, these observations are in line with earlier findings showing that cysteine residues in BAK are not required for BAK function in apoptosis [157]. Importantly, these findings confirm the functionality of mRuby2-BAK-WT and demonstrate that the BAK cysteine mutants are capable of inducing apoptotic cell death.

Re-expression of WT BAK in BAK^{-/-} MEFs also sensitized cells to Auranofin treatment confirming the importance of BAK for Auranofin-induced cell death (Figure 26 B). Interestingly, BAK^{-/-} MEFs expressing BAK cysteine mutants were significantly less sensitive to Auranofin-induced cell death and MEFs expressing the double cysteine mutant were especially resistant to Auranofin treatment.

These results further underscore the differences in cell death induced by Etoposide and Auranofin in MEFs. Mutating either one or both cysteines in BAK interferes with its function in Auranofin-induced cell death, but not in Etoposide-induced apoptosis, again highlighting the importance of BAK oxidation during Auranofin-induced cell death.
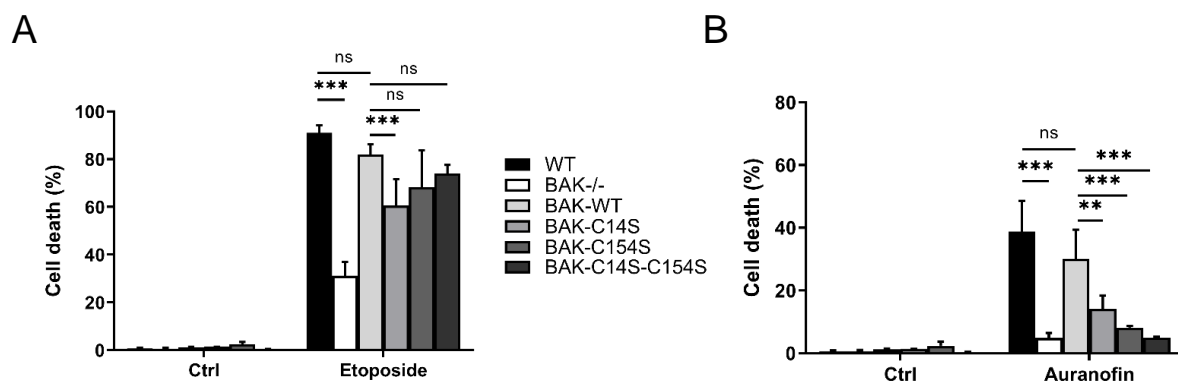
Figure 26. BAK$^{-/-}$ MEFs expressing BAK cysteine mutants are sensitive to Etoposide, but not Auranofin treatment. WT and BAK$^{-/-}$ MEFs and BAK$^{-/-}$ MEFs reconstituted with mRuby2-BAK-WT and BAK cysteine mutants were treated with 10 µM Etoposide (A) or 4 µM Auranofin (B) for 24 h. Cell death was measured using Sytox Green/Hoechst staining and fluorescence microscopy. Mean and SD of at least three experiments performed in triplicate are shown. Significances were assessed by one-way ANOVA followed by Tukey's post-hoc test, ns: not significant; ** p < 0.01; *** p < 0.001.

5.3.7 The BAK BH3 domain is needed for Auranofin- and Etoposide-induced cell death

Next, we introduced point mutations in the BAK BH3 domain to evaluate whether this domain is needed for induction of cell death upon treatment with Auranofin. The BH3 domain is critical for BAK dimerisation and interaction with BCL-2 proteins [157]. Point mutations in the BH3 domain of human BAK have been previously described and resulted in a loss of function [157]. We mutated the corresponding residues in murine BAK (I79 and D81) and expressed these mutants in BAK$^{-/-}$ MEFs (Figure 27 A). Both mutants were expressed to similar levels as endogenous BAK as determined by Western blotting (Figure 27 B). Mitochondrial localization of the BAK BH3 mutants was demonstrated using immunofluorescence analysis and staining against TOMM20 (Figure 27 C). As expected, the BAK BH3 mutants failed to induce cell death in BAK$^{-/-}$ MEFs upon stimulation with Etoposide (Figure 27 D). Interestingly, expression of these mutants also failed to resensitize BAK$^{-/-}$ MEFs to Auranofin-induced cell death (Figure 27 E). These results underscore the importance of the BH3 domain for BAK function in Etoposide- and Auranofin-induced cell death.
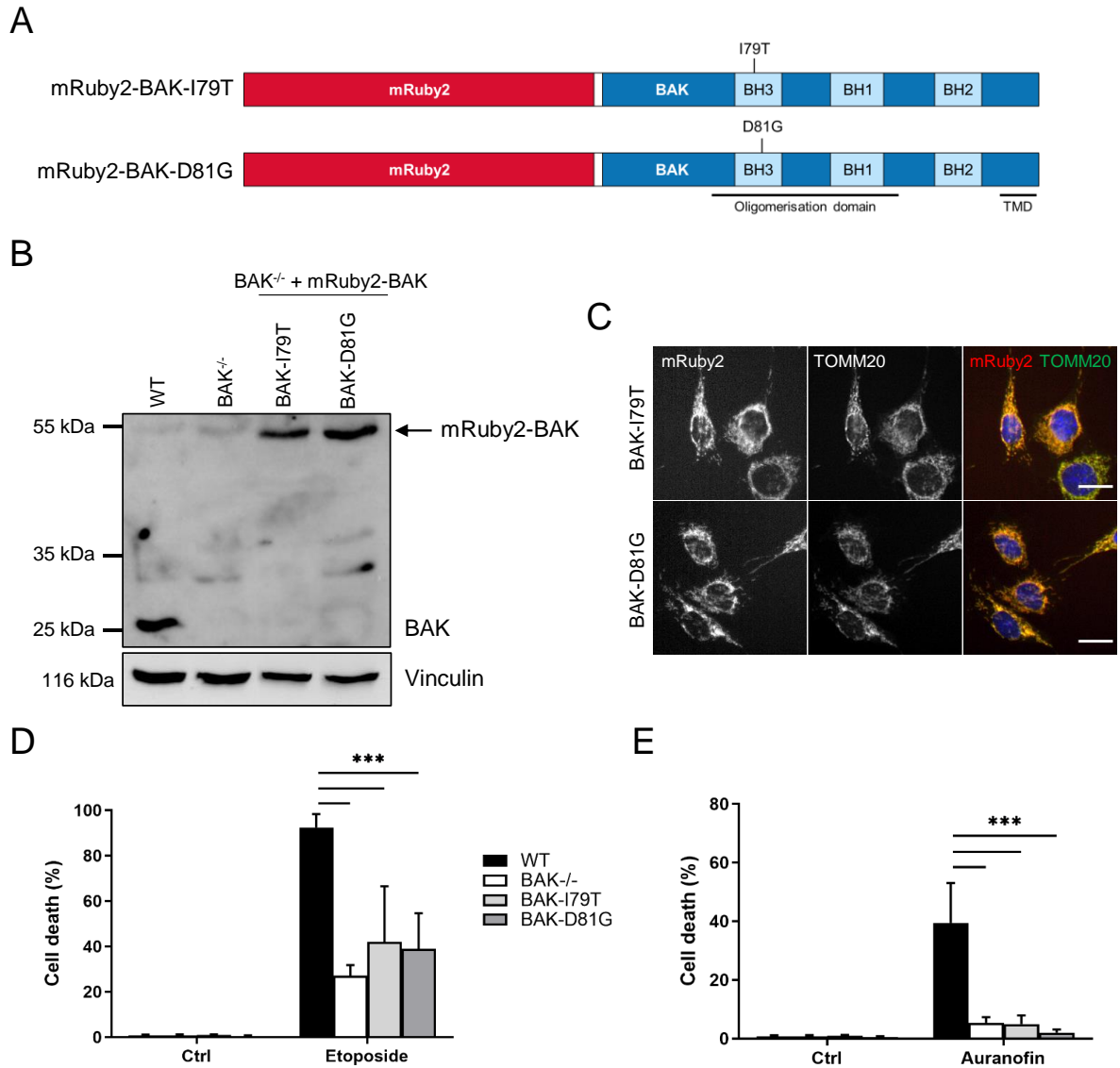
Figure 27. BAK BH3 mutants localize to mitochondria and do not resensitize BAK$^{-/-}$ MEFs to Auranofin- or Etoposide-induced cell death. (A) Schematic depiction of mRuby2-BAK with mutations in the BH3 domain. BH1-3: BCL-2 homology domain 1-3, TMD: transmembrane domain. (B) Lysates of WT and BAK$^{-/-}$ MEFs and BAK$^{-/-}$ MEFs reconstituted with mRuby2-BAK-I79T and mRuby2-BAK-D81G were analyzed by Western blotting for expression of BAK. Vinculin was used as loading control. Representative blot of two experiments is shown. (C) Immunofluorescence imaging of BAK$^{-/-}$ MEFs reconstituted with mRuby2-BAK-I79T and mRuby2-BAK-D81G stained against TOMM20. Scale bar = 20 μm. Representative images of two independent experiments are shown. (D, E) WT and BAK$^{-/-}$ MEFs and BAK$^{-/-}$ MEFs reconstituted with mRuby2-BAK-I79T and mRuby2-BAK-D81G were treated with 10 μM Etoposide (D) or 4 μM Auranofin (E) for 24 h. Cell death was measured using Sytox Green/Hoechst staining and fluorescence microscopy. Mean and SD of three experiments performed in triplicate are shown. Significances were assessed by one-way ANOVA followed by Tukey's post-hoc test, *** $p < 0.001$.

5.3.8 Mass spectrometry-based interaction analysis reveals changes in BAK interactome upon oxidation

Our previous results showed that cysteine residues in BAK are essential for Auranofin-induced cell death. To further understand the role of BAK in Auranofin-induced cell death and the relevance of the oxidation-sensitive BAK cysteine residues, we analyzed WT BAK and BAK-C14S-C154S protein-protein interactions during Auranofin treatment using an unbiased approach.

For this, BAK$^{-/-}$ MEFs expressing either WT BAK or BAK-C14S-C154S were treated with 4 µM Auranofin for 4 h. NEM was added before harvesting and throughout lysis to preserve the oxidation state of the proteins. Next, mRuby2-BAK and interaction partners were enriched using an RFP-trap that specifically recognizes mRuby2, followed by LC/MS. Intriguingly, we could identify oxidation of WT BAK on C14 after Auranofin treatment. Unfortunately, BAK C154 was not covered in this analysis and the oxidation state of this cysteine could not be determined.

In total, 396 proteins were identified in the analysis (Figure 28 A, Table 25). Binding of 121 proteins was independent of the presence of cysteine residues in BAK, however, 89 proteins bound preferentially to WT BAK. With this screen, we identified the well described BAK interaction partners BAX and BCL-X$_L$ that interact with BAK through their BH3 domain [149, 213]. These proteins were identified in both WT BAK- and BAK-C14S-C154S-containing samples and were not significantly enriched in either condition. This finding suggests that mutation of the BAK cysteine residues does not alter its BH3 domain which is essential for the regulation and execution of intrinsic apoptosis and explains why Etoposide-induced cell death is not reduced in MEFs expressing BAK-C14S-C154S.

Next, the 50 most significantly enriched BAK-WT and BAK-C14S-C154S interaction partners were sorted by significance and displayed in a heat-map according to fold change (log$_2$(BAK-WT/BAK-C14S-C154S)) (Figure 28 B). Proteins that were identified in the BAK-WT sample clustered in many different cellular processes that involve oxidation-reduction processes, vesicle-mediated transport, organic substance transport, localization and membrane organization (Figure 28 C). The uncharacterized protein C4orf3 homolog was enriched over 60-fold in BAK-WT expressing MEFs and was previously described as a regulator of calcium signaling [214]. Interestingly, we identified RAB11A/RAB11B that was also identified in the redox proteomics screen upon Auranofin treatment in Jurkat FD cells and that is involved in membrane trafficking (Figure 19 C).
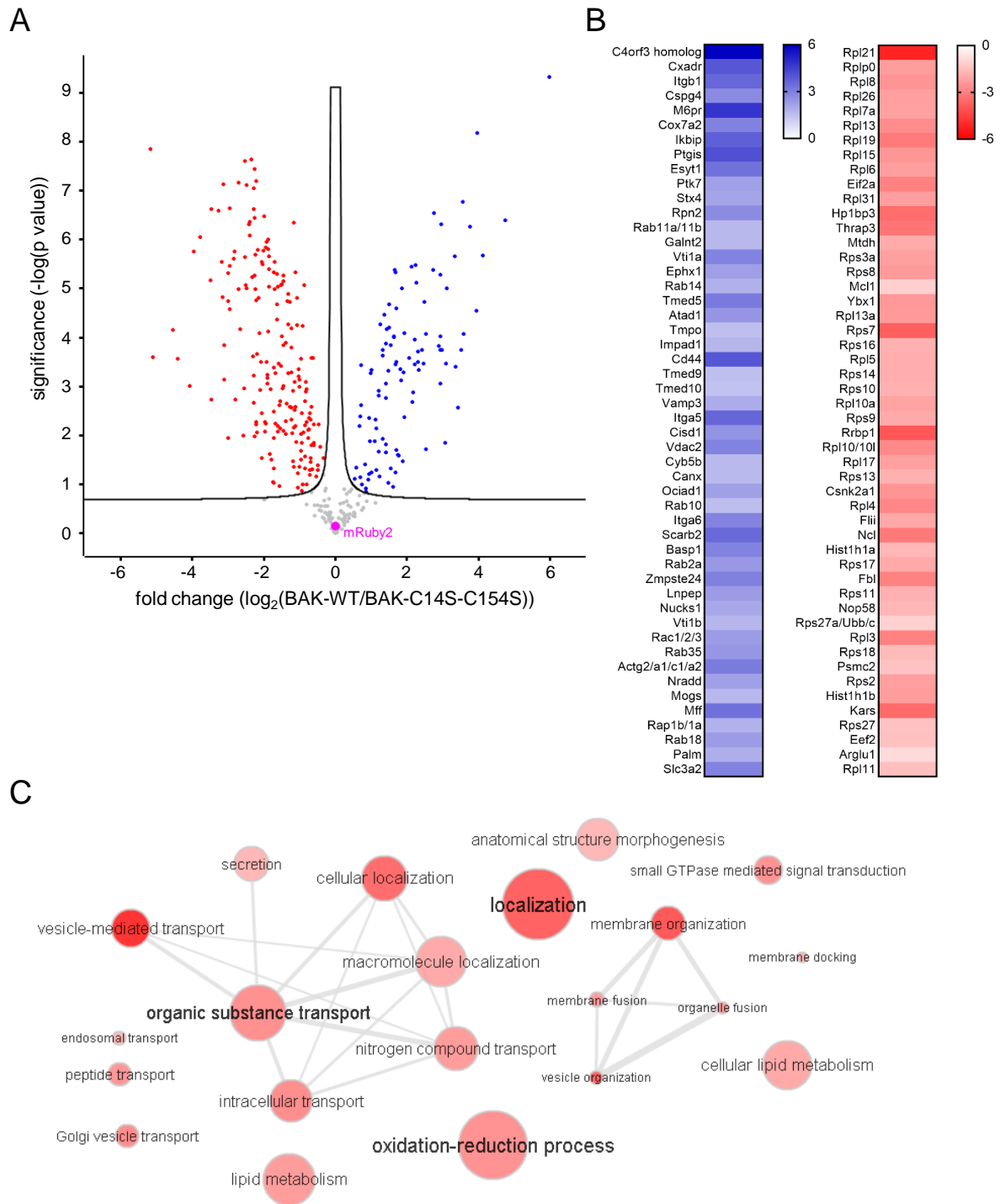
Figure 28. Cysteine residues influence BAK interactome upon Auranofin treatment. (A) BAK^{-/-} MEFs expressing mRuby2-BAK-WT or mRuby2-BAK-C14S-C154S were treated with 4 µM Auranofin for 4 h. Lysates were subjected to immunoprecipitation against mRuby2 and enriched proteins were analyzed by LC/MS. Results were normalized for mRuby2 expression (pink) and samples from mRuby2-BAK-WT were compared to samples from mRuby2-BAK-C14S-C154S expressing cells. Significant differentially enriched proteins are indicated in blue (up-regulated) and red (down-regulated) ($p < 0.05$, fold change > 1). Figure was generated by I. Wittig. (B) Top 50 differentially bound proteins are shown (gene names). Proteins significantly enriched in the BAK-WT sample are shown in blue, proteins significantly more bound to BAK-C14S-C154S in red. The lists were sorted by significance and colors assigned according to fold change (log2(BAK-WT/BAK-C14S-C154S)). (C) Clustering of proteins significantly enriched in mRuby2-BAK-WT expressing cells according to their involvement in cellular processes.

76

Proteins that were significantly more bound to BAK-C14S-C154S than to WT BAK were mainly ribosomal proteins (Figure 28 B). Of note, the anti-apoptotic BCL-2 protein MCL-1, a known binding partner of BAK [149], was among the 50 most significantly enriched proteins in the BAK-C14S-C154S sample.

Next, we validated the interaction of WT BAK with two proteins that were identified in the MS analysis, mitochondrial fission factor (MFF) and vesicle transport through interaction with t-SNAREs homolog 1A (VTI1A), using immunoprecipitation against mRuby2 and Western blotting. We determined interaction of BAK-WT with both tested proteins upon Auranofin treatment (Figure 29). Enrichment of MFF and VTI1A with BAK-C14S-C154S upon Auranofin treatment was weaker compared to the interaction with WT BAK, highlighting the importance of the BAK cysteine residues for this interaction.

In conclusion, we could demonstrate that Auranofin induced BAK-dependent cell death in MEFs. This cell death was caspase-independent, but could be rescued using ROS scavengers. BAK cysteine residues, as well as the BH3 domain, were critical for the induction of cell death upon Auranofin treatment. Of note, we could demonstrate Auranofin-induced BAK oxidation on C14. Additionally, we highlighted the importance of the BAK cysteine residues for the interaction of BAK with various proteins upon stimulation with Auranofin.

A

B
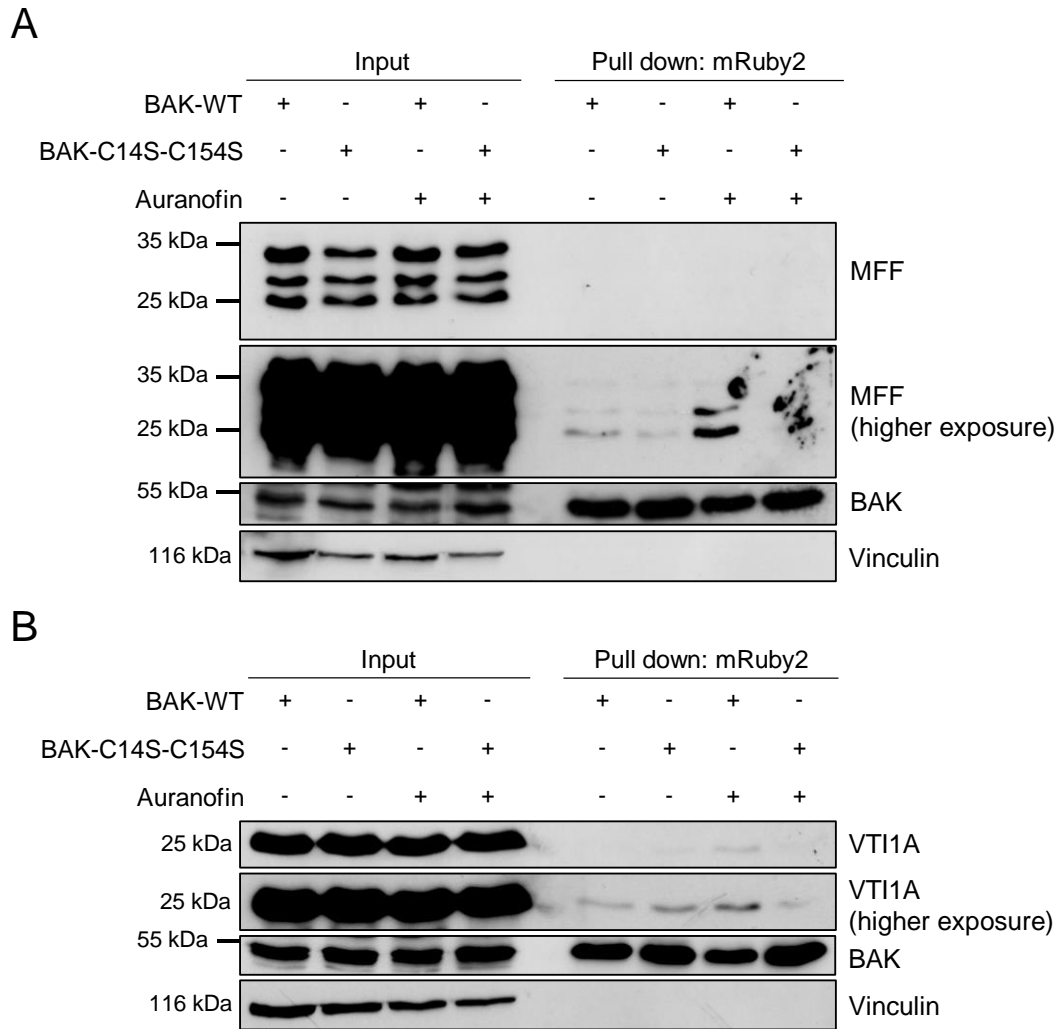
Figure 29. Interaction of mRuby2-BAK-WT with MFF and VTI1A is induced upon Auranofin treatment. BAK$^{-/-}$ MEFs reconstituted with mRuby2-BAK-WT or mRuby2-BAK-C14S-C154S were treated with 4 μM Auranofin for 4 h or left untreated. Lysates were subjected to immunoprecipitation against mRuby2 and enriched proteins were analyzed by SDS-PAGE and Western blotting. Pull-down of mRuby2-Bak was determined by blotting against BAK and enrichment of MFF (A) and VTI1A (B) was analyzed. Vinculin served as loading control. Representative blots of two independent experiments are shown.

6 Discussion

The aim of this study was to evaluate the potential of inhibitors of the Trx system for ALL therapy and to further understand the regulation of programmed cell death by ROS. In the first part of the study, we demonstrated that ALL cell lines are vulnerable to treatment with the Trx1-inhibitor PX-12. Focusing on Jurkat FD cells, we demonstrated that PX-12 induces intrinsic apoptosis and increases ROS levels. In the following part of the study, we revealed how the redox proteome of Jurkat FD cells becomes altered upon inhibition of TrxR with Auranofin. We identified oxidation of proteins involved in posttranslational modification and metabolism upon Auranofin treatment. In the third part of the study, we demonstrated that BAK oxidation is critical for Auranofin-induced cell death in MEFs. Furthermore, we highlighted the importance of BAK cysteine residues for its interaction with proteins involved in mitochondrial fission and vesicle transport, which might be important for mediating cell death in MEFs upon oxidative stimuli.

6.1 Unravelling the mechanism of PX-12-induced cell death in ALL cell lines

6.1.1 NOXA: An important player in PX-12-induced cell death

Extending the long-term survival of ALL patients suffering from relapse or belonging to a high-risk group is still challenging, highlighting the need for novel treatment options. Therefore, we explored the potential of the Trx1-inhibitor PX-12 to induce cell death in different ALL cell lines. We demonstrated that the Jurkat FD, KOPN-8 and REH ALL cell lines are sensitive to PX-12 treatment. Further experiments in Jurkat FD cells revealed that PX-12 induces mitochondria-mediated apoptosis, as BAK was rapidly activated upon PX-12 treatment and knock-down of BAK or the BH3-only protein NOXA could rescue cell death. Furthermore, rapid cleavage of caspase-9 and caspase-3 could be detected after PX-12 treatment and PX-12-induced cell death was inhibited by pre-treatment with the caspase inhibitor zVAD.fmk. In line with these findings, PX-12-mediated apoptosis induction was also shown in other cancer cell lines, such as lung cancer cells and cervical cancer cells [116, 202].

We further demonstrated that knock-down of NOXA attenuates PX-12-induced BAK activation and cell death. NOXA preferentially binds to MCL-1, which frees BAK and promotes BAK

oligomerization, MOMP and subsequent apoptosis [149, 151]. Indeed, NOXA binding targets MCL-1 for proteasomal degradation [149, 215]. NOXA is usually short-lived and rapidly degraded by the proteasome to ensure cell survival [216]. Notably, the activity of the 26S proteasome can be controlled by oxidation [217-219] and NOXA stabilization upon H_2O_2 treatment has been shown to rely, at least in part, on proteasome inhibition [220]. In line with these findings, we also observed increased NOXA levels upon PX-12 treatment. Whether this increase in NOXA protein levels is due to a PX-12-mediated decrease in proteasome activity needs to be determined.

Additionally, intracellular stress signals can activate NOXA expression. NOXA expression is regulated by several transcription factors, including activating transcription factor 4 (ATF4), p53, HIF-1, E2F-1 and c-MYC [220-224]. Since p53 is mutated in Jurkat cells, transcriptional regulation of NOXA by p53 can be excluded in this study [206, 225]. Interestingly, a role for the transcription factor ATF4 has been implicated in the control of NOXA expression during H_2O_2-induced intrinsic apoptosis in Jurkat cells [220]. Of note, ATF4 is activated by a variety of different cellular stress signals, including ER stress, hypoxia, nutrient deprivation and oxidative stress [226]. Importantly, ATF4 can promote adaptation to those stresses, however ATF4 induction has also been shown to mediate p53-independent apoptosis in leukemic cells [227]. Therefore, additional experiments are required to study the role of ATF4 and the transcriptional upregulation of NOXA in PX-12-treated ALL cells.

Of note, silencing of NOXA only partially rescues cell death induction upon PX-12 treatment, which might be due to insufficient siRNA-mediated knock-down. Alternatively, additional BH3-only proteins could be activated upon PX-12 treatment and contribute to cell death induction. Alternatively, PX-12 treatment could also lead to the activation of other apoptosis-inducing proteins or the inactivation of apoptosis-inhibiting proteins that were not investigated in this study.

6.1.2 Involvement of ROS in PX-12-induced cell death

PX-12 induced an increase in cellular and mitochondrial ROS levels in Jurkat FD cells, which could be decreased by pre-treatment with the thiol-containing GSH-precursor NAC. NAC pre-treatment also rescued PX-12-induced cell death. However, pre-treatment with the non-thiol-containing scavengers α-Toc or MnTBAP could neither reduce ROS levels, nor inhibit cell death induction upon PX-12 treatment. The relevance of the GSH pool in counteracting PX-12 cytotoxicity was reported previously. Firstly, several studies demonstrated a rescue of PX-12-induced cell death through NAC or GSH treatment in different cancer cell lines [113, 115, 202,

228]. Secondly, depletion of the cellular GSH pool has been reported after PX-12 treatment [116, 202] and GSH could act as an antioxidant and free radical scavenger, thereby limiting PX-12 cytotoxicity. It is, however, also feasible that GSH reacts directly with PX-12, which could limit its activity. A similar mechanism has been described for Auranofin, in which the gold ion undergoes adduct formation with GSH [229]. PX-12 does not contain a gold ion, however it has reported reactivity towards certain plasma components [122]. This hypothesis is further underscored by our findings that NAC, but not the non-thiol containing ROS scavengers, potently inhibit PX-12-induced cell death. By doing so, NAC could lead to the inactivation of PX-12, either directly, or through replenishment of the GSH pool. Further experiments are needed to assess the reactivity of PX-12 towards thiol-containing compounds.

As non-thiol containing scavengers had no effect on ROS levels and cell death induced by PX-12, we hypothesize that ROS production does only in part contribute to PX-12 cytotoxicity. Furthermore, knock-down of BAK or pre-treatment with pan-caspase inhibitor zVAD.fmk inhibited the increase in ROS seen after PX-12 treatment. An increase in ROS levels upon intrinsic apoptosis has been shown previously. For example, Cai et $al.$ could show that loss of cytochrome c inhibits the ETC and subsequently leads to increased $O_2^{\bullet-}$ production [172]. Interestingly, Ricci et $al.$ could demonstrate that caspases, which are activated upon cytochrome c release, lead to the disruption of complex I and II of the ETC and increased ROS production [230]. Therefore, it is possible that these effects also contribute to the elevated ROS levels that we observed upon PX-12 treatment.

Interestingly, PX-12 treatment led to increased PRDX3 dimer formation prior to the onset of cell death in Jurkat FD cells. Oxidized PRDX3 becomes usually reduced by mitochondrial Trx2 [231]. So far, PX-12 has only been described as an inhibitor of Trx1 [112]. However, inhibition of Trx2 by PX-12 cannot be ruled out as both Trx1 and Trx2, share the same active site motif that can be targeted by PX-12 [112, 232]. Of note, Trx2 has been reported to limit mitochondrial ROS production and apoptosis [233, 234]. A potential involvement of Trx2 in apoptosis induction could be related to its interaction with mitochondria-located ASK-1, which mediates JNK-independent apoptosis, cytochrome c release and caspase activation. Binding of Trx2 to ASK-1 might interfere with this pro-apoptotic function [235]. PX-12-mediated inhibition of Trx2 could release ASK-1 and contribute to the induction of intrinsic apoptosis. Additionally, the significance of Trx2 for cell survival might depend on its function to reduce PRDX3, since a crucial role for PRDX3 in maintaining mitochondrial function has been reported [236]. How exactly PRDX3 sustains mitochondrial membrane potential is not clear, but it might be possible that PRDX3 scavenges free radicals, thereby limiting the oxidation of components of the ETC or the mitochondrial membrane. Whether PX-12-mediated inhibition of Trx2 directly or through its ASK1 interaction contributes to cell death remains to be elucidated.

6.1.3 Clinical implications of PX-12 treatment in ALL

Understanding the mechanisms of PX-12-induced cell death in ALL is important to further advance its therapeutic potential. So far, PX-12 has been assessed in phase I and II clinical trials in solid tumors, but up till now, no significant antitumor activity could be shown [119-122]. The toxicity profile of PX-12 was, however, low and a Trx1 decrease in the plasma of study participants could indeed be detected [121]. Our study showed induction of cell death in all three tested ALL cell lines upon PX-12 treatment, therefore it might be possible that hematological malignancies could be more susceptible to PX-12 administration than solid cancers. In our experiments, relatively high PX-12 concentrations were applied that might be hard to achieve *in vivo*, questioning the applicability of PX-12 as a single agent therapy. Unraveling its mechanism of action could help to find novel combination therapies with a better therapeutic potential and need for lower doses. Indeed, PX-12-based combination therapies have been demonstrated previously, e.g. with arsenic trioxide [237], NF-κB inhibitors (Raninga 2015), or with 5-fluoruracil [113] or temozolomide [238] as a chemosensitizing agent.

As we could demonstrate an important role for pro-apoptotic BCL-2 proteins in PX-12-mediated cell death in Jurkat FD cells, drugs that limit the availability of anti-apoptotic BCL-2 proteins might sensitize cells to PX-12 treatment. Therefore, combining PX-12 with BH3 mimetics like S63845, which targets MCL-1 [239], could be a promising approach.

Additionally, it could be beneficial to combine PX-12 with compounds that promote apoptosis induction. Interestingly, Auranofin could sensitize ALL cell lines to apoptosis induced by the SMAC mimetic LCL161 [187]. SMAC mimetics antagonize inhibitor of apoptosis proteins (IAPs) that inhibit apoptosis induction either through inhibition of caspases or promoting pro-survival signaling pathways [240]. Combining PX-12 with SMAC mimetics might be a promising approach in ALL, as upregulation of IAP proteins has been described in primary ALL samples [241].

Additionally, drugs that target additional antioxidant systems, such as the GSH-depleting agents buthionine sulfoximine (BSO) [242] or Erastin [168], might further increase PX-12-induced ROS levels and promote harmful protein oxidation in ALL cells.

Interestingly, PX-12 has also been described as an anti-platelet [243] and an anti-microbial agent [100], so understanding the mechanisms of action could help to further repurpose this drug for diseases besides cancer.

6.2 Auranofin-induced changes in protein oxidation in Jurkat FD cells

Although a link between ROS and apoptosis has been established for almost 30 years [244, 245], how redox signaling precisely controls the induction and execution of cell death is still not completely understood. Using Auranofin, a well-described inhibitor of TrxR, we aimed to further understand the role of ROS as signaling molecules in cell death.

Auranofin, like PX-12, induced mitochondria-mediated apoptosis in Jurkat FD cells that could be rescued with either knock-down of BAK or pre-treatment with zVAD.fmk. These results were expected, as Auranofin has been described to induce intrinsic apoptosis in Jurkat cells [104]. As we were interested in identifying changes in protein oxidation upon cell death induction, we verified ROS increase shortly after Auranofin treatment. To identify Auranofin-induced protein oxidation, we employed an untargeted approach and performed a BIAM Switch Assay coupled to LC/MS. Using a similar approach, Loewe *et al.* could recently identify global changes in protein oxidation induced by NOX4, as well as a novel redox target of NOX4 [209]. Indeed, Auranofin treatment induced oxidation of over 200 proteins. Among those, we identified several known proteins that are oxidized upon Auranofin treatment, like members of the thioredoxin family including Trx1 and Trx2 that are reduced by the Auranofin targets TrxR1 and TrxR2. These results underscore the specificity of the TrxR inhibitor Auranofin and in line with these findings, we also identified oxidized PRDX1, PRDX2 and PRDX3, which are usually reduced by Trx1 and Trx2. In accordance with increased cytosolic and mitochondrial ROS levels, we could further identify oxidation of cytosolic and mitochondrial Trx and PRDX isoforms.

Additionally, we identified several proteins that have previously been described to be oxidized. For example, BCAT1, an aminotransferase involved in glutamate synthesis, whose activity is regulated through oxidation [246]. In addition, we have also identified PHPT1, a histidine phosphatase, that is known to be oxidized by H_2O_2 [247]. Furthermore, the tyrosine phosphatase PTP4A2 (also known as PRL-2) has also been described to be oxidized upon H_2O_2 treatment and could be reduced by thioredoxin-like protein 1 (also known as TRP32) [248].

Finally, we could validate Auranofin-induced oxidation of two proteins, APIP and PRMT1, by a BIAM Switch Assay followed by Western blotting.

APIP was initially described as an inhibitor of mitochondrial apoptosis as it competes with caspase-9 for binding to APAF-1 and thereby impedes caspase activation [249]. Additionally, APIP plays a role in the methionine salvage pathway as a 5-methylthioribulose-1-phosphate dehydratase [250-252]. Methionine is an essential amino acid and is required for protein

synthesis, methylation of DNA and proteins and synthesis of GSH [250]. Of note, metabolites of the methionine salvage pathway were also described to induce apoptosis [253, 254]. Furthermore, APIP was reported to regulate pyroptosis, an inflammatory type of programmed cell death [251]. Interestingly, Ko *et al.* could show that the APIP cysteine mutant C97A is catalytically inactive and impairs the function of APIP in methionine salvage. APIP C97A was however still able to suppress cell death induced by caspase-9 overexpression or Etoposide treatment [251, 252]. Of note, APIP C147 was identified as a possible site for H_2O_2-induced oxidation [255]. Whether oxidation of APIP at C147 alters its function was however not studied. Unfortunately, we could not identify the specific APIP oxidation site in our analysis necessitating further experiments. Whether APIP oxidation interferes with its function in apoptosis or the methionine salvage pathway remains to be elucidated.

PRMT1 is the major arginine methyltransferase in humans and involved in various cellular processes including regulation of transcription, RNA processing, DNA repair and signal transduction [256]. Of note, PRMT1 was reported to mediate oxidative stress-induced apoptosis via arginine methylation of FOXO1, which inhibits phosphorylation by Akt leading to nuclear translocation and induction of BIM expression [256]. Arginine methylation of BAD by PRMT1 was also shown to attenuate its phosphorylation by Akt. Methylation of BAD induces its mitochondrial translocation and interaction with BCL-X$_L$ promoting apoptosis induction [257]. These studies highlighted a pro-apoptotic function of PRMT1-mediated arginine methylation. On the contrary, PRMT1 also has anti-apoptotic functions, since PRMT1-mediated methylation of ASK-1 prevents ASK-1 activation by H_2O_2 and down-stream pro-apoptotic signaling [258]. Whether PRMT1 signaling induces or inhibits apoptosis might therefore depend on various factors, including the cell line, the stimulus or the PRMT1 isoform that is expressed. Interestingly, Morales *et al.* demonstrated that PRMT1 is a redox-sensitive enzyme whose methyltransferase activity can be reduced by H_2O_2-induced oxidation of at least two cysteine residues [259]. It might be possible that Auranofin-induced oxidation of PRMT1 could interfere with the anti-apoptotic function to promote cell death, but further experimentation is necessary to fully understand the role of PRMT1 oxidation in apoptosis induction.

In conclusion, we were able to detect changes in the redox proteome of Auranofin-treated cells. Determining whether these changes alter specific protein functions and signaling in apoptosis will be the interest of future research.

6.3 BAK oxidation in Auranofin-induced cell death in MEFs

6.3.1 Auranofin induces caspase-independent cell death in MEFs

Since we demonstrated BAK-dependent induction of intrinsic apoptosis upon Auranofin treatment in Jurkat FD cells, we assumed that Auranofin treatment would also trigger apoptosis in MEFs. Surprisingly, Auranofin-induced cell death in MEFs could not be rescued by pre-treatment with the caspase-inhibitor zVAD.fmk. The necroptosis inhibitor Nec-1s likewise failed to protect MEFs from Auranofin-induced cell death. Interestingly, we could demonstrate a ROS-dependency of this cell death mode. As cells were able to undergo caspase-dependent apoptosis upon Etoposide treatment, all proteins required for apoptosis execution are functionally expressed. It is possible that Auranofin induces caspase-independent apoptosis in MEFs since following MOMP, apoptosis inducing factor (AIF) and endonuclease G (EndoG) could be released, which translocate into the nucleus. AIF can then induce chromatin condensation and DNA fragmentation leading to cell death [260]. Of note, H_2O_2 treatment was shown to induce AIF release and nuclear translocation in HeLa cells [261], but whether Auranofin treatment leads to the release of AIF or EndoG needs to be determined.

6.3.2 BAK is oxidized upon Auranofin treatment

With use of the BIAM Switch Assay, we could demonstrate BAK oxidation upon Auranofin, but not Etoposide treatment, which could be validated using MS analysis that demonstrated oxidation of BAK C14 upon Auranofin treatment. Oxidation of BAK was reported previously by Rohde *et al.* upon a necroptotic stimulus, but the functional roles of this oxidation were not investigated [190]. Interestingly, H_2O_2-induced oxidation of BAX on cysteine 62 has been reported previously to promote its mitochondrial translocation and induction of apoptosis [262, 263].

As mutating one or both cysteine residues in BAK decreased Auranofin-, but not Etoposide-induced cell death in MEFs, we suggest that BAK oxidation is essential for cell death upon Auranofin treatment. Interestingly, cysteine-less BAK has previously been described to be able to form apoptotic pores in the mitochondrial membrane that lead to cytochrome c release [157, 264]. As BAK cysteine mutants can apparently still induce MOMP, but not cell death upon Auranofin treatment, we hypothesize that BAK has a different function in Auranofin-induced cell death. This hypothesis is underscored by the finding that binding of BAX and BCL-XL to

BAK is not altered upon mutation of its cysteine residues and might therefore not influence cell death induced by Auranofin treatment. We did however observe that BAK^{-/-} MEFs expressing BH3-mutated BAK were less vulnerable to Auranofin. As this domain is important for the interaction of BAK with various proteins and the formation of homodimers [157, 265, 266], it is possible that this domain is also needed for the non-apoptotic functions of BAK.

6.3.3 BAK has various functions in the cell

Apart from apoptosis induction, BAK has been implicated in autophagic cell death. BAK and BAX can be localized to lysosomes to induce lysosomal membrane permeabilization and subsequent cell death upon serum starvation [267]. Interestingly, this cell death was caspase-independent. Autophagy is an important cellular survival pathway that is induced upon nutrient deprivation [268]. Damaged mitochondria can also be eliminated by a specialized autophagic process called mitophagy. Mitochondria that are marked for mitophagy are engulfed by a phagophore forming the autophagosome that can subsequently fuse with lysosomes leading to the degradation of the mitochondria by lysosomal hydrolases. If the mitochondrial damage is still minor, mitochondrial fission or fusion can occur that redistributes damaged proteins and DNA. Interestingly, mitochondrial fission is also necessary for mitophagy as it targets the mitochondrial parts that are irreversibly damaged for mitophagic degradation. Dynamin-related protein 1 (DRP1), a member of the dynamin family, controls mitochondrial fission by forming constricting spirals around the mitochondria [269]. Recruitment of DRP1 to fission sites is mediated by MFF and mitochondrial dynamics proteins of 49 and 51 kDa (MID49 and MID51) [270-272]. Interestingly, we identified MFF in the BAK interaction MS analysis and could validate its interaction with WT BAK upon Auranofin treatment. Therfore, it is possible that Auranofin treatment leads to increased mitochondrial damage that induces mitophagy. We can speculate that BAK oxidation acts as a signal for damaged mitochondria, and via its interaction with MFF increases mitochondrial fission and ultimately mitophagy. This hypothesis is substantiated by the finding that proteins involved in vesicle-mediated transport, such as VTI1A, were also enriched in our MS analysis. Whether this pathway could act as a pro-survival mechanisms upon oxidative stress, or contribute to BAK localization in lysosomes and lysosomal membrane permeabilization and cell death remains unclear. Further analyses regarding BAK localization, mitochondrial network dynamics and lysosomal permeability upon Auranofin treatment will help to decipher this complex mechanism.

BAK and BAX can also be localized to the ER membrane. ER stress can induce BAK and BAX oligomerization and subsequent activation of caspase-12. Interestingly, ER-targeted BAK can

lead to calcium (Ca^{2+}) depletion of the ER [273]. Additionally, Scorrano *et al.* could demonstrate that BAK/BAX double knock-out MEFs release less Ca^{2+} from the ER upon H_2O_2 treatment, which results in decreased mitochondrial Ca^{2+} uptake and prevention of apoptosis. Expression of sarcoplasmic-endoplasmic reticulum Ca^{2+} ATPase (SERCA) that controls Ca^{2+} uptake in the ER could restore Ca^{2+} levels in the ER and oxidative stress-induced Ca^{2+} release [274]. Interestingly, Anderson *et al.* could identify two micropeptides, endoregulin (ELN) and another-regulin (ALN), which can inhibit SERCA activity in the ER [214]. Comparing the sequence of C4orf3 homolog, the peptide that displayed an over 60-fold enriched interaction with WT BAK in the MS analysis, revealed that it corresponds with the sequence of murine ALN that was reported by Anderson *et al.* [214]. Therefore, we could speculate that oxidative stimuli like Auranofin treatment triggers the interaction of BAK with ALN/C4orf3 homolog, which would free SERCA, resulting in increased ER Ca^{2+} uptake needed for cell death regulation by the ER. Further validation of this interaction and its impact on Ca^{2+} levels in the ER and mitochondria is necessary to strengthen this hypothesis.

Interestingly, BAK has also been connected to peroxisomal membrane permeabilization [275, 276]. As peroxisomes have important functions in many metabolic pathways, peroxisomal dysfunction is detrimental for the cell [277]. It was reported previously that voltage-dependent anion-selective channel protein 2 (VDAC2) regulates mitochondrial targeting of BAK and keeps it in an inactive monomeric conformation [278, 279]. Of note, the interaction of WT BAK with VDAC2 was identified in our MS screen as well. Hosoi *et al.* could demonstrate that VDAC2-deficiency leads to relocalization of BAK to peroxisomes and disturbance of peroxisome integrity. Interestingly, endogenous BAK can be localized to peroxisomes to control the release of catalase from peroxisomes, which could have an impact on cytosolic redox signaling and cellular survival. Importantly, BH3-only proteins BIM and PUMA were found to increase the BAK-dependent release of peroxisomal matrix proteins. This function of BAK was independent of BAX [275]. Whether Auranofin-treatment induces or inhibits peroxisomal targeting of BAK and thereby promotes cell death or cell survival necessitates further experimentation.

To conclude, we could demonstrate that Auranofin induces caspase-independent cell death in MEFs that depends on BAK oxidation. Which of the above described pathways is involved in Auranofin-induced cell death or whether several pathways contribute to the observed effects remains unclear at present and requires additional investigation.

6.4 Limitations and outlook

This study highlighted novel findings regarding redox regulation of cell death induction with a special focus on mitochondria and BAK. Several suggestions for future experiments have been discussed in the previous parts. However, there are some limitations to this study and some additional ideas that could be further explored.

First, we employed only pharmacological inhibitors of the thioredoxin system to induce ROS. We could validate their mechanism of action using a thioredoxin activity assay for PX-12-treated cells and identified oxidation of expected TrxR target proteins in the MS analysis of Auranofin-treated Jurkat FD cells. However, we cannot exclude off-target effects of the inhibitors that could potentially contribute to cell death induction as well. Therefore, genetic silencing of components of the Trx system might be useful to confirm and specifically study Trx-mediated effects. Additionally, it is necessary to validate the observed effects using further ROS-inducing stimuli to ensure the generality of the results.

Second, the analysis of PX-12-mediated cell death was performed in only one cell line. Extending the experiments to more cell lines, primary tumor samples and *in vivo* models will be necessary to fully elucidate the potential of PX-12 treatment for ALL therapy.

Third, Auranofin-induced cell death differed in Jurkat FD cells and MEFs. It will be interesting to explore why these cell lines react differently. It could be helpful to determine whether the proteins that were identified in the MS analysis in Jurkat FD cells are also oxidized in MEFs upon Auranofin treatment. Vice versa, identification of BAK interaction partners in Jurkat FD cells could shed light on the redox regulation of apoptosis. Additionally, further experiments are needed to validate the results from the MS analyses and to explore the functional impact of the changes observed upon Auranofin treatment in Jurkat FD cells and MEFs.

Additionally, oxidation of BAK C14 was identified in the MS analysis, but it is still unclear what kind of oxidative modification is induced upon Auranofin treatment. Employing BIAM Switch Assays with different reducing compounds or specialized reducing enzymes that reduce only certain oxidative modifications could help to answer this question. Additionally, whether BAK C154 is also oxidized upon Auranofin treatment needs to be determined. As we expressed all BAK mutants with a mRuby2-tag that also contains cysteines which can be oxidized, employing the BIAM Switch Assay followed by Western blotting to determine oxidation of each mutant is not possible. Therefore, further MS analyses are needed to cover more of the BAK sequence. Additionally, BAK mutants without the mRuby2-tag could be expressed.

7 Summary (Deutsche Zusammenfassung)

Leukämien sind neoplastische Erkrankungen des Blutes und des Knochenmarks und stellen die häufigsten Krebserkrankungen im Kindesalter dar. Die Leukämie, die hierbei am häufigsten auftritt, ist die akute lymphoblastische Leukämie (ALL), die durch maligne Transformation von lymphoiden Vorgängerzellen verursacht wird und zur Störung der normalen Hämatopoese führt. Zur Therapie der ALL wird häufig eine Kombination verschiedener Zytostatika verwendet, wobei in den letzten Jahren auch zielgerichtete, sogenannte „targeted" Therapien an Bedeutung gewonnen haben. Trotz steigender Überlebensraten sind die Aussichten für Erwachsene, Kleinkinder und Patienten, die einen Rückfall erleiden immer noch schlecht. Deswegen werden neue Therapieoptionen benötigt um die Überlebenschancen für alle Patienten zu vergrößern und die Nebenwirkungen der intensiven Chemotherapie zu verringern.

Reaktive Sauerstoffspezies (reactive oxygen species, ROS) sind Moleküle die durch die partielle Reduktion von Sauerstoff entstehen. Die am häufigsten in der Zelle vorkommenden ROS sind Wasserstoffperoxid (H_2O_2), das Hyperoxid-Anion ($O_2^{\bullet-}$) und das Hydroxyl-Radikal ($HO\bullet$). Wasserstoffperoxid ist weniger reaktiv als das Hyperoxid-Anion oder das Hydroxyl-Radikal, hat dadurch aber eine längere Halbwertszeit und kann zudem zelluläre Membranen durchdringen. ROS sind wichtige Signalmoleküle, die in einer Vielzahl von Signalwegen involviert sind. Hierbei spielt die Oxidation der Thiol-Gruppe von Cysteinen eine wichtige Rolle. Da hohe ROS-Level oxidativen Stress verursachen und zur irreversiblen Oxidation von zellulären Makromolekülen führen können, wird die Bildung und die Beseitigung von ROS stark kontrolliert. In der Zelle werden die meisten ROS in den Mitochondrien gebildet. Hierbei kann es während der Elektronentransportkette zur Bildung von Hyperoxid-Anionen aus molekularem Sauerstoff kommen. Hyperoxid-Anionen können weiterhin zu Wasserstoffperoxid dismutiert werden. Diese Reaktion wird durch die Mangan-Superoxid-Dismutase katalysiert. Weiterhin können ROS in der Zelle an Komplexen der NADPH-Oxidase (NOX) oder im endoplasmatischen Retikulum (ER) gebildet werden. Um ROS-Level im Gleichgewicht zu halten, exprimieren Zellen verschiedene antioxidative Moleküle und Enzyme. Das am häufigsten in der Zelle vorkommende nicht-enzymatische Antioxidans ist Glutathion (GSH). Ein wichtiges antioxidatives Enzym ist Katalase, welches die Reaktion von Wasserstoffperoxid zu Wasser und molekularem Sauerstoff katalysiert. Des Weiteren gibt es das Thioredoxin-System mit dem cytosolischen Thioredoxin 1 (Trx1), dem mitochondrialen Trx2 und den Thioredoxin Reduktasen (TrxR) 1, 2 und 3, die oxidiertes Trx in einer NADPH-abhängigen Reaktion reduzieren. Eine wichtige Funktion der Thioredoxine ist die Reduktion von oxidierten Peroxiredoxinen.

Interessanterweise wurden bei Krebszellen erhöhte ROS-Level gefunden, die zum Fortschreiten der Krebserkrankung und zur Metastasierung beitragen können. Die Oxidation von Proteinen in Wachstumsfaktor-Signalwegen kann beispielsweise die Signalwirkung verstärken und zur Zellproliferation beitragen. Des Weiteren können erhöhte ROS-Level zur Schädigung von DNA führen und die Mutagenese von Krebszellen erhöhen. Krebszellen profitieren zwar von erhöhten ROS-Leveln, jedoch sind zu hohe ROS-Level toxisch für die Zelle. Um sich daher vor oxidativer Schädigung zu schützen sind Krebszellen stark von antioxidativen Systemen abhängig. Dies macht Krebszellen besonders anfällig für Behandlungen die ROS induzieren. So konnte schon gezeigt werden, dass Inhibitoren des Trx-Systems das Wachstum von Tumorzellen hemmen und Zelltod in Tumorzellen verursachen. Die Anti-Tumor-Wirkung von Auranofin, einem TrxR-Inhibitor, wurde in verschiedenen Modellen gezeigt und bereits in klinischen Studien untersucht. Des Weiteren zeigte PX-12, ein irreversibler Trx1-Inhibitor, eine wachstumshemmende Wirkung in verschiedenen Krebszelllinien.

Der programmierte Zelltod spielt eine wichtige Rolle in der Entwicklung mehrzelliger Organismen, der Gewebehomöostase und auch als Antwort auf intra- und extrazelluläre Stress-Signale. Dabei stellt die Apoptose den am besten beschriebenen Mechanismus des programmierten Zelltodes dar. Apoptose kann entweder durch extrinsische oder intrinsische Signale aktiviert werden. Die extrinsische Apoptose kann durch Bindung verschiedener Liganden (TNFα, FAS Ligand, TRAIL) an ihre Rezeptoren (TNF Rezeptor 1, TRAIL Rezeptor 1 oder 2) an der Zelloberfläche initiiert werden. Diese Bindung löst die Bildung verschiedener Signalkomplexe aus, die letztendlich zur proteolytischen Spaltung und Aktivierung von Caspase-8 führt. Aktive Caspase-8 kann weiterhin Caspase-3 und -7 aktivieren, was zur Spaltung verschiedener Proteine und schließlich zum Zelltod führt.

Die intrinsische Apoptose kann durch verschiedene Stress-Signale wie DNA-Schädigung, Störungen des Zellzyklus oder oxidativem Stress, ausgelöst werden. Dieser Signalweg führt zur Permeabilisierung der äußeren Mitochondrienmembran und zum Freiwerden verschiedener Proteine, die Apoptose auslösen. Der intrinsische Apoptose-Signalweg wird durch die Familie der BCL-2 Proteine kontrolliert. Diese umschließt die anti-apoptotischen Proteine BCL-2, BCL-X$_L$, MCL-1, BCL-W und BCL2A1, die pro-apoptotischen Effektorproteine BAK und BAX und die pro-apoptotischen BH3-only Proteine BIM, BID, PUMA, NOXA, BAD und BMF. Wenn BAK oder BAX nicht durch anti-apoptotische BCL-2 Proteine inhibiert werden, können diese durch die Bindung spezieller pro-apoptotischer BH3-only Proteine aktiviert werden und dimerisieren. Diese Homodimere sind essentiell für die weitere Oligomerisierung von BAK und BAX und die Bildung von Poren in der äußeren Mitochondrienmembran. BH3-only Proteine können auch anti-apoptotische BCL-2 Proteine binden und so die

Interaktion dieser Proteine mit BAK und BAX stören. Unter normalen Umständen besteht ein Gleichgewicht zwischen pro- und anti-apoptotischen Proteinen, welches die Induktion der Apoptose verhindert. Durch Stress-Signale kann dieses Gleichgewicht zugunsten der pro-apoptotischen Proteine verschoben werden.

ROS und oxidativer Stress können programmierten Zelltod durch verschiedene Signalwege induzieren. So spielen ROS, unter anderem bei der Apoptose, der Nekroptose und der Ferroptose eine Rolle. Jedoch ist der genaue Mechanismus, der oxidative Signalwirkung und Zelltod verbindet nicht vollständig bekannt.

Da eine Störung der zellulären Redox-Homöostase während der Entwicklung und dem Verlauf der Leukämie berichtet wurde, war das Ziel dieser Arbeit, das Potential von Inhibitoren des Trx-Systems für die Therapie der ALL zu untersuchen. Zusätzlich wollten wir die Rolle von ROS und der dadurch versursachten Proteinoxidation bei der Induktion und der Ausführung des programmierten Zelltodes besser verstehen.

Im ersten Teil dieser Arbeit konnten wir zeigen, dass der Trx1-Inhibitor PX-12 in drei ALL Zelllinien eine dosis-abhängige Abnahme der Zellviabilität und eine Zunahme des Zelltodes verursachte. Weitere Analysen in FADD-defizienten (FD) Jurkat Zellen ergaben, dass die PX-12-Behandlung einen Anstieg von ROS und der durch Oxidation ausgelösten Dimerbildung von Peroxiredoxin-3 zur Folge hatte. Interessanterweise konnte Zelltod durch die Vorbehandlung mit dem Thiol-enthaltenden Antioxidans N-Acetylcysteine, aber nicht mit Thiol-freien Antioxidantien, inhibiert werden. Der durch PX-12-Behandlung induzierte Zelltod konnte weiterhin durch Vorbehandlung mit dem Caspasen-Inhibitor zVAD.fmk verhindert werden. Überdies führte die Behandlung mit PX-12 zur Spaltung von Caspase-3 und -9 und zur Aktivierung des pro-apoptotischen Effektorproteins BAK. Wir schlussfolgerten deshalb, dass die PX-12-Behandlung zur Aktivierung der intrinsischen Apoptose in Jurkat FD Zellen führte. Wir konnten weiterhin darlegen, dass der Knock-down von BAK oder die Vorbehandlung mit zVAD.fmk den PX-12-induzierten Anstieg der ROS-Level verhinderte. Außerdem konnten wir eine wichtige Rolle des BH3-only Proteins NOXA in der von PX-12 ausgelösten Apoptose zeigen, da ein Knock-down von NOXA sowohl Zelltod als auch die Aktivierung von BAK verhinderte. Diese Ergebnisse geben neue Erkenntnisse über den Mechanismus des PX-12-abhängigen Zelltodes in ALL Zelllinien, welche dazu beitragen können neue Kombinationstherapien zu entwickeln. Weiterhin unterstreichen diese Ergebnisse das Potential von PX-12 für die Behandlung der ALL. Diese Resultate müssen in weiteren Zelllinien, primären Proben oder in Tiermodellen bestätigt werden.

Um die weiteren Vorgänge, die zum durch Trx-Inhibition induzierten Zelltod führen, besser zu verstehen, untersuchten wir im zweiten Teil dieser Arbeit Änderungen in der globalen Proteinoxidation in Jurkat FD Zellen. Dazu behandelten wir Jurkat FD Zellen mit dem

Thioredoxin-Reduktase-Inhibitor Auranofin. Zuerst untersuchten wir den Zelltodmechanismus, der durch Auranofin-Behandlung in Jurkat FD Zellen ausgelöst wird. Auranofin löste hierbei die Spaltung von Caspase-3 und -9 und die Aktivierung von BAK aus. Der Zelltod konnte entweder durch Vorbehandlung mit zVAD.fmk, aber nicht mit Nekroptose-Inhibitoren, oder durch Knock-down von BAK verhindert werden. Unsere Ergebnisse passen zu vorherigen Studien, in denen die Induktion von intrinsischer Apoptose nach Auranofin-Behandlung berichtet wurde. Weiterhin konnten wir eine Erhöhung der ROS-Level nach Auranofin-Behandlung feststellen. Zur Analyse der globalen Proteinoxidation verwendeten wir einen BIAM-Switch-Assay gefolgt von Massenspektrometrie. Mit dem BIAM-Switch-Assay können gezielt oxidierte Proteine angereichert werden, die dann durch Massenspektrometrie identifiziert werden können. Mit dieser Analyse konnten wir zeigen, dass die Behandlung mit Auranofin zur Oxidation von über 200 Proteinen führte. Wie erwartet, konnten wir die Oxidation von Trx1, Trx2 und verschiedenen Peroxiredoxinen nach Auranofin-Behandlung zeigen. Außerdem konnten wir die Oxidation von APAF1-interacting protein (APIP) und Protein arginine N-methyltransferase (PRMT1) darlegen, die beide mit der Regulation von Apoptose in Verbindung stehen. Mit dieser Untersuchung konnten wir zeigen, dass die Behandlung mit Auranofin zu Veränderungen der globalen Proteinoxidation beiträgt. Ob die Funktionalität der beschriebenen Proteine durch Oxidation verändert wird und dies zur Induktion der Apoptose beiträgt, muss weiter untersucht werden.

Da wir BAK als wichtiges Protein beim PX-12- und Auranofin-induzierten Zelltod identifizieren konnten, wollten wir die Beteiligung von BAK im ROS-vermittelten Zelltod im dritten Teil der Arbeit weiter untersuchen. Erste Analysen in Wildtyp (WT) und BAK$^{-/-}$ murinen embryonalen Fibroblasten (MEFs) zeigten, dass BAK essentiell für den von Auranofin-induzierten Zelltod in MEFs war. Interessanterweise war dieser Zelltod in MEFs unabhängig von Caspasen, was wir durch Versuche, den Zelltod mit zVAD.fmk zu inhibieren, zeigen konnten. Interessanterweise konnte der Auranofin-abhängige Zelltod aber durch Vorbehandlung mit den Antioxidantien α-Tocopherol, Butylhydroxyanisol oder 2-tert-Butylhydrochinon gehemmt werden. Diese Ergebnisse zeigen, dass der von Auranofin ausgelöste Zelltod in MEFs ROS-abhängig ist. Um sicherzustellen, dass die von uns verwendeten MEFs Apoptose induzieren können, behandelten wir diese Zellen mit Etoposid, welches als Auslöser der intrinsischen Apoptose beschrieben wurde. Etoposid-Behandlung löste in WT MEFs Zelltod aus, der durch Vorbehandlung mit zVAD.fmk inhibiert werden konnte. Wie erwartet, waren BAK$^{-/-}$ MEFs vor Etoposid-induziertem Zelltod geschützt. Zusätzlich konnten wir zeigen, dass die Behandlung mit Auranofin, aber nicht mit Etoposid, die Oxidation von BAK auslöste. Um die Rolle der Auranofin-abhängigen BAK-Oxidation in der Zelltodinduktion besser zu verstehen, exprimierten wir BAK-Fusionsproteine mit einem fluoreszierenden Markerprotein in BAK$^{-/-}$ MEFs. BAK wurde hierbei mit der WT Sequenz oder als Mutante exprimiert, bei der

92

mindestens eines der zwei Oxidations-sensitiven Cysteine zu Oxidations-insensitivem Serin mutiert wurde. Die Mutation der Cysteine änderte dabei nicht die Lokalisation von BAK in der äußeren Mitochondrienmembran, da wir eine Co-Lokalisation aller BAK Mutanten mit TOMM20, einem Protein der äußeren Mitochondrienmembran, zeigen konnten. Expression des WT BAK Proteins konnte außerdem BAK$^{-/-}$ MEFs für die Behandlung mit Auranofin oder Etoposid resensibilisieren. Interessanterweise starben auch BAK$^{-/-}$ MEFs, welche die BAK-Cystein-Mutanten exprimierten, durch die Behandlung mit Etoposid. Diese Zellen starben dagegen weniger nach Auranofin-Behandlung, als solche die WT BAK exprimierten. Diese Ergebnisse zeigten, dass die Cysteine in BAK eine wichtige Rolle beim Auranofin-induzierten Zelltod in MEFs spielen.

Weiterhin untersuchten wir, ob die BH3-Domäne von BAK für den durch Auranofin ausgelösten Zelltod benötigt wird. Dazu brachten wir bereits beschriebene Punktmutationen in die BAK-Sequenz ein, die einen Funktionsverlust der BH3-Domäne verursachen. BAK$^{-/-}$ MEFs, die diese BH3-Mutanten exprimierten, starben nicht durch die Behandlung mit Auranofin oder Etoposid. Um die Rolle von BAK im Auranofin-induzierten Zelltod besser zu verstehen, untersuchten wir die Interaktionspartner von WT BAK und Cystein-freiem BAK nach der Behandlung mit Auranofin. Dazu führten wir eine Co-Immunpräzipitation mit anschließender massenspektrometrischer Analyse durch. Mit dieser Analyse konnten wir auch die Oxidation von BAK an Cystein 14 bestätigen. Leider wurde nicht die gesamte Sequenz von BAK erfasst und somit können wir nicht bestätigen, ob auch Cystein 154 nach der Behandlung mit Auranofin oxidiert war. Hierfür sind weitere Analysen notwendig. Wir konnten außerdem feststellen, dass sich einige Interaktionspartner von WT BAK und Cystein-freiem BAK unterschieden. So interagierte WT BAK nach Auranofin-Behandlung mit Proteinen, die eine Rolle im Vesikeltransport, in Oxidations-Reduktionsprozessen und in der zellulären Lokalisation spielen. Das Protein, das am meisten mit WT BAK angereichert wurde, war C4orf3 homolog, welches auch als Another-regulin (ALN) beschrieben wurde und an der Regulation der Calcium-Aufnahme in das ER beteiligt ist. Weiterhin konnten wir die Interaktion von WT BAK mit den Proteinen Mitochondrial fission factor (MFF), welches an der Fission von Mitochondrien beteiligt ist, und Vesicle transport through interaction with t-SNAREs homolog 1A (VTI1A), welches eine Rolle im Vesikeltransport spielt, bestätigen. Interessanterweise unterschied sich die Interaktion mit Proteinen, die an der Regulation der Apoptose beteiligt sind, wie BAX und BCL-X$_L$, nicht zwischen WT BAK und Cystein-freiem BAK. Unsere Ergebnisse weisen auf eine wichtige Rolle der Oxidation von BAK im Auranofin-induzierten Zelltod hin. Weiterhin konnten wir neue oxidationsabhängige Interaktionspartner von BAK identifizieren. Wie genau die Funktion von BAK durch Oxidation verändert wird und welche Rolle die gezeigten Interaktionspartner beim Auranofin-induzierten Zelltod spielen, muss in weiteren Experimenten gezeigt werden.

Zusammenfassend unterstreicht diese Arbeit das Potential von ROS-induzierenden Behandlungen für die Therapie der ALL und zeigt neue Erkenntnisse für die Redox-Regulation des programmierten Zelltodes auf.

8 References

1. Pui, C.H., L.L. Robison, and A.T. Look, *Acute lymphoblastic leukaemia.* Lancet, 2008. **371**(9617): p. 1030-43.
2. Hunger, S.P. and C.G. Mullighan, *Acute Lymphoblastic Leukemia in Children.* N Engl J Med, 2015. **373**(16): p. 1541-52.
3. Kuhlen, M., J.H. Klusmann, and J.I. Hoell, *Molecular Approaches to Treating Pediatric Leukemias.* Front Pediatr, 2019. **7**: p. 368.
4. Kato, M. and A. Manabe, *Treatment and biology of pediatric acute lymphoblastic leukemia.* Pediatr Int, 2018. **60**(1): p. 4-12.
5. Armstrong, S.A. and A.T. Look, *Molecular genetics of acute lymphoblastic leukemia.* J Clin Oncol, 2005. **23**(26): p. 6306-15.
6. Shurtleff, S.A., et al., *TEL/AML1 fusion resulting from a cryptic t(12;21) is the most common genetic lesion in pediatric ALL and defines a subgroup of patients with an excellent prognosis.* Leukemia, 1995. **9**(12): p. 1985-9.
7. Hong, D., et al., *Initiating and cancer-propagating cells in TEL-AML1-associated childhood leukemia.* Science, 2008. **319**(5861): p. 336-9.
8. Kurzrock, R., J.U. Gutterman, and M. Talpaz, *The molecular genetics of Philadelphia chromosome-positive leukemias.* N Engl J Med, 1988. **319**(15): p. 990-8.
9. Ren, R., *Mechanisms of BCR-ABL in the pathogenesis of chronic myelogenous leukaemia.* Nat Rev Cancer, 2005. **5**(3): p. 172-83.
10. Druker, B.J., et al., *Effects of a selective inhibitor of the Abl tyrosine kinase on the growth of Bcr-Abl positive cells.* Nat Med, 1996. **2**(5): p. 561-6.
11. Pehlivan, K.C., B.B. Duncan, and D.W. Lee, *CAR-T Cell Therapy for Acute Lymphoblastic Leukemia: Transforming the Treatment of Relapsed and Refractory Disease.* Curr Hematol Malig Rep, 2018. **13**(5): p. 396-406.
12. Ray, P.D., B.W. Huang, and Y. Tsuji, *Reactive oxygen species (ROS) homeostasis and redox regulation in cellular signaling.* Cell Signal, 2012. **24**(5): p. 981-90.
13. Gorrini, C., I.S. Harris, and T.W. Mak, *Modulation of oxidative stress as an anticancer strategy.* Nat Rev Drug Discov, 2013. **12**(12): p. 931-947.
14. Hancock, J.T., R. Desikan, and S.J. Neill, *Role of reactive oxygen species in cell signalling pathways.* Biochem Soc Trans, 2001. **29**(Pt 2): p. 345-50.
15. Paulsen, C.E. and K.S. Carroll, *Cysteine-mediated redox signaling: chemistry, biology, and tools for discovery.* Chem Rev, 2013. **113**(7): p. 4633-79.
16. D'Autréaux, B. and M.B. Toledano, *ROS as signalling molecules: mechanisms that generate specificity in ROS homeostasis.* Nature Reviews Molecular Cell Biology, 2007. **8**: p. 813.
17. Henzler, T. and E. Steudle, *Transport and metabolic degradation of hydrogen peroxide in Chara corallina: model calculations and measurements with the pressure probe suggest transport of H_2O_2 across water channels.* J Exp Bot, 2000. **51**(353): p. 2053-66.
18. Bienert, G.P., J.K. Schjoerring, and T.P. Jahn, *Membrane transport of hydrogen peroxide.* Biochim Biophys Acta, 2006. **1758**(8): p. 994-1003.
19. Murphy, M.P., *How mitochondria produce reactive oxygen species.* Biochem J, 2009. **417**(1): p. 1-13.
20. Holmstrom, K.M. and T. Finkel, *Cellular mechanisms and physiological consequences of redox-dependent signalling.* Nat Rev Mol Cell Biol, 2014. **15**(6): p. 411-21.
21. Trachootham, D., J. Alexandre, and P. Huang, *Targeting cancer cells by ROS-mediated mechanisms: a radical therapeutic approach?* Nat Rev Drug Discov, 2009. **8**(7): p. 579-91.
22. Sies, H. and D.P. Jones, *Reactive oxygen species (ROS) as pleiotropic physiological signalling agents.* Nat Rev Mol Cell Biol, 2020. **21**(7): p. 363-383.

23. Zeeshan, H.M., et al., *Endoplasmic Reticulum Stress and Associated ROS.* Int J Mol Sci, 2016. **17**(3): p. 327.

24. Sies, H., *Glutathione and its role in cellular functions.* Free Radic Biol Med, 1999. **27**(9-10): p. 916-21.

25. Castaldo, S.A., et al., *The Tumorigenic Roles of the Cellular REDOX Regulatory Systems.* Oxid Med Cell Longev, 2016. **2016**: p. 8413032.

26. Meister, A. and M.E. Anderson, *Glutathione.* Annu Rev Biochem, 1983. **52**: p. 711-60.

27. Kaplowitz, N., et al., *GSH transporters: molecular characterization and role in GSH homeostasis.* Biol Chem Hoppe Seyler, 1996. **377**(5): p. 267-73.

28. Bachhawat, A.K., et al., *Glutathione transporters.* Biochim Biophys Acta, 2013. **1830**(5): p. 3154-64.

29. Meister, A., *Glutathione, ascorbate, and cellular protection.* Cancer Res, 1994. **54**(7 Suppl): p. 1969s-1975s.

30. Traber, M.G. and J.F. Stevens, *Vitamins C and E: beneficial effects from a mechanistic perspective.* Free Radic Biol Med, 2011. **51**(5): p. 1000-13.

31. Gould, R.L. and R. Pazdro, *Impact of Supplementary Amino Acids, Micronutrients, and Overall Diet on Glutathione Homeostasis.* Nutrients, 2019. **11**(5).

32. Glorieux, C. and P.B. Calderon, *Catalase, a remarkable enzyme: targeting the oldest antioxidant enzyme to find a new cancer treatment approach.* Biol Chem, 2017. **398**(10): p. 1095-1108.

33. Lazarow, P.B. and C. de Duve, *The synthesis and turnover of rat liver peroxisomes. V. Intracellular pathway of catalase synthesis.* J Cell Biol, 1973. **59**(2 Pt 1): p. 507-24.

34. Lee, S., S.M. Kim, and R.T. Lee, *Thioredoxin and thioredoxin target proteins: from molecular mechanisms to functional significance.* Antioxid Redox Signal, 2013. **18**(10): p. 1165-207.

35. Holmgren, A., *Thioredoxin. 6. The amino acid sequence of the protein from escherichia coli B.* Eur J Biochem, 1968. **6**(4): p. 475-84.

36. Lillig, C.H. and A. Holmgren, *Thioredoxin and related molecules - From biology to health and disease.* Antioxidants & Redox Signaling, 2007. **9**(1): p. 25-47.

37. Collet, J.F. and J. Messens, *Structure, function, and mechanism of thioredoxin proteins.* Antioxid Redox Signal, 2010. **13**(8): p. 1205-16.

38. Zhang, J., et al., *Targeting the Thioredoxin System for Cancer Therapy.* Trends Pharmacol Sci, 2017. **38**(9): p. 794-808.

39. Dillet, V., H.J. Dyson, and D. Bashford, *Calculations of electrostatic interactions and pKas in the active site of Escherichia coli thioredoxin.* Biochemistry, 1998. **37**(28): p. 10298-306.

40. Zhang, J., et al., *Small molecule inhibitors of mammalian thioredoxin reductase as potential anticancer agents: An update.* Med Res Rev, 2019. **39**(1): p. 5-39.

41. Huber, R.E. and R.S. Criddle, *Comparison of the chemical properties of selenocysteine and selenocystine with their sulfur analogs.* Arch Biochem Biophys, 1967. **122**(1): p. 164-73.

42. Zhong, L. and A. Holmgren, *Essential role of selenium in the catalytic activities of mammalian thioredoxin reductase revealed by characterization of recombinant enzymes with selenocysteine mutations.* J Biol Chem, 2000. **275**(24): p. 18121-8.

43. Conrad, M., et al., *Essential role for mitochondrial thioredoxin reductase in hematopoiesis, heart development, and heart function.* Molecular and cellular biology, 2004. **24**(21): p. 9414-9423.

44. Jakupoglu, C., et al., *Cytoplasmic thioredoxin reductase is essential for embryogenesis but dispensable for cardiac development.* Mol Cell Biol, 2005. **25**(5): p. 1980-8.

45. Hampton, M.B., et al., *Peroxiredoxin Involvement in the Initiation and Progression of Human Cancer.* Antioxidants & Redox Signaling, 2017. **28**(7): p. 591-608.

46. Peskin, A.V., et al., *The high reactivity of peroxiredoxin 2 with H(2)O(2) is not reflected in its reaction with other oxidants and thiol reagents.* J Biol Chem, 2007. **282**(16): p. 11885-92.

47. Stocker, S., et al., *A role for 2-Cys peroxiredoxins in facilitating cytosolic protein thiol oxidation.* Nat Chem Biol, 2018. **14**(2): p. 148-155.

48. Johansson, C., C.H. Lillig, and A. Holmgren, *Human mitochondrial glutaredoxin reduces S-glutathionylated proteins with high affinity accepting electrons from either glutathione or thioredoxin reductase.* J Biol Chem, 2004. **279**(9): p. 7537-43.

49. Lubos, E., J. Loscalzo, and D.E. Handy, *Glutathione peroxidase-1 in health and disease: from molecular mechanisms to therapeutic opportunities.* Antioxid Redox Signal, 2011. **15**(7): p. 1957-97.

50. Margis, R., et al., *Glutathione peroxidase family - an evolutionary overview.* FEBS J, 2008. **275**(15): p. 3959-70.

51. Yant, L.J., et al., *The selenoprotein GPX4 is essential for mouse development and protects from radiation and oxidative damage insults.* Free Radic Biol Med, 2003. **34**(4): p. 496-502.

52. Yang, W.S., et al., *Regulation of ferroptotic cancer cell death by GPX4.* Cell, 2014. **156**(1-2): p. 317-331.

53. Reddie, K.G. and K.S. Carroll, *Expanding the functional diversity of proteins through cysteine oxidation.* Curr Opin Chem Biol, 2008. **12**(6): p. 746-54.

54. Biteau, B., J. Labarre, and M.B. Toledano, *ATP-dependent reduction of cysteine-sulphinic acid by S. cerevisiae sulphiredoxin.* Nature, 2003. **425**(6961): p. 980-4.

55. Chang, T.S., et al., *Characterization of mammalian sulfiredoxin and its reactivation of hyperoxidized peroxiredoxin through reduction of cysteine sulfinic acid in the active site to cysteine.* J Biol Chem, 2004. **279**(49): p. 50994-1001.

56. Gilbert, H.F., *Molecular and cellular aspects of thiol-disulfide exchange.* Adv Enzymol Relat Areas Mol Biol, 1990. **63**: p. 69-172.

57. Meng, T.C., T. Fukada, and N.K. Tonks, *Reversible oxidation and inactivation of protein tyrosine phosphatases in vivo.* Mol Cell, 2002. **9**(2): p. 387-99.

58. Bae, Y.S., et al., *Epidermal growth factor (EGF)-induced generation of hydrogen peroxide. Role in EGF receptor-mediated tyrosine phosphorylation.* J Biol Chem, 1997. **272**(1): p. 217-21.

59. Schieber, M. and N.S. Chandel, *ROS function in redox signaling and oxidative stress.* Curr Biol, 2014. **24**(10): p. R453-62.

60. Leslie, N.R., et al., *Redox regulation of PI 3-kinase signalling via inactivation of PTEN.* EMBO J, 2003. **22**(20): p. 5501-10.

61. Dansen, T.B., et al., *Redox-sensitive cysteines bridge p300/CBP-mediated acetylation and FoxO4 activity.* Nat Chem Biol, 2009. **5**(9): p. 664-72.

62. Eijkelenboom, A. and B.M. Burgering, *FOXOs: signalling integrators for homeostasis maintenance.* Nat Rev Mol Cell Biol, 2013. **14**(2): p. 83-97.

63. Klotz, L.O. and H. Steinbrenner, *Cellular adaptation to xenobiotics: Interplay between xenosensors, reactive oxygen species and FOXO transcription factors.* Redox Biol, 2017. **13**: p. 646-654.

64. Itoh, K., et al., *An Nrf2/small Maf heterodimer mediates the induction of phase II detoxifying enzyme genes through antioxidant response elements.* Biochem Biophys Res Commun, 1997. **236**(2): p. 313-22.

65. Hayes, J.D. and A.T. Dinkova-Kostova, *The Nrf2 regulatory network provides an interface between redox and intermediary metabolism.* Trends Biochem Sci, 2014. **39**(4): p. 199-218.

66. Yamamoto, M., T.W. Kensler, and H. Motohashi, *The KEAP1-NRF2 System: a Thiol-Based Sensor-Effector Apparatus for Maintaining Redox Homeostasis.* Physiol Rev, 2018. **98**(3): p. 1169-1203.

67. Liu, B., Y. Chen, and D.K. St Clair, *ROS and p53: a versatile partnership.* Free Radic Biol Med, 2008. **44**(8): p. 1529-35.

68. Velu, C.S., et al., *Human p53 is inhibited by glutathionylation of cysteines present in the proximal DNA-binding domain during oxidative stress.* Biochemistry, 2007. **46**(26): p. 7765-80.

69. Hornsveld, M. and T.B. Dansen, *The Hallmarks of Cancer from a Redox Perspective.* Antioxid Redox Signal, 2016. **25**(6): p. 300-25.

70. Bensaad, K., et al., *TIGAR, a p53-inducible regulator of glycolysis and apoptosis.* Cell, 2006. **126**(1): p. 107-20.

71. Cheung, E.C., R.L. Ludwig, and K.H. Vousden, *Mitochondrial localization of TIGAR under hypoxia stimulates HK2 and lowers ROS and cell death.* Proc Natl Acad Sci U S A, 2012. **109**(50): p. 20491-6.

72. Kruiswijk, F., C.F. Labuschagne, and K.H. Vousden, *p53 in survival, death and metabolic health: a lifeguard with a licence to kill.* Nat Rev Mol Cell Biol, 2015. **16**(7): p. 393-405.

73. Polyak, K., et al., *A model for p53-induced apoptosis.* Nature, 1997. **389**(6648): p. 300-5.

74. Rivera, A. and S.A. Maxwell, *The p53-induced gene-6 (proline oxidase) mediates apoptosis through a calcineurin-dependent pathway.* J Biol Chem, 2005. **280**(32): p. 29346-54.

75. Wang, D.B., et al., *p53 and mitochondrial function in neurons.* Biochim Biophys Acta, 2014. **1842**(8): p. 1186-97.

76. Jiang, P., et al., *p53 regulates biosynthesis through direct inactivation of glucose-6-phosphate dehydrogenase.* Nat Cell Biol, 2011. **13**(3): p. 310-6.

77. Szatrowski, T.P. and C.F. Nathan, *Production of large amounts of hydrogen peroxide by human tumor cells.* Cancer Res, 1991. **51**(3): p. 794-8.

78. Toyokuni, S., et al., *Persistent oxidative stress in cancer.* FEBS Lett, 1995. **358**(1): p. 1-3.

79. Panieri, E. and M.M. Santoro, *ROS homeostasis and metabolism: a dangerous liason in cancer cells.* Cell Death Dis, 2016. **7**(6): p. e2253.

80. Ziech, D., et al., *Reactive oxygen species (ROS)--induced genetic and epigenetic alterations in human carcinogenesis.* Mutat Res, 2011. **711**(1-2): p. 167-73.

81. Ishikawa, K., et al., *ROS-generating mitochondrial DNA mutations can regulate tumor cell metastasis.* Science, 2008. **320**(5876): p. 661-4.

82. Porporato, P.E., et al., *A mitochondrial switch promotes tumor metastasis.* Cell Rep, 2014. **8**(3): p. 754-66.

83. Cat, B., et al., *Enhancement of tumor invasion depends on transdifferentiation of skin fibroblasts mediated by reactive oxygen species.* J Cell Sci, 2006. **119**(Pt 13): p. 2727-38.

84. Jezierska-Drutel, A., S.A. Rosenzweig, and C.A. Neumann, *Role of oxidative stress and the microenvironment in breast cancer development and progression.* Adv Cancer Res, 2013. **119**: p. 107-25.

85. Vafa, O., et al., *c-Myc can induce DNA damage, increase reactive oxygen species, and mitigate p53 function: a mechanism for oncogene-induced genetic instability.* Mol Cell, 2002. **9**(5): p. 1031-44.

86. Irani, K., et al., *Mitogenic signaling mediated by oxidants in Ras-transformed fibroblasts.* Science, 1997. **275**(5306): p. 1649-52.

87. Lim, J.K.M. and G. Leprivier, *The impact of oncogenic RAS on redox balance and implications for cancer development.* Cell Death Dis, 2019. **10**(12): p. 955.

88. Carew, J.S., et al., *Mitochondrial DNA mutations in primary leukemia cells after chemotherapy: clinical significance and therapeutic implications.* Leukemia, 2003. **17**(8): p. 1437-47.

89. Van Houten, B., V. Woshner, and J.H. Santos, *Role of mitochondrial DNA in toxic responses to oxidative stress.* DNA Repair (Amst), 2006. **5**(2): p. 145-52.

90. Fulton, A.M. and Y.C. Chong, *The role of macrophage-derived TNFa in the induction of sublethal tumor cell DNA damage.* Carcinogenesis, 1992. **13**(1): p. 77-81.

91. Klimova, T. and N.S. Chandel, *Mitochondrial complex III regulates hypoxic activation of HIF.* Cell Death Differ, 2008. **15**(4): p. 660-6.

92. Jeon, S.M., N.S. Chandel, and N. Hay, *AMPK regulates NADPH homeostasis to promote tumour cell survival during energy stress.* Nature, 2012. **485**(7400): p. 661-+.

93. DeBerardinis, R.J. and N.S. Chandel, *Fundamentals of cancer metabolism.* Science Advances, 2016. **2**(5).

94. Maiti, A.K., *Gene network analysis of oxidative stress-mediated drug sensitivity in resistant ovarian carcinoma cells.* Pharmacogenomics Journal, 2010. **10**(2): p. 94-104.

95. Yang, H., et al., *The role of cellular reactive oxygen species in cancer chemotherapy.* J Exp Clin Cancer Res, 2018. **37**(1): p. 266.

96. Blodgett, R.C., Jr., M.A. Heuer, and R.G. Pietrusko, *Auranofin: a unique oral chrysotherapeutic agent.* Semin Arthritis Rheum, 1984. **13**(3): p. 255-73.

97. Zou, T., et al., *Chemical biology of anticancer gold(III) and gold(I) complexes.* Chem Soc Rev, 2015. **44**(24): p. 8786-801.

98. Shaw, I.C., *Gold-based therapeutic agents.* Chem Rev, 1999. **99**(9): p. 2589-600.

99. Gandin, V., et al., *Cancer cell death induced by phosphine gold(I) compounds targeting thioredoxin reductase.* Biochem Pharmacol, 2010. **79**(2): p. 90-101.

100. May, H.C., et al., *Repurposing Auranofin, Ebselen, and PX-12 as Antimicrobial Agents Targeting the Thioredoxin System.* Front Microbiol, 2018. **9**: p. 336.

101. Gromer, S., et al., *Human placenta thioredoxin reductase. Isolation of the selenoenzyme, steady state kinetics, and inhibition by therapeutic gold compounds.* J Biol Chem, 1998. **273**(32): p. 20096-101.

102. Rigobello, M.P., et al., *Gold complexes inhibit mitochondrial thioredoxin reductase: consequences on mitochondrial functions.* J Inorg Biochem, 2004. **98**(10): p. 1634-41.

103. Rigobello, M.P., et al., *Induction of mitochondrial permeability transition by auranofin, a gold(I)-phosphine derivative.* Br J Pharmacol, 2002. **136**(8): p. 1162-8.

104. Cox, A.G., et al., *The thioredoxin reductase inhibitor auranofin triggers apoptosis through a Bax/Bak-dependent process that involves peroxiredoxin 3 oxidation.* Biochem Pharmacol, 2008. **76**(9): p. 1097-109.

105. Liu, N., et al., *Clinically used antirheumatic agent auranofin is a proteasomal deubiquitinase inhibitor and inhibits tumor growth.* Oncotarget, 2014. **5**(14): p. 5453-71.

106. Mirabelli, C.K., et al., *Evaluation of the in vivo antitumor activity and in vitro cytotoxic properties of auranofin, a coordinated gold compound, in murine tumor models.* Cancer Res, 1985. **45**(1): p. 32-9.

107. Marzano, C., et al., *Inhibition of thioredoxin reductase by auranofin induces apoptosis in cisplatin-resistant human ovarian cancer cells.* Free Radic Biol Med, 2007. **42**(6): p. 872-81.

108. Pessetto, Z.Y., et al., *Drug repurposing for gastrointestinal stromal tumor.* Mol Cancer Ther, 2013. **12**(7): p. 1299-309.

109. Fiskus, W., et al., *Auranofin induces lethal oxidative and endoplasmic reticulum stress and exerts potent preclinical activity against chronic lymphocytic leukemia.* Cancer Res, 2014. **74**(9): p. 2520-32.

110. Fan, C., et al., *Enhancement of auranofin-induced lung cancer cell apoptosis by selenocystine, a natural inhibitor of TrxR1 in vitro and in vivo.* Cell Death Dis, 2014. **5**: p. e1191.

111. Chen, X., et al., *Anti-rheumatic agent auranofin induced apoptosis in chronic myeloid leukemia cells resistant to imatinib through both Bcr/Abl-dependent and -independent mechanisms.* Oncotarget, 2014. **5**(19): p. 9118-32.

112. Kirkpatrick, D.L., et al., *Mechanisms of inhibition of the thioredoxin growth factor system by antitumor 2-imidazolyl disulfides.* Biochem Pharmacol, 1998. **55**(7): p. 987-94.

113. Li, G.Z., et al., *PX-12 inhibits the growth of hepatocelluar carcinoma by inducing S-phase arrest, ROS-dependent apoptosis and enhances 5-FU cytotoxicity.* Am J Transl Res, 2015. **7**(9): p. 1528-40.

114. Wang, F., et al., *Thioredoxin-1 inhibitor, 1-methylpropyl 2-imidazolyl disulfide, inhibits the growth, migration and invasion of colorectal cancer cell lines.* Oncol Rep, 2015. **33**(2): p. 967-73.

115. Raninga, P.V., et al., *Inhibition of thioredoxin 1 leads to apoptosis in drug-resistant multiple myeloma.* Oncotarget, 2015. **6**(17): p. 15410-24.

116. Shin, H.R., B.R. You, and W.H. Park, *PX-12-induced HeLa cell death is associated with oxidative stress and GSH depletion.* Oncol Lett, 2013. **6**(6): p. 1804-1810.

117. Samaranayake, G.J., et al., *Thioredoxin-1 protects against androgen receptor-induced redox vulnerability in castration-resistant prostate cancer.* Nat Commun, 2017. **8**(1): p. 1204.

118. Shao, L., et al., *Thioredoxin expression in primary T-cell acute lymphoblastic leukemia and its therapeutic implication.* Cancer Res, 2001. **61**(19): p. 7333-8.

119. Ramanathan, R.K., et al., *A randomized phase II study of PX-12, an inhibitor of thioredoxin in patients with advanced cancer of the pancreas following progression after a gemcitabine-containing combination.* Cancer Chemother Pharmacol, 2011. **67**(3): p. 503-9.

120. Ramanathan, R.K., et al., *A phase I trial of PX-12, a small-molecule inhibitor of thioredoxin-1, administered as a 72-hour infusion every 21 days in patients with advanced cancers refractory to standard therapy.* Invest New Drugs, 2012. **30**(4): p. 1591-6.

121. Ramanathan, R.K., et al., *A Phase I pharmacokinetic and pharmacodynamic study of PX-12, a novel inhibitor of thioredoxin-1, in patients with advanced solid tumors.* Clin Cancer Res, 2007. **13**(7): p. 2109-14.

122. Baker, A.F., et al., *A phase IB trial of 24-hour intravenous PX-12, a thioredoxin-1 inhibitor, in patients with advanced gastrointestinal cancers.* Invest New Drugs, 2013. **31**(3): p. 631-641.

123. Galluzzi, L., et al., *Molecular mechanisms of cell death: recommendations of the Nomenclature Committee on Cell Death 2018.* Cell Death Differ, 2018. **25**(3): p. 486-541.

124. Fuchs, Y. and H. Steller, *Live to die another way: modes of programmed cell death and the signals emanating from dying cells.* Nat Rev Mol Cell Biol, 2015. **16**(6): p. 329-44.

125. Degterev, A. and J. Yuan, *Expansion and evolution of cell death programmes.* Nat Rev Mol Cell Biol, 2008. **9**(5): p. 378-90.

126. Schweichel, J.U. and H.J. Merker, *The morphology of various types of cell death in prenatal tissues.* Teratology, 1973. **7**(3): p. 253-66.

127. Green, D.R., T.H. Oguin, and J. Martinez, *The clearance of dying cells: table for two.* Cell Death Differ, 2016. **23**(6): p. 915-26.

128. Ashkenazi, A. and V.M. Dixit, *Death receptors: signaling and modulation.* Science, 1998. **281**(5381): p. 1305-8.

129. Li, J., Q. Yin, and H. Wu, *Structural basis of signal transduction in the TNF receptor superfamily.* Adv Immunol, 2013. **119**: p. 135-53.

130. Vanden Berghe, T., et al., *Regulated necrosis: the expanding network of non-apoptotic cell death pathways.* Nat Rev Mol Cell Biol, 2014. **15**(2): p. 135-47.

131. Czabotar, P.E., et al., *Control of apoptosis by the BCL-2 protein family: implications for physiology and therapy.* Nat Rev Mol Cell Biol, 2014. **15**(1): p. 49-63.

132. Pop, C. and G.S. Salvesen, *Human caspases: activation, specificity, and regulation.* J Biol Chem, 2009. **284**(33): p. 21777-81.

133. Fuentes-Prior, P. and G.S. Salvesen, *The protein structures that shape caspase activity, specificity, activation and inhibition.* Biochem J, 2004. **384**(Pt 2): p. 201-32.

134. Fulda, S., *Therapeutic opportunities based on caspase modulation.* Semin Cell Dev Biol, 2018. **82**: p. 150-157.

135. Germain, M., et al., *Cleavage of automodified poly(ADP-ribose) polymerase during apoptosis. Evidence for involvement of caspase-7.* J Biol Chem, 1999. **274**(40): p. 28379-84.

136. Nagata, S., et al., *Exposure of phosphatidylserine on the cell surface.* Cell Death Differ, 2016. **23**(6): p. 952-61.

137. Segawa, K., et al., *Caspase-mediated cleavage of phospholipid flippase for apoptotic phosphatidylserine exposure.* Science, 2014. **344**(6188): p. 1164-8.

138. Poon, I.K., et al., *Apoptotic cell clearance: basic biology and therapeutic potential.* Nat Rev Immunol, 2014. **14**(3): p. 166-80.

139. Adams, J.M. and S. Cory, *The BCL-2 arbiters of apoptosis and their growing role as cancer targets.* Cell Death Differ, 2018. **25**(1): p. 27-36.

140. Roos, W.P., A.D. Thomas, and B. Kaina, *DNA damage and the balance between survival and death in cancer biology.* Nat Rev Cancer, 2016. **16**(1): p. 20-33.

141. Brumatti, G., M. Salmanidis, and P.G. Ekert, *Crossing paths: interactions between the cell death machinery and growth factor survival signals.* Cell Mol Life Sci, 2010. **67**(10): p. 1619-30.

142. Pihan, P., A. Carreras-Sureda, and C. Hetz, *BCL-2 family: integrating stress responses at the ER to control cell demise.* Cell Death Differ, 2017. **24**(9): p. 1478-1487.

143. Tait, S.W. and D.R. Green, *Mitochondria and cell death: outer membrane permeabilization and beyond.* Nat Rev Mol Cell Biol, 2010. **11**(9): p. 621-32.

144. Hsu, Y.T., K.G. Wolter, and R.J. Youle, *Cytosol-to-membrane redistribution of Bax and Bcl-X(L) during apoptosis.* Proc Natl Acad Sci U S A, 1997. **94**(8): p. 3668-72.

145. Wolter, K.G., et al., *Movement of Bax from the cytosol to mitochondria during apoptosis.* J Cell Biol, 1997. **139**(5): p. 1281-92.

146. Suzuki, M., R.J. Youle, and N. Tjandra, *Structure of Bax: coregulation of dimer formation and intracellular localization.* Cell, 2000. **103**(4): p. 645-54.

147. Todt, F., et al., *Differential retrotranslocation of mitochondrial Bax and Bak.* EMBO J, 2015. **34**(1): p. 67-80.

148. Edlich, F., et al., *Bcl-x(L) retrotranslocates Bax from the mitochondria into the cytosol.* Cell, 2011. **145**(1): p. 104-16.

149. Willis, S.N., et al., *Proapoptotic Bak is sequestered by Mcl-1 and Bcl-xL, but not Bcl-2, until displaced by BH3-only proteins.* Genes Dev, 2005. **19**(11): p. 1294-305.

150. van Delft, M.F. and D.C. Huang, *How the Bcl-2 family of proteins interact to regulate apoptosis.* Cell Res, 2006. **16**(2): p. 203-13.

151. Chen, L., et al., *Differential targeting of prosurvival Bcl-2 proteins by their BH3-only ligands allows complementary apoptotic function.* Mol Cell, 2005. **17**(3): p. 393-403.

152. Letai, A., et al., *Distinct BH3 domains either sensitize or activate mitochondrial apoptosis, serving as prototype cancer therapeutics.* Cancer Cell, 2002. **2**(3): p. 183-92.

153. Kim, H., et al., *Hierarchical regulation of mitochondrion-dependent apoptosis by BCL-2 subfamilies.* Nat Cell Biol, 2006. **8**(12): p. 1348-58.

154. Robin, A.Y., et al., *Crystal structure of Bax bound to the BH3 peptide of Bim identifies important contacts for interaction.* Cell Death Dis, 2015. **6**: p. e1809.

155. Czabotar, P.E., et al., *Bax crystal structures reveal how BH3 domains activate Bax and nucleate its oligomerization to induce apoptosis.* Cell, 2013. **152**(3): p. 519-31.

156. Moldoveanu, T., et al., *BID-induced structural changes in BAK promote apoptosis.* Nat Struct Mol Biol, 2013. **20**(5): p. 589-97.

157. Dewson, G., et al., *To Trigger Apoptosis, Bak Exposes Its BH3 Domain and Homodimerizes via BH3:Groove Interactions.* Molecular Cell, 2008. **30**(3): p. 369-380.

158. Dewson, G., et al., *Bax dimerizes via a symmetric BH3:groove interface during apoptosis.* Cell Death Differ, 2012. **19**(4): p. 661-70.

159. Brouwer, J.M., et al., *Bak core and latch domains separate during activation, and freed core domains form symmetric homodimers.* Mol Cell, 2014. **55**(6): p. 938-946.

160. Chen, H.C., et al., *An interconnected hierarchical model of cell death regulation by the BCL-2 family.* Nat Cell Biol, 2015. **17**(10): p. 1270-81.

161. O'Neill, K.L., et al., *Inactivation of prosurvival Bcl-2 proteins activates Bax/Bak through the outer mitochondrial membrane.* Genes Dev, 2016. **30**(8): p. 973-88.

162. Salvador-Gallego, R., et al., *Bax assembly into rings and arcs in apoptotic mitochondria is linked to membrane pores.* EMBO J, 2016. **35**(4): p. 389-401.

163. Grosse, L., et al., *Bax assembles into large ring-like structures remodeling the mitochondrial outer membrane in apoptosis.* EMBO J, 2016. **35**(4): p. 402-13.

164. Cosentino, K. and A.J. Garcia-Saez, *Bax and Bak Pores: Are We Closing the Circle?* Trends Cell Biol, 2017. **27**(4): p. 266-275.

165. Ke, F., et al., *BCL-2 family member BOK is widely expressed but its loss has only minimal impact in mice.* Cell Death Differ, 2012. **19**(6): p. 915-25.

166. Stehle, D., et al., *Contribution of BH3-domain and Transmembrane-domain to the Activity and Interaction of the Pore-forming Bcl-2 Proteins Bok, Bak, and Bax.* Sci Rep, 2018. **8**(1): p. 12434.

167. Einsele-Scholz, S., et al., *Bok is a genuine multi-BH-domain protein that triggers apoptosis in the absence of Bax and Bak.* J Cell Sci, 2016. **129**(11): p. 2213-23.

168. Dixon, S.J., et al., *Ferroptosis: an iron-dependent form of nonapoptotic cell death.* Cell, 2012. **149**(5): p. 1060-72.

169. Yang, W.S. and B.R. Stockwell, *Ferroptosis: Death by Lipid Peroxidation.* Trends Cell Biol, 2016. **26**(3): p. 165-176.

170. Richter, C., *Oxidative damage to mitochondrial DNA and its relationship to ageing.* Int J Biochem Cell Biol, 1995. **27**(7): p. 647-53.

171. Orrenius, S., V. Gogvadze, and B. Zhivotovsky, *Calcium and mitochondria in the regulation of cell death.* Biochem Biophys Res Commun, 2015. **460**(1): p. 72-81.

172. Cai, J. and D.P. Jones, *Superoxide in apoptosis. Mitochondrial generation triggered by cytochrome c loss.* J Biol Chem, 1998. **273**(19): p. 11401-4.

173. Ichijo, H., et al., *Induction of apoptosis by ASK1, a mammalian MAPKKK that activates SAPK/JNK and p38 signaling pathways.* Science, 1997. **275**(5296): p. 90-4.

174. Di Meo, S. and P. Venditti, *Evolution of the Knowledge of Free Radicals and Other Oxidants.* Oxid Med Cell Longev, 2020. **2020**: p. 9829176.

175. Yamamoto, K., H. Ichijo, and S.J. Korsmeyer, *BCL-2 is phosphorylated and inactivated by an ASK1/Jun N-terminal protein kinase pathway normally activated at G(2)/M.* Mol Cell Biol, 1999. **19**(12): p. 8469-78.

176. Matsuzawa, A., et al., *Physiological roles of ASK1-mediated signal transduction in oxidative stress- and endoplasmic reticulum stress-induced apoptosis: advanced findings from ASK1 knockout mice.* Antioxid Redox Signal, 2002. **4**(3): p. 415-25.

177. Zhang, A.Y., et al., *Acid sphingomyelinase and its redox amplification in formation of lipid raft redox signaling platforms in endothelial cells.* Antioxid Redox Signal, 2007. **9**(7): p. 817-28.

178. Blaser, H., et al., *TNF and ROS Crosstalk in Inflammation.* Trends Cell Biol, 2016. **26**(4): p. 249-261.

179. Redza-Dutordoir, M. and D.A. Averill-Bates, *Activation of apoptosis signalling pathways by reactive oxygen species.* Biochim Biophys Acta, 2016. **1863**(12): p. 2977-2992.

180. Mellier, G. and S. Pervaiz, *The three Rs along the TRAIL: resistance, re-sensitization and reactive oxygen species (ROS).* Free Radic Res, 2012. **46**(8): p. 996-1003.

181. Zamzami, N., et al., *Bid acts on the permeability transition pore complex to induce apoptosis.* Oncogene, 2000. **19**(54): p. 6342-50.

182. Karch, J., et al., *Bax and Bak function as the outer membrane component of the mitochondrial permeability pore in regulating necrotic cell death in mice.* Elife, 2013. **2**: p. e00772.

183. Murphy, J.M., et al., *The pseudokinase MLKL mediates necroptosis via a molecular switch mechanism.* Immunity, 2013. **39**(3): p. 443-53.

184. Schenk, B. and S. Fulda, *Reactive oxygen species regulate Smac mimetic/TNFalpha-induced necroptotic signaling and cell death.* Oncogene, 2015. **34**(47): p. 5796-806.

185. Fulda, S., *Regulation of necroptosis signaling and cell death by reactive oxygen species.* Biol Chem, 2016. **397**(7): p. 657-60.

186. Zhang, Y., et al., *RIP1 autophosphorylation is promoted by mitochondrial ROS and is essential for RIP3 recruitment into necrosome.* Nat Commun, 2017. **8**: p. 14329.

187. Hass, C., et al., *Sensitization of acute lymphoblastic leukemia cells for LCL161-induced cell death by targeting redox homeostasis.* Biochem Pharmacol, 2016. **105**: p. 14-22.

188. Roder, C. and M.J. Thomson, *Auranofin: repurposing an old drug for a golden new age.* Drugs R D, 2015. **15**(1): p. 13-20.

189. Habermann, K.J., et al., *Targeting redox homeostasis in rhabdomyosarcoma cells: GSH-depleting agents enhance auranofin-induced cell death.* Cell Death Dis, 2017. **8**(10): p. e3067.

190. Rohde, K., et al., *A Bak-dependent mitochondrial amplification step contributes to Smac mimetic/glucocorticoid-induced necroptosis.* Cell Death Differ, 2017. **24**(1): p. 83-97.

191. Juo, P., et al., *FADD is required for multiple signaling events downstream of the receptor Fas.* Cell Growth Differ, 1999. **10**(12): p. 797-804.

192. McArthur, K., et al., *BAK/BAX macropores facilitate mitochondrial herniation and mtDNA efflux during apoptosis.* Science, 2018. **359**(6378).

193. Eden, E., et al., *GOrilla: a tool for discovery and visualization of enriched GO terms in ranked gene lists.* BMC Bioinformatics, 2009. **10**: p. 48.

194. Cox, J. and M. Mann, *MaxQuant enables high peptide identification rates, individualized p.p.b.-range mass accuracies and proteome-wide protein quantification.* Nat Biotechnol, 2008. **26**(12): p. 1367-72.

195. Tyanova, S., et al., *The Perseus computational platform for comprehensive analysis of (prote)omics data.* Nat Methods, 2016. **13**(9): p. 731-40.

196. Supek, F., et al., *REVIGO summarizes and visualizes long lists of gene ontology terms.* PLoS One, 2011. **6**(7): p. e21800.

197. Fuhrmann, D.C., I. Wittig, and B. Brune, *TMEM126B deficiency reduces mitochondrial SDH oxidation by LPS, attenuating HIF-1alpha stabilization and IL-1beta expression.* Redox Biol, 2019. **20**: p. 204-216.

198. Schurmann, C., et al., *The polarity protein Scrib limits atherosclerosis development in mice.* Cardiovasc Res, 2019. **115**(14): p. 1963-1974.

199. Ehrenfeld, V. and S. Fulda, *Thioredoxin inhibitor PX-12 induces mitochondria-mediated apoptosis in acute lymphoblastic leukemia cells.* Biol Chem, 2019.

200. Irwin, M.E., N. Rivera-Del Valle, and J. Chandra, *Redox control of leukemia: from molecular mechanisms to therapeutic opportunities.* Antioxid Redox Signal, 2013. **18**(11): p. 1349-83.

201. Tourneur, L. and G. Chiocchia, *FADD: a regulator of life and death.* Trends Immunol, 2010. **31**(7): p. 260-9.

202. You, B.R., H.R. Shin, and W.H. Park, *PX-12 inhibits the growth of A549 lung cancer cells via G2/M phase arrest and ROS-dependent apoptosis.* Int J Oncol, 2014. **44**(1): p. 301-8.

203. Peskin, A.V., et al., *Hyperoxidation of peroxiredoxins 2 and 3: rate constants for the reactions of the sulfenic acid of the peroxidatic cysteine.* J Biol Chem, 2013. **288**(20): p. 14170-7.

204. Wei, M.C., et al., *tBID, a membrane-targeted death ligand, oligomerizes BAK to release cytochrome c.* Genes Dev, 2000. **14**(16): p. 2060-71.

205. Meijerink, J.P., et al., *Hematopoietic malignancies demonstrate loss-of-function mutations of BAX.* Blood, 1998. **91**(8): p. 2991-7.

206. Gioia, L., et al., *A genome-wide survey of mutations in the Jurkat cell line.* BMC Genomics, 2018. **19**(1): p. 334.

207. Albert, M.C., K. Brinkmann, and H. Kashkar, *Noxa and cancer therapy: Tuning up the mitochondrial death machinery in response to chemotherapy.* Mol Cell Oncol, 2014. **1**(1): p. e29906.

208. Jaffrey, S.R. and S.H. Snyder, *The biotin switch method for the detection of S-nitrosylated proteins.* Sci STKE, 2001. **2001**(86): p. pl1.

209. Lowe, O., et al., *BIAM switch assay coupled to mass spectrometry identifies novel redox targets of NADPH oxidase 4.* Redox Biol, 2019. **21**: p. 101125.

210. Dagnell, M., E.E. Schmidt, and E.S.J. Arner, *The A to Z of modulated cell patterning by mammalian thioredoxin reductases.* Free Radic Biol Med, 2018. **115**: p. 484-496.

211. Johnston, A.S., S.E. Lehnart, and J.R. Burgoyne, *Ca(2+) signaling in the myocardium by (redox) regulation of PKA/CaMKII.* Front Pharmacol, 2015. **6**: p. 166.

212. Hande, K.R., *Etoposide: four decades of development of a topoisomerase II inhibitor.* Eur J Cancer, 1998. **34**(10): p. 1514-21.

213. Pena-Blanco, A. and A.J. Garcia-Saez, *Bax, Bak and beyond - mitochondrial performance in apoptosis.* FEBS J, 2018. **285**(3): p. 416-431.

214. Anderson, D.M., et al., *Widespread control of calcium signaling by a family of SERCA-inhibiting micropeptides.* Sci Signal, 2016. **9**(457): p. ra119.

215. Czabotar, P.E., et al., *Structural insights into the degradation of Mcl-1 induced by BH3 domains.* Proc Natl Acad Sci U S A, 2007. **104**(15): p. 6217-22.

216. Baou, M., et al., *Role of NOXA and its ubiquitination in proteasome inhibitor-induced apoptosis in chronic lymphocytic leukemia cells.* Haematologica, 2010. **95**(9): p. 1510-8.

217. Reinheckel, T., et al., *Comparative resistance of the 20S and 26S proteasome to oxidative stress.* Biochem J, 1998. **335 (Pt 3)**: p. 637-42.

218. Ishii, T., et al., *Oxidative modification of proteasome: identification of an oxidation-sensitive subunit in 26 S proteasome.* Biochemistry, 2005. **44**(42): p. 13893-901.

219. Wang, X., et al., *Regulation of the 26S proteasome complex during oxidative stress.* Sci Signal, 2010. **3**(151): p. ra88.

220. Aikawa, T., et al., *Noxa is necessary for hydrogen peroxide-induced caspase-dependent cell death.* FEBS Lett, 2010. **584**(4): p. 681-8.

221. Oda, E., et al., *Noxa, a BH3-only member of the Bcl-2 family and candidate mediator of p53-induced apoptosis.* Science, 2000. **288**(5468): p. 1053-8.

222. Kim, J.Y., et al., *BH3-only protein Noxa is a mediator of hypoxic cell death induced by hypoxia-inducible factor 1alpha.* J Exp Med, 2004. **199**(1): p. 113-24.

223. Hershko, T. and D. Ginsberg, *Up-regulation of Bcl-2 homology 3 (BH3)-only proteins by E2F1 mediates apoptosis.* J Biol Chem, 2004. **279**(10): p. 8627-34.

224. Nikiforov, M.A., et al., *Tumor cell-selective regulation of NOXA by c-MYC in response to proteasome inhibition.* Proc Natl Acad Sci U S A, 2007. **104**(49): p. 19488-93.

225. Cheng, J. and M. Haas, *Frequent mutations in the p53 tumor suppressor gene in human leukemia T-cell lines.* Mol Cell Biol, 1990. **10**(10): p. 5502-9.

226. Wortel, I.M.N., et al., *Surviving Stress: Modulation of ATF4-Mediated Stress Responses in Normal and Malignant Cells.* Trends Endocrinol Metab, 2017. **28**(11): p. 794-806.

227. Ishizawa, J., et al., *ATF4 induction through an atypical integrated stress response to ONC201 triggers p53-independent apoptosis in hematological malignancies.* Sci Signal, 2016. **9**(415): p. ra17.

228. Li, G., et al., *Upregulation of connexin43 contributes to PX-12-induced oxidative cell death.* Tumour Biol, 2016. **37**(6): p. 7535-46.

229. Albert, A., et al., *Speciation analysis of the antirheumatic agent Auranofin and its thiol adducts by LC/ESI-MS and LC/ICP-MS.* J Anal Atom Spectrom, 2012. **27**(6): p. 975-981.

230. Ricci, J.E., R.A. Gottlieb, and D.R. Green, *Caspase-mediated loss of mitochondrial function and generation of reactive oxygen species during apoptosis.* J Cell Biol, 2003. **160**(1): p. 65-75.

231. Miranda-Vizuete, A., A.E. Damdimopoulos, and G. Spyrou, *The mitochondrial thioredoxin system.* Antioxid Redox Signal, 2000. **2**(4): p. 801-10.

232. Kekulandara, D.N., et al., *Redox-Inactive Peptide Disrupting Trx1-Ask1 Interaction for Selective Activation of Stress Signaling.* Biochemistry, 2018. **57**(5): p. 772-780.

233. Tanaka, T., et al., *Thioredoxin-2 (TRX-2) is an essential gene regulating mitochondria-dependent apoptosis.* EMBO J, 2002. **21**(7): p. 1695-703.

234. Nonn, L., et al., *The absence of mitochondrial thioredoxin 2 causes massive apoptosis, exencephaly, and early embryonic lethality in homozygous mice.* Mol Cell Biol, 2003. **23**(3): p. 916-22.

235. Zhang, R., et al., *Thioredoxin-2 inhibits mitochondria-located ASK1-mediated apoptosis in a JNK-independent manner.* Circ Res, 2004. **94**(11): p. 1483-91.

236. Wonsey, D.R., K.I. Zeller, and C.V. Dang, *The c-Myc target gene PRDX3 is required for mitochondrial homeostasis and neoplastic transformation.* Proc Natl Acad Sci U S A, 2002. **99**(10): p. 6649-54.

237. Tan, Y., et al., *Thioredoxin-1 inhibitor PX-12 induces human acute myeloid leukemia cell apoptosis and enhances the sensitivity of cells to arsenic trioxide.* Int J Clin Exp Pathol, 2014. **7**(8): p. 4765-73.

238. Haas, B., et al., *Thioredoxin Confers Intrinsic Resistance to Cytostatic Drugs in Human Glioma Cells.* Int J Mol Sci, 2018. **19**(10).

239. Kotschy, A., et al., *The MCL1 inhibitor S63845 is tolerable and effective in diverse cancer models.* Nature, 2016. **538**(7626): p. 477-482.

240. Fulda, S. and D. Vucic, *Targeting IAP proteins for therapeutic intervention in cancer.* Nat Rev Drug Discov, 2012. **11**(2): p. 109-24.

241. Hundsdoerfer, P., et al., *XIAP expression is post-transcriptionally upregulated in childhood ALL and is associated with glucocorticoid response in T-cell ALL.* Pediatr Blood Cancer, 2010. **55**(2): p. 260-6.

242. Griffith, O.W. and A. Meister, *Potent and specific inhibition of glutathione synthesis by buthionine sulfoximine (S-n-butyl homocysteine sulfoximine).* J Biol Chem, 1979. **254**(16): p. 7558-60.

243. Metcalfe, C., et al., *Thioredoxin Inhibitors Attenuate Platelet Function and Thrombus Formation.* PLoS One, 2016. **11**(10): p. e0163006.

244. Hockenbery, D.M., et al., *Bcl-2 functions in an antioxidant pathway to prevent apoptosis.* Cell, 1993. **75**(2): p. 241-51.

245. Kane, D.J., et al., *Bcl-2 inhibition of neural death: decreased generation of reactive oxygen species.* Science, 1993. **262**(5137): p. 1274-7.

246. Coles, S.J., J.T. Hancock, and M.E. Conway, *Differential redox potential between the human cytosolic and mitochondrial branched-chain aminotransferase.* Acta Biochim Biophys Sin (Shanghai), 2012. **44**(2): p. 172-6.

247. Martin, D.R., et al., *Structural and activity characterization of human PHPT1 after oxidative modification.* Sci Rep, 2016. **6**: p. 23658.

248. Ishii, T., Y. Funato, and H. Miki, *Thioredoxin-related protein 32 (TRP32) specifically reduces oxidized phosphatase of regenerating liver (PRL).* J Biol Chem, 2013. **288**(10): p. 7263-70.

249. Cho, D.H., et al., *Induced inhibition of ischemic/hypoxic injury by APIP, a novel Apaf-1-interacting protein.* J Biol Chem, 2004. **279**(38): p. 39942-50.

250. Mary, C., et al., *Functional identification of APIP as human mtnB, a key enzyme in the methionine salvage pathway.* PLoS One, 2012. **7**(12): p. e52877.

251. Ko, D.C., et al., *Functional genetic screen of human diversity reveals that a methionine salvage enzyme regulates inflammatory cell death.* Proc Natl Acad Sci U S A, 2012. **109**(35): p. E2343-52.

252. Kang, W., et al., *Structural and biochemical basis for the inhibition of cell death by APIP, a methionine salvage enzyme.* Proc Natl Acad Sci U S A, 2014. **111**(1): p. E54-61.

253. Tang, B., et al., *The methionine salvage pathway compound 4-methylthio-2-oxobutanate causes apoptosis independent of down-regulation of ornithine decarboxylase.* Biochem Pharmacol, 2006. **72**(7): p. 806-15.

254. Basu, I., et al., *A transition state analogue of 5'-methylthioadenosine phosphorylase induces apoptosis in head and neck cancers.* J Biol Chem, 2007. **282**(29): p. 21477-86.

255. Fu, L., et al., *Systematic and Quantitative Assessment of Hydrogen Peroxide Reactivity With Cysteines Across Human Proteomes.* Mol Cell Proteomics, 2017. **16**(10): p. 1815-1828.

256. Yamagata, K., et al., *Arginine methylation of FOXO transcription factors inhibits their phosphorylation by Akt.* Mol Cell, 2008. **32**(2): p. 221-31.

257. Sakamaki, J., et al., *Arginine methylation of BCL-2 antagonist of cell death (BAD) counteracts its phosphorylation and inactivation by Akt.* Proc Natl Acad Sci U S A, 2011. **108**(15): p. 6085-90.

258. Cho, J.H., et al., *Arginine methylation-dependent regulation of ASK1 signaling by PRMT1.* Cell Death Differ, 2012. **19**(5): p. 859-70.

259. Morales, Y., et al., *Redox Control of Protein Arginine Methyltransferase 1 (PRMT1) Activity.* J Biol Chem, 2015. **290**(24): p. 14915-26.

260. Orrenius, S., V. Gogvadze, and B. Zhivotovsky, *Mitochondrial oxidative stress: implications for cell death.* Annu Rev Pharmacol Toxicol, 2007. **47**: p. 143-83.

261. Pallepati, P. and D. Averill-Bates, *Mild thermotolerance induced at 40 degrees C increases antioxidants and protects HeLa cells against mitochondrial apoptosis induced by hydrogen peroxide: Role of p53.* Arch Biochem Biophys, 2010. **495**(2): p. 97-111.

262. D'Alessio, M., et al., *Oxidative Bax dimerization promotes its translocation to mitochondria independently of apoptosis.* FASEB J, 2005. **19**(11): p. 1504-6.

263. Nie, C., et al., *Cysteine 62 of Bax is critical for its conformational activation and its proapoptotic activity in response to H2O2-induced apoptosis.* J Biol Chem, 2008. **283**(22): p. 15359-69.

264. Mandal, T., et al., *Assembly of Bak homodimers into higher order homooligomers in the mitochondrial apoptotic pore.* Sci Rep, 2016. **6**: p. 30763.

265. Aouacheria, A., et al., *Redefining the BH3 Death Domain as a 'Short Linear Motif'.* Trends Biochem Sci, 2015. **40**(12): p. 736-748.

266. Aluvila, S., et al., *Organization of the mitochondrial apoptotic BAK pore: oligomerization of the BAK homodimers.* J Biol Chem, 2014. **289**(5): p. 2537-51.

267. Karch, J., et al., *Autophagic cell death is dependent on lysosomal membrane permeability through Bax and Bak.* Elife, 2017. **6**.

268. Gozuacik, D. and A. Kimchi, *Autophagy and cell death.* Curr Top Dev Biol, 2007. **78**: p. 217-45.

269. Youle, R.J. and A.M. van der Bliek, *Mitochondrial fission, fusion, and stress.* Science, 2012. **337**(6098): p. 1062-5.

270. Gandre-Babbe, S. and A.M. van der Bliek, *The novel tail-anchored membrane protein Mff controls mitochondrial and peroxisomal fission in mammalian cells.* Mol Biol Cell, 2008. **19**(6): p. 2402-12.

271. Otera, H., et al., *Mff is an essential factor for mitochondrial recruitment of Drp1 during mitochondrial fission in mammalian cells.* J Cell Biol, 2010. **191**(6): p. 1141-58.

272. Kalia, R., et al., *Structural basis of mitochondrial receptor binding and constriction by DRP1.* Nature, 2018. **558**(7710): p. 401-405.

273. Zong, W.X., et al., *Bax and Bak can localize to the endoplasmic reticulum to initiate apoptosis.* J Cell Biol, 2003. **162**(1): p. 59-69.

274. Scorrano, L., et al., *BAX and BAK regulation of endoplasmic reticulum Ca2+: a control point for apoptosis.* Science, 2003. **300**(5616): p. 135-9.

275. Hosoi, K.I., et al., *The VDAC2-BAK axis regulates peroxisomal membrane permeability.* J Cell Biol, 2017. **216**(3): p. 709-722.

276. Fujiki, Y., et al., *BAK regulates catalase release from peroxisomes.* Mol Cell Oncol, 2017. **4**(3): p. e1306610.

277. Chipuk, J.E. and M.P. Luna-Vargas, *The peroxisomes strike BAK: Regulation of peroxisome integrity by the Bcl-2 family.* J Cell Biol, 2017. **216**(3): p. 547-549.

278. Cheng, E.H., et al., *VDAC2 inhibits BAK activation and mitochondrial apoptosis.* Science, 2003. **301**(5632): p. 513-7.

279. Setoguchi, K., H. Otera, and K. Mihara, *Cytosolic factor- and TOM-independent import of C-tail-anchored mitochondrial outer membrane proteins.* EMBO J, 2006. **25**(24): p. 5635-47.

9 Appendix

Table 24: Significantly enriched proteins identified in the MS analysis of Jurkat FD cells. Fold changes are shown for Auranofin-treated cells compared to control (Ctrl). Table was generated by I. Wittig.

Gene names	Majority protein IDs	-Log Student's T-test p-value Auranofin/Ctrl	Fold change Auranofin/Ctrl
C16orf87	H3BQL3;Q6PH81	7.64	7.23
TOR1AIP2	Q9H496	5.83	5.66
NAA40	Q86UY6	5.64	31.63
IAH1	H7C5G1;Q2TAA2	5.55	3.43
FBXO22	Q8NEZ5;H3BRE0;H3BTH6	4.98	11.31
PFN2	C9J712;P35080;C9JQ45	4.74	3.16
BUD31	P41223;C9JNV2;C9JCD9	4.65	3.93
TXNDC17	Q9BRA2;I3L2R6	4.01	3.07
RFX5	F8W689;P48382	3.72	4.35
BCAT1	P54687	3.48	4.57
PHPT1	Q9NRX4	3.44	4.56
MNAT1	P51948;H0YJ92;H0YJF2	3.42	2.69
RPS26/S26P11	P62854;Q5JNZ5	3.31	2.40
PTP4A2	Q12974	3.21	2.24
APIP	Q96GX9;S4R3D6	3.15	2.01
NUDT5	A6NFX8;Q9UKK9;H0YEY4;A6NCQ0;A6NJU6	3.09	1.68
SMYD5	E2QRN5;F8WEJ9;C9IYN9;Q6GMV2	3.00	3.78
PDLIM1	O00151	2.98	2.20
RNF5	Q99942;A0A140TA09	2.89	2.41
RAB11A/11B	B4DQU5;H3BMH2;H3BSC1;P62491;Q15907	2.89	10.29
PGPEP1	Q9NXJ5;U3KQ24;U3KQG9;S4R2Y9	2.88	6.50
TXN	P10599	2.84	2.51
GEMIN5	Q8TEQ6	2.82	3.86
OGFOD2	Q6N063;F5H145	2.79	4.41
PRMT1	A0A087X1W2;E9PKG1;H7C2I1;Q99873	2.79	9.60
DPF2	J3KMZ8;Q92785;E9PN04	2.77	2.32
RNF20	Q5VTR2	2.72	4.40
FUS	P35637;H3BPE7	2.71	2.35
PPP2R2A/B/D	E5RFR9;Q00005;P63151;Q66LE6	2.71	2.40
IDI1	Q13907;C9JKM8	2.67	2.23
NUBP2	Q9Y5Y2;B7Z6P0;H3BQR2	2.66	2.53
MTFR1L	E9PLD2;Q9H019	2.55	3.30
ZNF346	B7Z4N4;B7Z4J8;D6RJ07;Q9UL40	2.54	10.69
PITHD1	Q9GZP4	2.53	12.65
DNAJA1	P31689	2.52	2.14
RNF168	Q8IYW5	2.52	3.55
BOLA1	Q9Y3E2	2.51	2.39
ADH5	P11766	2.50	1.92
TOMM40	O96008	2.49	2.32
PDCD2L	Q9BRP1	2.47	2.47
NHLRC2	Q8NBF2	2.45	2.66
SS18L2	Q9UHA2	2.44	3.03
CEP72	Q9P209	2.42	2.50
INTS12	D6R9Y5;A0A1B0GX90	2.41	2.36
GLRX	P35754	2.40	2.34
ZNF787	A0A087WUD1;Q6DD87	2.38	6.34
QTRT1	Q9BXR0;K7ESP6	2.33	13.20
ZC3H14	H0YJA2;Q6PJT7;G3V5I6;G3V256	2.28	3.82
GMPR/2	A0A0B4J281;H0YMG3	2.28	2.91
NPLOC4	Q8TAT6	2.27	8.08
SF3B6	Q9Y3B4	2.25	7.49
KCMF1	Q9P0J7	2.23	2.33
C8orf33	Q9H7E9	2.21	4.73
PDXP	Q96GD0	2.20	9.75
CEP63	D6R9Q4;D6RAY6;Q96MT8	2.19	2.78
INCENP	Q9NQS7	2.17	3.16
HARS	P12081;B3KWE1;B4DDD8;B4E1C5	2.16	3.25
HK2	P52789	2.07	4.13
REPIN1	E7EVL6;C9JZE3;C9JYJ8;Q9BWE0	2.07	5.02
PPME1	Q9Y570	2.03	5.62
KCTD5	Q9NXV2	1.98	6.25
ZNHIT2	E9PQB8;Q9UHR6	1.97	4.42

Gene names	Majority protein IDs	-Log Student's T-test p-value Auranofin/Ctrl	Fold change Auranofin/Ctrl
SPRYD7	Q5W111	2.56	1.67
SRSF3	P84103;A0A087X2D0	2.41	1.60
CSNK2B	Q5SRQ6;P67870;Q5SRQ3;N0E472;A0A0G2JM12	2.40	1.58
POLR2C	P19387	2.40	1.80
TIA1	C9JTN7;F8W8I6;P31483;E5RGV5	2.38	1.72
SLBP	F8W8D3;Q14493;H7C4H8;H0YAE8;E7EUV9	2.31	2.00
PRDX1	A0A0A0MSI0;Q06830	2.28	1.69
TYMS	P04818	2.23	1.51
PRDX2	P32119;A6NIW5	2.21	1.94
PPA2	Q9H2U2	2.19	1.89
DENR	O43583;F8VVL1	2.18	1.38
ZCCHC3	Q9NUD5	2.18	2.41
SEC61B	P60468	2.11	2.56
COX5B	P10606	2.11	1.56
PPP4R1	J3KRU1;J3QL26;J3KSB0;J3QLA6;J3QQV0;Q8TF05	2.11	2.35
PWP1	Q13610;B4DJV5	2.10	1.71
MIF	P14174	2.09	1.61
TRA2B	P62995;H7C2L4;H7BXF3	2.09	1.71
FAM118A	B0QY29;Q9NWS6	2.09	1.33
PHF6	A0A0D9SGE8;Q8IWS0;Q5JRC6	2.06	2.96
VRK3	M0R073;M0QYA8;Q8IV63	2.05	1.84
MTCH2	Q9Y6C9;E9PIE4	2.05	2.49
NOB1	H3BUR4;Q9ULX3	2.04	2.86
MAZ	I3L2Z5;A0A087WWR2;P56270;H3BQI4	2.04	1.52
PPA1	Q15181	2.02	1.99
CLPX	O76031	2.01	2.89
COMMD4	A0A0B4J287;Q9H0A8;H3BM91	2.00	2.91
DTWD2	D6REE2;D6RBD8;Q8NBA8	1.99	2.59
HDGF	P51858	1.99	1.54
DCTN4	Q9UJW0	1.97	3.52
ATXN10	Q9UBB4	1.96	1.90
CLPP	M0R208;Q16740;M0QYV5	1.96	1.40
CIAPIN1	Q6FI81;H3BV90;H3BT65;H3BUG4;H3BQ23;H3BPG7	1.96	2.14
SH2D1A	O60880	1.93	2.54
PSMB3	P49720;A0A087WY10;A0A087WUL2;A0A087WXQ8	1.91	2.38
API5	G3V1C3;Q9BZZ5	1.90	2.76
BDH2	D6RBF6;D6RFG2;D6R9U8;D6RIR6;Q9BUT1	1.88	2.03
PHF5A	Q7RTV0	1.88	1.73
SCAF8	A0A0A0MT33;Q9UPN6	1.87	6.37
RPP25L	Q8N5L8	1.87	1.57
RNF187	Q5TA31	1.86	2.78
TAF15	Q92804;A0A075B7D9	1.84	1.88
MAFG	I3L2F8	1.81	8.51
LIMS1	C9JF46;A0A0J9YXC7;P48059	1.81	2.36
TRIM28	Q13263	1.80	1.83
CHAMP1	Q96JM3	1.78	1.79
PDCL	Q13371;H0Y5D3;H0Y3M0	1.77	2.97
ZPR1	H7C0E5;H7BZM7;O75312	1.77	2.03
CARHSP1	Q9Y2V2;H3BSW7;H3BUY4;H3BPY5;H3BNU9	1.76	1.94
MAP2K4	P45985	1.76	2.19
SPHKAP	Q2M3C7	1.76	15.10
RNF181	Q9P0P0;F8WBU5;C9J391;C9J1C6;H7C426	1.76	1.81
BRIX1	Q8TDN6	1.75	1.67
PPIG	C9JN15;E9PG73;Q13427;C9JT64;C9J679;C9JM79	1.75	1.73
ZNF22	P17026	1.75	5.69
NDUFS1	B4DJ81;P28331	1.75	1.40
CENPV	Q7Z7K6	1.74	1.78
PSMG4	D6REN3;E2QRC7;D6RB92;Q5JS54;H7C465	1.71	2.43
VEZF1	J3QSH4;Q14119;J9JIC7	1.71	3.56
PDCD2	Q16342;F5GWT2;J3QK82;A0A087WYJ3;F5H4V9	1.70	2.26
NUMA1	A0A087WY61;Q14980;H0YFY6	1.70	1.74
PSMB8	Q5JNW7;A0A140T998;X5D2R7;P28062	1.68	1.73
PDLIM2	Q96JY6;C9JS55;A0A087WVI1	1.67	4.55
TMOD3	Q9NYL9;H0YKU1;H0YNJ8	1.67	1.73
LPXN	O60711;B7Z5P7	1.67	1.93
IKBKG	Q9Y6K9;A0A087WUW6;A0A087X1B1	1.66	7.58
ING1	A0A087WXF7;A0A0C4DFW2;Q9UK53	1.64	2.20
TPX2	Q9ULW0	1.64	1.65
IGBP1	P78318	1.63	1.69
UROD	A0A1B0GVZ4;P06132;Q5T446;A0A1B0GVN9	1.63	1.62
PPAT	Q06203	1.62	1.59
BCL11B	D3YTK1;Q9C0K0	1.62	2.22
NIFK	Q9BYG3;C9J6C5	1.62	1.44
BCCIP	Q9P287	1.61	1.58

Gene names	Majority protein IDs	-Log Student's T-test p-value Auranofin/Ctrl	Fold change Auranofin/Ctrl
ING4	E9PJ14;A4KYM5;Q9UNL4	1.61	2.85
RPP30	Q5VU11;P78346	1.60	1.53
MRPL12	B4DLN1;P52815	1.60	2.49
NAA10	P41227;F8W808;A8MWP7	1.59	1.66
DRG1	Q9Y295;F8WEE0	1.58	2.86
LYAR	Q9NX58	1.58	6.57
ALKBH5	Q6P6C2	1.58	1.41
PHC2	B3KPJ4;A0A0A0MSI2;Q8IXK0	1.58	3.44
LCMT1	Q9UIC8	1.56	2.13
RBM4/4B	Q9BWF3;E9PB51;D6R9K7;J3QRR5;Q9BQ04	1.56	1.45
CCDC77	F5H0W5;Q9BR77	1.55	2.01
TARDBP	Q13148;B1AKP7;G3V162	1.55	1.75
NOP2	P46087;F5H5X6	1.55	1.26
GNL3	Q9BVP2	1.54	1.30
XPNPEP1	Q5T6H7;Q9NQW7	1.54	1.76
RBM42	K7EQ03;K7EP90;Q9BTD8	1.54	3.80
EIF5B	A0A087WUT6;O60841	1.53	2.10
RNASEH2B	A0A087WXR7;Q5TBB1;A0A087WZJ6	1.51	1.54
SDHB	P21912;A0A087WXX8;A0A087WWT1	1.51	1.68
PEPD	P12955	1.51	2.09
CAMK4	Q16566	1.50	1.44
TSR2	Q969E8	1.50	1.85
TIMM23	O14925	1.50	2.05
PTRH2	J3KQ48;Q9Y3E5	1.50	2.17
ACSL4	O60488	1.50	1.62
RUNX1	Q01196;H9KVB1;A8MZI9;C9JWM1	1.50	1.33
PAK4	M0R2X4;O96013	1.49	1.88
TUBA1C	F5H5D3;Q9BQE3;F8VVB9	1.49	3.53
GIMAP1	Q8WWP7	1.49	2.44
GLCCI1	Q86VQ1;H7C0B2	1.48	1.87
ZNF598	H3BQQ2;Q86UK7	1.48	2.46
CCDC86	Q9H6F5	1.48	1.95
PPM1G	O15355	1.47	1.60
ABHD17B	Q5VST6	1.46	2.74
IKZF1	A0A0A0MRA0;R9R4D9	1.46	1.72
LRRFIP1	Q32MZ4	1.45	1.61
SRP19	A0A087WWU9;P09132	1.45	1.54
TCOF1	J3KQ96;E7ETY2;Q13428	1.45	1.62
CHORDC1	Q9UHD1;E9PPQ5	1.44	1.34
S100A4	P26447	1.44	2.16
ABCF1	H0YGW7;Q8NE71	1.44	1.39
RNF214	E9PN76;Q8ND24	1.44	1.98
C5orf22	Q49AR2;E5RFG1;B4DR92;E5RHP8	1.44	3.14
GINS1	Q14691	1.44	3.45
ZYX	Q15942;H0Y2Y8	1.43	1.63
SRSF10	Q6IQ42;Q5JRI1;O75494	1.42	1.40
TXN2	M0QXH0;Q99757	1.41	2.85
DAZAP1	K7EQ02;K7EQ55;K7EK33;Q96EP5	1.41	1.50
MRPS18B	Q9Y676;A0A0G2JIC6	1.40	5.21
SCO1	J3QL56;O75880	1.40	5.45
GTF2F1	M0R0Z3;M0R0R9;M0QXD6;P35269	1.39	3.96
MAP7D1	Q3KQU3	1.39	1.61
PSMD10	B1AJY5;B1AJY7;O75832	1.39	1.46
RRM1	P23921	1.39	2.44
PRDX3	P30048	1.36	1.53
TCEB2	Q15370;A0A0B4J296;B8ZZU8	1.35	1.61
SPATS2L	B8ZZZ7;Q9NUQ6	1.35	1.94
NTMT1	Q9BV86	1.35	1.60
CDCA7	Q9BWT1	1.35	1.53
TARS	P26639	1.34	1.70
EWSR1	H7BY36;A0A0D9SFL3;B0QYK0	1.34	1.53
BABAM1	M0QYV1;M0R3F4;M0R2A4	1.34	2.58
ZFP42	H0YJV7;Q96MM3;O15391;P25490	1.33	1.52
C20orf27	Q9GZN8;H7BYU9	1.33	1.75
GLYR1	K7EMM8;Q49A26	1.33	1.50
PTPN1	P18031;B4DSN5	1.33	7.00
TRAF3IP3	E2QRE5;Q9Y228;C9JBA0;B1AJU2;C9J0C0	1.32	1.55
PSMA6	G3V5Z7;P60900;G3V295;G3V3I1;G3V3U4	1.31	1.45

Table 25: Interaction partners of mRuby2-BAK identified in the MS analysis. Results were normalized to mRuby2 expression. Fold changes are shown as mRuby2-BAK-WT (WT) compared to mRuby2-BAK-C14S-C154S (SS). Table was generated by I. Wittig.

Gene names	Majority protein IDs	-Log Student's T-test p-value WT/SS	fold change WT/SS
C4orf3 homolog	Q99M08	9.32	62.27
M6pr	P24668	6.40	26.64
Ptgis	O35074	5.67	17.26
Cxadr	P97792	8.19	15.46
Cd44	P15379	4.54	15.40
Ikbip	Q9DBZ1	6.26	13.44
Itga5	P11688	4.08	11.97
Itgb1	P09055	6.78	11.85
Scarb2	O35114	3.75	11.46
Pgrmc2	Q80UU9	2.57	10.77
Mff	Q6PCP5	3.40	10.26
Esyt1	Q3U7R1	5.67	10.11
Tmed5	Q9CXE7	5.00	8.66
Actg2;Acta1;Actc1;Acta2	P63268;P68134;P68033;P62737	3.47	8.54
Glipr2	Q9CYL5	1.86	8.32
Zmpste24	Q80W54	3.74	7.86
Cox7a2	P48771	6.31	7.79
Vti1a	O89116	5.29	7.67
Basp1	Q91XV3	3.75	7.67
Slc3a2	P10852	3.06	7.64
Vdac2	Q60930	4.02	7.62
Itga6	Q61739	3.83	7.40
Cspg4	Q8VHY0	6.55	6.72
Rpn2	Q9DBG6	5.38	6.61
Cisd1	Q91WS0	4.08	5.76
Mlec	Q6ZQI3	1.71	5.75
Atad1	Q9D5T0	4.72	5.60
Rab35	Q6PHN9	3.48	5.51
Rab2a	P53994	3.74	5.33
Rab18	P35293	3.33	5.00
Lnpep	Q8C129	3.71	4.97
Rac2;Rac1;Rac3	Q05144;P63001;P60764	3.50	4.96
Ephx1	Q9D379	5.13	4.78
Ptk7	Q8BKG3	5.49	4.70
Nradd	Q8CJ26	3.46	4.66
Ociad1	Q9CRD0	3.96	4.65
Rab6a	P35279	2.89	4.51
Vdac1	Q60932	2.68	4.43
Stx4	P70452	5.46	4.38
Nucks1	Q80XU3	3.58	4.17
Vamp3	P63024	4.10	3.81
Stx7	O70439	2.37	3.76
Palm	Q9Z0P4	3.28	3.71
Vamp4	O70480	1.47	3.68
Rab14	Q91V41	5.01	3.63
Lman2	Q9DBH5	3.13	3.56
Rap1b;Rap1a	Q99JI6;P62835	3.35	3.53
Spcs3	Q6ZWQ7	1.59	3.42
Degs1	O09005	1.60	3.37
Vti1b	O88384	3.51	3.26
Impad1	Q80V26	4.59	3.25
H2-K1	P01901;P14428;P03991;P04223	1.70	3.23
Mogs	Q80UM7	3.45	3.19
Galnt2	Q6PB93	5.34	3.18
Chmp6	P0C0A3	1.25	3.18
Rab11a;Rab11b	P62492;P46638	5.38	3.15
Canx	P35564	4.01	3.12
Cyb5b	Q9CQX2	4.02	3.10
Por	P37040	0.94	3.06
Rab10	P61027	3.85	2.93
Mfge8	P21956	1.32	2.93
Tmpo	Q61029;Q61033	4.69	2.82
Tmed9	Q99KF1	4.21	2.81
Vapb	Q9QY76	3.32	2.80
Atp5f1	Q9CQQ7	1.03	2.76
Tmed10	Q9D1D4	4.17	2.68
Lrp1	Q91ZX7	3.06	2.67
Igf2r	Q07113	1.65	2.66
Rab1A	P62821	1.82	2.65

Gene names	Majority protein IDs	-Log Student's T-test p-value WT/SS	fold change WT/SS
Cpd	O89001	2.77	2.65
Snap23	O09044	3.87	2.65
Lnp	Q7TQ95	4.46	2.59
Vapa	Q9WV55	3.74	2.49
Ldlr	P35951	1.92	2.48
Vamp8	O70404	3.64	2.48
Cyb5r3	Q9DCN2	4.27	2.40
Ncbp2	Q9CQ49	1.16	2.35
Ssr3	Q9DCF9	1.66	2.32
Ccdc167	Q9D162	2.81	2.31
Hmox2	O70252	2.91	2.31
Sec11a	Q9R0P6	1.29	2.21
Golm1	Q91XA2	2.14	2.20
Actn1	Q7TPR4	0.61	2.18
Mrc2	Q64449	2.32	2.15
Cyb5a	P56395	1.87	2.13
Slc7a5	Q9Z127	1.25	2.02
Hmox1	P14901	3.34	2.00
Bsg	P18572	3.27	1.98
Glud1	P26443	1.88	1.96
Anxa2	P07356	1.21	1.93
Cyb5r1	Q9DB73	2.35	1.91
Glg1	Q61543	1.09	1.88
	P0DN34	0.66	1.82
Lyar	Q08288	0.92	1.81
Slc2a1	P17809	0.85	1.80
Mxra7	Q9CZH7	1.41	1.76
Mdh2	P08249	0.81	1.74
Tm9sf4	Q8BH24	0.53	1.71
Rab8a	P55258	1.00	1.68
Prpf38b	Q80SY5	0.47	1.67
Tmem43	Q9DBS1	2.61	1.64
Myof	Q69ZN7	3.44	1.64
Gpd2	Q64521	1.14	1.63
Cox4i1	P19783	2.39	1.61
Bak1	O08734	0.76	1.60
Pgrmc1	O55022	2.18	1.59
Atp5h	Q9DCX2	0.58	1.55
Bcap29	Q61334	0.60	1.55
Phb2	O35129	1.34	1.51
Bloc1s5	Q8R015	0.41	1.46
Cox6c	Q9CPQ1	1.11	1.45
Cav1;Cav3	P49817;P51637	0.34	1.44
Gnb2l1	P68040	0.43	1.43
Rsrc2	A2RTL5	0.36	1.40
Ermp1	Q3UVK0	0.89	1.37
Cwc25	Q9DBF7	0.54	1.34
Sco2	Q8VCL2	0.39	1.32
Alg9	Q8VDI9	0.86	1.32
Snw1	Q9CSN1	0.32	1.30
H2-D1;H2-L	P01899;P01897	0.86	1.30
Rab8b	P61028	0.57	1.28
Hnrnpa2b1	O88569	0.38	1.27
Nelfe	P19426	0.25	1.26
	Q8CIL4	0.65	1.25
Lman1	Q9D0F3	0.80	1.25
Flnb	Q80X90	0.31	1.21
Hsd17b12	O70503	0.37	1.21
Stx8	O88983	0.23	1.20
Phb	P67778	0.32	1.19
Rab7a	P51150	0.90	1.18
Tmem2	Q5FWI3	0.17	1.18
Stx2	Q00262	0.24	1.17
Rab5c	P35278	0.23	1.16
Dld	O08749	0.26	1.16
Emc7	Q9EP72	0.61	1.16
Cox5a	P12787	0.41	1.16
D8Ertd738e	Q8R1F0	0.08	1.13
Cpsf7	Q8BTV2	0.28	1.13
Puf60	Q3UEB3	0.44	1.12
Emc2	Q9CRD2	0.45	1.11
Rpn1	Q91YQ5	0.60	1.09
Epha2	Q03145	0.12	1.09
Atp1a1	Q8VDN2	0.31	1.07

Gene names	Majority protein IDs	-Log Student's T-test p-value WT/SS	fold change WT/SS
Rnps1	Q99M28	0.10	1.06
Hsp90aa1	P07901	0.14	1.05
Bax	Q07813	0.16	1.04
Ube2j1	Q9JJZ4	0.06	1.03
Srsf1	Q6PDM2	0.05	1.03
Snrnp70	Q62376	0.02	1.03
Hspa8;Hspa2	P63017;P17156	0.04	1.02
Fip1l1	Q9D824	0.02	1.01
Nsrp1	Q5NCR9	0.01	1.01
Atp5a1	Q03265	0.01	1.00
Srsf2	Q62093	0.01	1.00
Ruby	XMRUBY2	0.15	1.00
Emc4	Q9CZX9	0.01	-1.01
Apc2	Q9Z1K7	0.02	-1.02
Shmt2	Q9CZN7	0.06	-1.02
Atp5c1	Q91VR2	0.03	-1.02
Znf593	Q9DB42	0.05	-1.03
Cmtm4	Q8CJ61	0.05	-1.03
Rps25	P62852	0.12	-1.04
Vat1	Q62465	0.10	-1.05
Nudt21	Q9CQF3	0.18	-1.06
P4hb	P09103	0.31	-1.07
Fau	P62862	0.10	-1.09
Myl6	Q60605	0.23	-1.09
Xxylt1	Q3U4G3	0.28	-1.09
Fam32a	Q9CR80	0.43	-1.10
Ckap4	Q8BMK4	0.40	-1.11
Actn4	P57780	0.26	-1.11
Sart1	Q9Z315	0.32	-1.11
Srp14	P16254	0.39	-1.12
Ppib	P24369	0.42	-1.13
Bcl2l1	Q64373	0.35	-1.13
Pdia3	P27773	0.70	-1.13
Emc8	O70378	0.32	-1.14
Hnrnpa3	Q8BG05	0.29	-1.14
Atp5b	P56480	0.55	-1.16
Snrnp27	Q8K194	0.37	-1.17
Myh9	Q8VDD5	0.22	-1.20
Capns1	O88456	0.92	-1.20
Atpif1	O35143	0.43	-1.22
Tma16	Q9CR02	0.55	-1.23
Arl6ip4	Q9JM93	0.87	-1.23
Tma7	Q8K003	0.29	-1.24
Acadl	P51174	0.68	-1.24
Bcap31	Q61335	1.20	-1.26
Actb	P60710	1.54	-1.26
Myh10	Q61879	0.32	-1.28
Cct5	P80316	0.46	-1.32
Cfl1	P18760	0.55	-1.32
Sptan1	P16546	1.77	-1.35
Dhx8	A2A4P0	0.47	-1.37
Cpsf6	Q6NVF9	2.23	-1.39
Frg1	P97376	1.29	-1.40
Emc1	Q8C7X2	0.57	-1.41
Srsf7	Q8BL97	1.39	-1.41
Rbm39	Q8VH51	1.15	-1.46
Tpm3	P21107	0.57	-1.49
Hmgb2	P30681	0.36	-1.50
Sptbn1	Q62261	2.22	-1.52
Vcp	Q01853	1.79	-1.52
Sub1	P11031	1.84	-1.53
Hspa5	P20029	3.59	-1.55
	Q9D937	1.31	-1.57
Dars	Q922B2	0.84	-1.60
Anxa1	P10107	2.59	-1.60
Hmgb1	P63158	1.80	-1.60
Hsp90b1	P08113	3.59	-1.60
Zmat2	Q9CPW7	1.53	-1.61
Serpinh1	P19324	2.32	-1.62
Hnrnpa1	P49312	1.45	-1.62
Srsf3	P84104	2.45	-1.64
Psip1	Q99JF8	1.29	-1.64
Hspa9	P38647	1.19	-1.64
Lamc1	P02468	2.35	-1.66

Gene names	Majority protein IDs	-Log Student's T-test p-value WT/SS	fold change WT/SS
Luc7l2	Q7TNC4	2.12	-1.66
Hist1h1c	P15864	2.10	-1.69
Atp5i	Q06185	1.94	-1.69
Tpm1	P58771	0.58	-1.75
Eif5b	Q05D44	2.28	-1.75
Nufip2	Q5F2E7	2.95	-1.76
Eif3e	P60229	0.99	-1.76
Rpl22l1	Q9D7S7	2.90	-1.78
Nol12	Q8BG17	3.09	-1.78
Eef1g	Q9D8N0	2.21	-1.80
Hdgfrp2	Q3UMU9	2.70	-1.81
Mrps26	Q80ZS3	1.32	-1.81
Mmtag2	Q99LX5	1.56	-1.82
Arglu1	Q3UL36	5.08	-1.84
Lonp1	Q8CGK3	2.06	-1.85
Hsp90ab1	P11499	4.23	-1.90
Gnl2	Q99LH1	0.99	-1.90
Srsf6	Q3TWW8	0.87	-1.90
Gapdh	P16858	2.45	-1.92
Tubb5;Tubb2b;Tubb2a;Tubb3	P99024;Q9CWF2;Q7TMM9;Q9ERD7	1.85	-1.92
Rpsa	P14206	3.57	-1.95
Ddx42	Q810A7	2.03	-1.95
Rbmxl1;Rbmx	Q91VM5;Q9WV02	1.50	-1.96
Ebna1bp2	Q9D903	1.69	-1.96
Ran	P62827	3.14	-2.00
Ruvbl2	Q9WTM5	3.00	-2.00
Myl12b	Q3THE2	1.36	-2.01
Nop16	Q9CPT5	3.35	-2.02
Ccdc124	Q9D8X2	3.21	-2.03
Tuba1c;Tuba1a;Tuba1b;Tuba3a	P68373;P68369;P05213;P05214	1.22	-2.06
Cct8	P42932	0.92	-2.08
Rpl30	P62889	4.26	-2.09
	Q0VG62	4.81	-2.10
Ddx18	Q8K363	1.86	-2.14
Atxn2l	Q7TQH0	2.19	-2.17
Sf3b4	Q8QZY9	2.58	-2.18
Rps27a;Ubb;Ubc	P62983;P0CG49;P0CG50	5.34	-2.18
Eno1	P17182	3.09	-2.19
Tra2b	P62996	2.51	-2.20
Mcl1	P97287	6.35	-2.22
Cbx5	Q61686	1.36	-2.23
Hnrnpab	Q99020	2.16	-2.26
Slc4a7	Q8BTY2	1.47	-2.28
Srsf10	Q9R0U0	2.92	-2.29
Rps19bp1	Q8C6B9	2.05	-2.30
Hspa4	Q61316	2.56	-2.33
Srrm1	Q52KI8	3.29	-2.33
Hspd1	P63038	3.80	-2.35
Abcf1	Q6P542	4.18	-2.35
Polr1d	P97304	2.33	-2.36
Rpl22	P67984	4.73	-2.40
Flnc	Q8VHX6	2.59	-2.42
Pdap1	Q3UHX2	3.27	-2.49
Rps19	Q9CZX8	4.89	-2.50
Ptrf	O54724	4.27	-2.50
Rpl23a	P62751	4.74	-2.54
Hmga1	P17095	2.65	-2.59
Calu	O35887	2.03	-2.60
Aldoa	P05064	2.29	-2.60
Zc3h15	Q3TIV5	3.90	-2.62
Rps27	Q6ZWU9	5.15	-2.73
Psmc2	P46471	5.27	-2.74
Atp5o	Q9DB20	2.10	-2.75
Hist1h2bp;Hist1h2bk;Hist1h2bc	Q8CGP2;Q8CGP1;Q6ZWY9	3.02	-2.76
Rpl35	Q6ZWV7	3.84	-2.76
Tubb4b	P68372	2.96	-2.79
Ppia	P17742	4.02	-2.81
Eef2	P58252	5.09	-2.83
Nop2	Q922K7	3.42	-2.86
Rpl11	Q9CXW4	5.08	-2.86
Rps12	P63323	2.15	-2.91
Sars	P26638	2.70	-2.93
Nop56	Q9D6Z1	2.62	-2.95
Plec	Q9QXS1	0.96	-2.97

Gene names	Majority protein IDs	-Log Student's T-test p-value WT/SS	fold change WT/SS
Ywhag	P61982	3.47	-3.01
Hnrnpc	Q9Z204	2.19	-3.03
Raly	Q64012	2.08	-3.04
Flna	Q8BTM8	5.04	-3.07
Rps18	P62270	5.30	-3.08
Rps20	P60867	4.36	-3.09
Hist1h1d	P43277	4.68	-3.12
Lap3	Q9CPY7	2.24	-3.19
Cactin	Q9CS00	3.27	-3.19
Rps3	P62908	5.00	-3.27
Hist1h1a	P43275	5.55	-3.27
Nop58	Q6DFW4	5.34	-3.29
Aldh2	P47738	1.32	-3.30
Rpl12	P35979	1.95	-3.31
Eif3c	Q8R1B4	1.03	-3.31
Cdk1	P11440	3.38	-3.32
Rpl29	P47915	2.49	-3.32
Anxa4	P97429	1.05	-3.36
H3f3a;Hist1h3b;Hist1h3a;H3f3c	P84244;P84228;P68433;P02301	1.50	-3.44
Mcm2	P97310	2.94	-3.52
Ywhaz	P63101	1.61	-3.57
Rps15	P62843	5.03	-3.61
Rps13	P62301	5.66	-3.63
Rps11	P62281	5.41	-3.65
Eef1d	P57776	4.13	-3.65
Rps16	P14131	6.01	-3.66
Rps10	P63325	5.81	-3.68
Edf1	Q9JMG1	3.18	-3.71
Eif3b	Q8JZQ9	3.24	-3.76
Drg1	P32233	3.06	-3.76
Nap1l1;Nap1l4	P28656;Q78ZA7	3.51	-3.79
Rpl5	P47962	5.95	-3.80
Kpna2	P52293	2.24	-3.84
Rps14	P62264	5.84	-3.85
Epb41l2	O70318	2.08	-3.89
Eif3d	O70194	2.27	-3.90
Mtdh	Q80WJ7	6.49	-3.98
Rps26	P62855	0.69	-3.99
Rps9	Q6ZWN5	5.77	-4.02
Rps17	P63276	5.50	-4.11
Pkm	P52480	2.45	-4.13
Flii	Q9JJ28	5.56	-4.16
Hist1h1e	P43274	1.53	-4.17
Smarca5	Q91ZW3	3.50	-4.20
Eif3i	Q9QZD9	2.93	-4.27
Rpl18	P35980	4.09	-4.37
Rps4x	P62702	4.81	-4.46
Rpl10a	P53026	5.79	-4.50
Eif3a	P23116	3.66	-4.56
Aco2	Q99KI0	2.07	-4.56
Hmgn1	P18608	2.28	-4.61
Rpl35a	O55142	2.23	-4.64
Nolc1	E9Q5C9	4.76	-4.67
Rpl7a	P12970	7.20	-4.67
Igf2bp2	Q5SF07	5.00	-4.70
Rpl17	Q9CPR4	5.69	-4.74
Rps3a	P97351	6.45	-4.77
Rpl26	P61255	7.45	-4.81
Rps2	P25444	5.26	-4.81
Eif1ax;Eif1a	Q8BMJ3;Q60872	1.98	-4.82
Vars	Q9Z1Q9	3.22	-4.86
Hnrnpu	Q8VEK3	2.66	-4.88
Rpl6	P47911	7.05	-4.88
Rpl31	P62900	6.63	-4.89
Hdlbp	Q8VDJ3	3.61	-4.91
Hist1h1b	P43276	5.23	-5.04
Rplp0	P14869	7.64	-5.10
Rpl13a	P19253	6.08	-5.26
Rps8	P62242	6.37	-5.26
Ybx1	P62960	6.31	-5.37
Rps6	P62754	5.01	-5.55
Rpl15	Q9CZM2	7.12	-5.58
Rpl7	P14148	5.08	-5.65
Rpl8	P62918	7.62	-5.75

Gene names	Majority protein IDs	-Log Student's T-test p-value WT/SS	fold change WT/SS
Csnk2a1	Q60737	5.65	-5.78
Snd1	Q78PY7	2.97	-5.87
Hnrnpk	P61979	2.00	-5.97
Pa2g4	P50580	4.17	-6.37
Ssb	P32067	4.99	-6.55
Rpl13	P47963	7.17	-6.55
Rplp2	P99027	2.73	-6.97
Rpl10;Rpl10l	Q6ZWV3;P86048	5.76	-7.01
Rpl4	Q9D8E6	5.61	-7.14
Rps5	P97461	4.57	-7.70
Eif2a	Q8BJW6	6.64	-7.73
Fbl	P35550	5.47	-7.74
Rpl3	P27659	5.32	-7.93
Rps24	P62849	1.95	-7.95
Ybx3	Q9JKB3	4.74	-8.04
Rpl14	Q9CR57	3.85	-8.61
Syncrip	Q7TMK9	3.14	-8.64
Rpl19	P84099	7.13	-8.71
Rpl28	P41105	4.83	-8.97
Ncl	P09405	5.55	-8.98
Thrap3	Q569Z6	6.59	-9.57
Hp1bp3	Q3TEA8	6.62	-10.99
Rpl9	P51410	2.73	-11.06
Kars	Q99MN1	5.17	-11.18
Rps7	P62082	6.06	-13.74
Rrbp1	Q99PL5	5.77	-15.60
Rpl27	P61358	3.01	-16.71
Rpl27a	P14115	3.57	-21.23
Alyref;Alyref2	O08583;Q9JJW6	4.16	-23.10
Rpl34	Q9D1R9	3.59	-34.27
Rpl21	O09167	7.86	-36.17

10 Acknowledgments

12 Eidesstattliche Erklärung

Ich, Vanessa Ehrenfeld geb. Zimmermann, erkläre hiermit an Eides statt, dass ich die vorgelegte Dissertation mit dem Titel

„Regulation of cell death signaling by the thioredoxin system in healthy and malignant cells"

selbständig angefertigt und mich anderer Hilfsmittel als der in ihr angegebenen nicht bedient habe, insbesondere, dass alle Entlehnungen aus anderen Schriften mit Angabe der betreffenden Schrift gekennzeichnet sind. Alle Beiträge von Kollegen und Kolleginnen werden in der Arbeit explizit erwähnt und sind im Folgenden nochmals aufgeführt. Das unten aufgeführte Material wurde im Rahmen von Forschungskooperationen erstellt:

- Figure 19 B. Auranofin treatment induces changes in global protein oxidation in Jurkat FD cells; Kollaborationspartner: Dr. Ilka Wittig, Funktionelle Proteomik, Fachbereich Medizin, Goethe-Universität Frankfurt; Beitrag des Kollaborationspartners: Probenaufbereitung, Massenspektrometrische Analyse, Datenanalyse und statistische Auswertung; eigener Beitrag: Vorbereitung der Zellen, Aufbereitung der Abbildung.
- Figure 28 A. Cysteine residues influence BAK interactome upon Auranofin treatment; Kollaborationspartner: Dr. Ilka Wittig, Funktionelle Proteomik, Fachbereich Medizin, Goethe-Universität Frankfurt; Beitrag des Kollaborationspartners: Probenaufbereitung, Massenspektrometrische Analyse, Datenanalyse und statistische Auswertung; eigener Beitrag: Vorbereitung der Zellen, Aufbereitung der Abbildung.
- Table 24. Significantly enriched proteins identified in the MS analysis of Jurkat FD cells; Kollaborationspartner: Dr. Ilka Wittig, Funktionelle Proteomik, Fachbereich Medizin, Goethe-Universität Frankfurt; Beitrag des Kollaborationspartners: Probenaufbereitung, Massenspektrometrische Analyse, Datenanalyse und statistische Auswertung; eigener Beitrag: Vorbereitung der Zellen, Aufbereitung der Tabelle.
- Table 25. Interaction partners of mRuby2-BAK identified in the MS analysis; Kollaborationspartner: Dr. Ilka Wittig, Funktionelle Proteomik, Fachbereich Medizin, Goethe-Universität Frankfurt; Beitrag des Kollaborationspartners: Probenaufbereitung, Massenspektrometrische Analyse, Datenanalyse und statistische Auswertung; eigener Beitrag: Vorbereitung der Zellen, Aufbereitung der Tabelle.

Die folgenden Teile der Dissertation sind bereits veröffentlich worden [199]:

- Figure 7. PX-12 decreases cell viability and causes cell death in ALL cell lines.
- Figure 8. PX-12 induces cell death in a time-dependent manner in Jurkat FD cells.
- Figure 9. PX-12 decreases Trx activity that is accompanied by ROS formation in Jurkat FD cells.
- Figure 10. PRDX3 dimer formation is increased upon PX-12 treatment.
- Figure 11. NAC rescues PX-12-induced cell death and ROS increase.
- Figure 12. PX-12 induces caspase-dependent cell death.
- Figure 13. BAK is activated upon PX-12 treatment and involved in cell death induction and ROS increase.
- Figure 14. NOXA is involved in PX-12-mediated cell death and BAK activation.

Ich versichere, die Grundsätze der guten wissenschaftlichen Praxis beachtet, und nicht die Hilfe einer kommerziellen Promotionsvermittlung in Anspruch genommen zu haben.

Frankfurt am Main, den 27.07.2020

Vanessa Ehrenfeld